OCCURRENCE OF MULTIPLE FLUID PHASES ACROSS A BASIN, IN THE SAME SHALE GAS FORMATION – EAGLE FORD SHALE EXAMPLE

A Dissertation

by

YAO TIAN

Submitted to the Office of Graduate and Professional Studies of
Texas A&M University
in partial fulfillment of the requirements for the degree of

DOCTOR OF PHILOSOPHY

Chair of Committee,	Walter B. Ayers
Committee Members,	William D. McCain, Jr.
	Zoya Heidari
	Yuefeng Sun
Head of Department,	A. Daniel Hill

May 2014

Major Subject: Petroleum Engineering

Copyright 2014 Yao Tian

ABSTRACT

Shale gas and oil are playing a significant role in US energy independence by reversing declining production trends. Successful exploration and development of the Eagle Ford Shale Play requires reservoir characterization, recognition of fluid regions, and the application of optimal operational practices in all regions.

Using stratigraphic and petrophysical analyses, we evaluated key parameters, of reservoir depth and thickness, fluid composition, reservoir pressure, total organic carbon (TOC), and number of limestone and organic-rich marl interbeds of the Lower Eagle Ford Shale. Spatial statistics were used to identify key reservoir parameters affecting Eagle Ford production. We built reservoir models of various fluid regions and history matched production data. Well deliverability was modeled to optimize oil production rate by designing appropriate operational parameters.

From NW to SE, Eagle Ford fluids evolve from oil, to gas condensate and, finally, to dry gas, reflecting greater depth and thermal maturity. From outcrop, the Eagle Ford Shale dips southeastward; depth exceeds 13,000 ft at the Sligo Shelf Margin. We divided Eagle Ford Shale into three layers. The Lower Eagle Ford is present throughout the study area; it is more than 275 ft thick in the Maverick Basin depocenter and thins to less than 50 ft on the northeast. In the Lower Eagle Ford Shale, a strike-elongate trend of high TOC, high average gamma ray values, and low bulk density extends from Maverick Co.

northeastward through Guadalupe Co. Both limestone and organic-rich marl beds increase in number from fewer than 2 near outcrop to more than 20 at the shelf margins. Average thicknesses of Lower Eagle Ford limestone and organic-rich marl beds are low (< 5 ft.) in the La Salle – DeWitt trend, coincident with the most productive gas and oil wells. Eagle Ford Shale was divided into 5 production regions in South Texas that coincide with the regional, strike-elongate trends of geologic parameters, which suggests that these parameters significantly impact Eagle Ford Shale production.

Eagle Ford Shale production (barrels of oil equivalent, BOE) increases consistently with depth, increases with Lower Eagle Ford thickness (up to 180-ft thickness), and increases with TOC (up to 7%). P values analyses suggest high certainty of the relationship between the production and five reservoir parameters tested in regression models.

Multiple good history matches of a gas condensate well suggest significant uncertainties in reservoir parameters. Oil production rate is not sensitive to oil relative permeability for the gas condensate well model. We were unable to match the production history for the volatile oil wells, possibly because gas of lift. Reservoir modeling suggests low bottomhole flowing pressure was the key to optimize cumulative oil production.

Concepts and models developed in this study may assist operators in making critical Eagle Ford Shale development decisions; they may be transferable to other shale plays.

DEDICATION

I dedicate 30% of this work to my husband, Linfeng Bi, without whom this project could have been finished 1 year earlier. A happy marriage negatively impacts efficiency– immensely.

I dedicate 30% of this work to my advisor, Dr. W.B. Ayers. Without his tremendous support, wise guidance, and constant encouragement through the journey, I could never finish this project.

I dedicate 40% of this work to my parents, Wanlu Tian and Minhang Zheng, who shown me the beauty of knowledge and gave me the strength and perseverance to chase the dream and reach for the stars.

This dissertation is only the beginning of my brilliant journey.

ACKNOWLEDGEMENTS

I thank my committee members, Dr. Ayers, Dr. McCain, Dr. Heidari, and Dr. Sun, for their guidance and support throughout the course of this research. Your comments, insights, and questions have been very beneficial in the completion of this project. I express my sincere gratefulness for everything you did for me.

I also thank my friends and colleagues and faculty and staff of the Harold Vance Department of Petroleum Engineering for making my time at Texas A&M University a great experience.

I also extend my gratitude to the Drillinginfo, Texas Railroad Commission, and IHS for the data they provided.

TABLE OF CONTENTS

Page

ABSTRACT ii

DEDICATION iv

ACKNOWLEDGEMENTS v

TABLE OF CONTENTS vi

LIST OF FIGURES ix

LIST OF TABLES xvii

CHAPTER I INTRODUCTION 1

Eagle Ford Shale Geological Features 5
Reservoir Properties 10
Production 11
Statement of the Problem, Objectives, and Methods 14

CHAPTER II REGIONAL PRODUCTION TRENDS AND FLUID PROPERTIES 16

Regional Production Analysis 16
Fluid Identification 16
Oil Gravity and Gas Specific Gravity 20
Reservoir Pressure and Pressure Gradient 23
Stimulation Practice in Eagle Ford Shale 25

CHAPTER III STRUCTURAL AND STRATIGRAPHIC ANALYSES 29

Methods 29
Structural Setting 30
Thicknesses of Eagle Ford Shale Units 34

CHAPTER IV PETROPHYSICAL EVALUATION OF KEY RESERVOIR PARAMETERS 40

TOC Analyses by Well Logs 40
Bulk Density and Gamma Ray—Qualitatively Assessment of TOC 41
Spectral Gamma Ray Analysis—Qualitative Assessment of TOC 43

Passey's ΔR Methods—Quantitative Assessment of TOC 46
Cyclicity 53

CHAPTER V QUANTITATIVE EVALUATION OF KEY RESERVOIR PARAMETERS 61

Methods 62
Data Preparation 62
Distribution Pattern Identification 62
Skewness Identification 63
Transformation to Normality 64
Covariance Function Fitting 65
Gaussian Distribution Data Prediction 66
Poisson Distribution Data Prediction 66
Prediction Results 67
Gaussian Data Group Prediction 69
Poisson Distribution Prediction 76
Fitting Regression Models 79
Regression Result Interpretation 83
Coefficient Analysis 83
Depth vs. BOE Production 84
Thickness vs. BOE 85
TOC vs. BOE Production 85
Number of Limestone Beds vs. BOE Production 86
Average Bed Thickness vs. BOE Production 87
P-value Analyses 88
Limitations 90

CHAPTER VI RESERVOIR MODELING 91

Production Data Used in Reservoir Modeling 91
Volatile and Gas Condensate Well Modeling 94
Reservoir Geometry 94
Model Setup 97
Reservoir Properties 97
Relative Permeability 99
Transmissibility Multiplier 101
Pressure/Volume/Temperature (PVT) Data Acquisition 102
Volatile Oil and Gas Condensate Wells Simulation Results 105
Gas Condensate Well History Match 105
Gas Condensate Model Sensitivity Analysis 116
Volatile Well Model Simulation Results 119
Oil Production Optimization 124
Dry Gas Well Modelling 125

Data Gathering 125
Dry Gas Model History Match Results 128

CHAPTER VII DISCUSSION 130

Regions 1 and 2 131
Region 3 133
Region 4 133
Region 5 134

CHAPTER VIII CONCLUSIONS 135

REFERENCES 138

LIST OF FIGURES

Page

Fig. 1—US dry natural gas production by source, 1990–2040, TCF (EIA 2012a). 1

Fig. 2—Petroleum and other liquid fuels supply by source, 1970–2040 (million barrels per day) (EIA 2014). 2

Fig. 3—Monthly dry gas production of shale plays (billion cubic feet (Bcf)/day) (EIA 2012b).....2

Fig. 4—Texas Eagle Ford Shale drilling permits issued 2008 through 2013 (TRC 2014).....3

Fig. 5—Review of emerging resources: US shale gas and shale oil plays (EIA 2011).....4

Fig. 6—Texas Eagle Ford Shale: production of oil, gas condensate, and gas wells, 2008 through 2012 (TRC 2013a–c). 4

Fig. 7—Structural top of Eagle Ford Shale (Hentz and Ruppel 2010). 6

Fig. 8—Map of the western part of the Western Gulf Province showing main structural features. Modified from Condon and Dyman (2006).....7

Fig. 9—Lithostratigraphy of the Eagle Ford Shale in Texas (Hentz and Ruppel 2010, after Childs et al. 1988). 8

Fig. 10—Isopach map of the Lower Eagle Ford Shale (Hentz and Ruppel 2010).....9

Fig. 11—Isopach map of the Upper Eagle Ford Shale (Hentz and Ruppel 2010). 10

Fig. 12—Maturation window of Eagle Ford Shale hydrocarbon (Fan et al. 2011). 12

Fig. 13—Eagle Ford Shale peak monthly gas production. Data from Drillinginfo (2013). 17

Fig. 14—Eagle Ford Shale peak monthly oil production. Data from Drillinginfo (2013). 17

Fig. 15—Fluid types of Eagle Ford Shale identified by the average GOR from first three months. Data from Drillinginfo (2013). 18

Fig. 16—Heptane-plus content map for Eagle Ford wells. Data from TRC (2013). 19

Fig. 17—GOR Profile for (a) black oil wells, (b) for volatile oil wells, and (c) gas condensate wells. The heavy red line in average GOR. Data retrieved from HPDI (2012). 21

Fig. 18—Oil API gravity increases from northwest to southeast. Data from Drillinginfo (2013). 22

Fig. 19—Gas specific gravity increases from southeast to northwest. Data from Drillinginfo (2013). 23

Fig. 20—Eagle Ford Shale reservoir pressure of from PVT analysis results. Data from TRC (2013). 24

Fig. 21—Eagle Ford Shale pressure gradient. Data from TRC (2013). 25

Fig. 22—Number of hydraulic fracture stages stimulated in Eagle Ford Wells, by operators. Data from Drilliginfo (2012). 26

Fig. 23—Number of hydraulic fracture stages vs. first 6 month production of SM Energy wells. Data from Drillinginfo (2012). 27

Fig. 24—Number of hydraulic fracture stages vs. first 6 months production of Anadarko wells. Data from Drillinginfo (2012). 27

Fig. 25—Number of hydraulic fracture stages vs. first 6 month production of Marathon Oil Company wells. Data from Drillinginfo (2012). 28

Fig. 26—Number of hydraulic fracture stages vs. first 6 month production of ConocoPhillips wells. Data from Drillinginfo (2012). 28

Fig. 27—Structure base of the Eagle Ford Shale. 30

Fig. 28—Type log in Maverick County showing three units identified in the Eagle Ford Shale (The Exploration Company, Paloma E 1 53). See Fig. 27 for location. 31

Fig. 29—Density vs. neutron porosity crossplot for Eagle Ford Shale units and Buda Limestone. 32

Fig. 30—PEF vs. gamma ray crossplot for Eagle Ford Shale units and Buda Limestone. 33

Fig. 31—Deep resistivity vs. gamma ray crossplot for Eagle Ford Shale units and Buda Limestone. 34

Fig. 32—Cross section of Eagle Ford Shale showing the three stratigraphic subdivisions. See Figure 27 for locations. 35

Fig. 33—Thickness of total Eagle Ford Shale. 36

Fig. 34—Thickness of Lower Eagle Ford Shale. 37

Fig. 35—Thickness of total Upper Eagle Ford Shale. 38

Fig. 36—Thickness of lower unit of Upper Eagle Ford Shale. 38

Fig. 37—Thickness of upper unit of Upper Eagle Ford Shale. 39

Fig. 38—Average gamma ray response of the Lower Eagle Ford Shale, based on more than 500 wells. 42

Fig. 39—Average of bulk density of Lower Eagle Ford Shale. 42

Fig. 40—Spectral gamma ray analysis of Eagle Ford Shale, Well D, Harle 1, LaSalle County. See Figure 39 for well location. 43

Fig. 41—Lithologic analyses of Eagle Ford Shale. Well D, Harle 1, LaSalle County. See Figure 39 for well location. 45

Fig. 42—Spectral gamma ray analysis of Eagle Ford Shale, Well E, Pruski Henry 1, Gonzales County. See Figure 39 for well location. 46

Fig. 43—Lower Eagle Ford LOM map. Contour interval is 0.5 LOM units. (Cardneaux 2012) 48

Fig. 44—Level of maturity of Lower Eagle Ford Shale, (interpreted from map by Cardneaux 2012) 48

Fig. 45—TOC of Lower Eagle Ford, determined using resistivity and bulk density logs (Eq. 2). 49

Fig. 46—TOC of Lower Eagle Ford, determined using resistivity and sonic logs (Eq. 3). 49

Fig. 47—Average TOC of Lower Eagle Ford Shale, determined by using Eqs. 2 and 3. 50

Fig. 48—Average TOC of Lower-Upper Eagle Ford Shale, determined using Eqs. 2 and 3. 50

Fig. 49—Average TOC of Upper-Upper Eagle Ford Shale determined using Eqs. 2 and 3. 51

Fig. 50—Lower Eagle Ford ORM and limestone interbeds. See Fig. 52 for well locations. 55

Fig. 51—Schematic showing gamma ray cutoffs used to count the numbers of Lower Eagle Ford Shale limestone and ORM beds. 56

Fig. 52—Number of limestone bed of Lower Eagle Ford Shale. 57

Fig. 53—Number of ORM bed in the Lower Eagle Ford Shale. 58

Fig. 54—Average bed thickness of Lower Eagle Ford Shale. 59

Fig. 55—Schematic workflow for quantifying influences on production from various geological parameters. 63

Fig. 56—(a) Unit slope on Q-Q plot for Gaussian distribution; (b) Curved pattern on Q-Q plot, suggesting skewness (Skbkekas 2009). 64

Fig. 57—Log transformation with λ being zero (Scott and Lane 2008). 65

Fig. 58—Spatial map of first 6 month barrel of oil equivalent production of Eagle Ford Shale in South Texas. Coordinates uses North American Datum 1927 (NAD27) in meters. 68

Fig. 59—Histogram and Q-Q plot of depth data. 69

Fig. 60—(a) Histogram of thickness of Lower Eagle Ford Shale, (b) Q-Q plot of thickness, (c) Box-Cox transformation result, and (d) Q-Q plot of thickness data after Box-Cox transformation. 70

Fig. 61—Skewness elimination workflow by Q-Q plots and Box-Cox transformation. 71

Fig. 62—Depth of Lower Eagle Ford Shale by stratigraphic analyses on vertical wells. Coordinates uses NAD27 system in meters. 72

Fig. 63—Depth of Lower Eagle Ford Shale predicted for Eagle Ford production wells locations by kriging. Coordinates uses NAD27 system in meters. 72

Fig. 64—Thickness of Lower Eagle Ford Shale by stratigraphic analyses on vertical wells. Coordinates uses NAD27 system in meters. 73

Fig. 65—Thickness of Lower Eagle Ford Shale predicted for Eagle Ford production well locations by kriging. Coordinates uses NAD27 system in meters. 73

Fig. 66—Average bed thickness of Lower Eagle Ford Shale calculated at vertical wells. Coordinates uses NAD27 system in meters. 74

Fig. 67—Average bed thickness of Lower Eagle Ford Shale predicted for Eagle Ford production well locations by kriging. Coordinates uses NAD27 system in meters. 74

Fig. 68—TOC calculated at vertical wells by petrophysical analyses. Coordinates uses NAD27 system in meters. 75

Fig. 69—TOC predicted for Eagle Ford production well locations by kriging. Coordinates uses NAD27 system in meters. 75

Fig. 70—Histogram and Q-Q plot of number of limestone beds. 76

Fig. 71—MCMC sampling of intercept (β), variance ($\sigma 2$), and spatial range (ϕ) for the number of limestone beds. 77

Fig. 72—Number of limestone beds at vertical wells. Coordinates uses NAD27 system in meters. 78

Fig. 73—Number of limestone beds predicted for Eagle Ford production well locations by Bayesian prediction. Coordinates uses NAD27 system in meters. 78

Fig. 74—Transformation of production data for Gaussian distribution without skewness. 80

Fig. 75—First 6 months' BOE prediction from model 1. Coordinates uses NAD27 system in meters. 81

Fig. 76—First 6 months' BOE prediction from model 2. Coordinates uses NAD27 system in meters. 82

Fig. 77—First 6 months' BOE prediction from model 3. Coordinates uses NAD27 system in meters. 82

Fig. 78—Depth vs. production correlation of regression model 3. 84

Fig. 79—Total thickness of Lower Eagle Ford Shale vs. production correlation of regression model 3. 85

Fig. 80—Average TOC of Lower Eagle Ford Shale vs. production correlation of regression model 3. 86

Fig. 81—Number of limestone beds in Lower Eagle Ford Shale vs. production correlation of regression model 3. 87

Fig. 82—Average bed thickness of Lower Eagle Ford Shale vs. production correlation of regression model 3. 88

Fig. 83—Production history for gas condensate well. 91

Fig. 84—Production history for volatile oil well No. 1. 92

Fig. 85—Production history for volatile oil well No. 2. 92

Fig. 86—Production history for dry gas well (Bazen et al. 2012). 93

Fig. 87—Lateral length distribution of Eagle Ford Shale horizontal wells. Data from Drillinginfo (2012). 95

Fig. 88—Geometry for base case reservoir model for all production regions. 96

Fig. 89—Fracture permeability of the fracturing plan. 98

Fig. 90—Relative permeability generated by Corey's correlation for organic-rich marl. 100

Fig. 91—Relative permeability generated by Corey's correlation for the limestone beds. 100

Fig. 92—Pressure-dependent permeability for hydraulic fracture, ORM, and limestone (Honarpour et al. 2012). 101

Fig. 93—Pressure-dependent porosity for ORM and calcite-rich rocks. 102

Fig. 94—Phase diagram used in the volatile oil model. 104

Fig. 95—Phase diagram used in the gas condensate model. 104

Fig. 96—Low relative permeability used in the history match process. 105

Fig. 97—Model 1 of good history match results. 108

Fig. 98—Model 2 of good history match results. 109

Fig. 99—Model 3 of good history match results. 110

Fig. 100—Model 4 of good history match results. 111

Fig. 101—Model 5 of good history match results with higher porosity. 112

Fig. 102—Model 6 of good history match results with higher water saturation. 113

Fig. 103—Model 7 of good history match results with higher porosity and water saturation. 114

Fig. 104—Three relative permeability cases used in the sensitivity analysis. 117

Fig. 105—Gas condensate well sensitivity analysis of relative permeability on cumulative oil production. 117

Fig. 106—Gas condensate well sensitivity analysis of porosity on cumulative oil production. 118

Fig. 107—Gas condensate well sensitivity analysis of water saturation on cumulative oil production. 118

Fig. 108—Gas condensate well sensitivity analysis of fracture permeability on cumulative oil production. 119

Fig. 109—Simulation results showing proper pressure decline prediction but inaccurate simulated GOR on volatile oil well model No. 1. 120

Fig. 110—Simulation results showing proper pressure decline prediction but inaccurate simulated GOR on volatile oil well model No. 2. 121

Fig. 111—Simulation results showing accurate simulated GOR but inaccurate simulated pressure on volatile oil well model No. 1. 122

Fig. 112—Oil production forecast with two different bottomhole pressures. 125

Fig. 113—Production and pressure history of 250 days for Eagle Ford dry gas well (Bazen et al. 2010). 126

Fig. 114—Log image in publication vs. the well log images available in Drillinginfo database (Bazen et al. 2012; Drillinginfo 2013). 127

Fig. 115—Digitized well log showing layering in the reservoir model (digitized from image in Drillinginfo). 127

Fig. 116—Two models of a dry gas well showing good matches between pressure history and simulated pressure. 128

Fig. 117—Eagle Ford Shale production region subdivisions displayed on Eagle Ford GOR map (Fig. 15). 131

Fig. 118—Summary of "central trends" of key Eagle Ford Shale reservoir properties (Figs, 27,34, 39, 37, 47, 52 through 54) that affect productivity. Displayed on Eagle Ford GOR map (Fig. 15). 132

LIST OF TABLES

Page

Table 1—Typical Completion for Horizontal Eagle Ford Wells in the Gas and Liquid-Rich Areas 13

Table 2—The Coefficients of Geological Parameters from Three Models 83

Table 3—P-values and Significant Codes of Geological Parameters in Regression Model 3. 89

Table 4—Reservoir and Fracture Properties for the Dry Gas Wells 94

Table 5—Reservoir Model Geometry Design 96

Table 6—Depth and Thickness for Reservoir Models of Gas Condensate and Volatile Oil Regions 98

Table 7—Reservoir Properties for Input Before History Match 98

Table 8—Summary of Fluid Properties Used in The Reservoir Models for PVT Behavior 103

Table 9—Composition and C7+ Properties for the Reservoir Models 103

Table 10—Summary of Reservoir Properties of Gas Condensate Models with Good History Match Results 115

Table 11—Fracture Permeability Decreasing from Center to Outer Boundary of History Match Results 115

Table 12—Water Saturation Used in the Dry Gas Reservoir Model from Two History Matches 129

Table 13—Porosity Used in the Dry Gas Reservoir Model from Two History Match Results 129

Table 14—Summary of Generalized Reservoir Properties of Lower Eagle Ford Among Five Production Regions. 130

CHAPTER I

INTRODUCTION

From 2010 to 2011, total US gas production increased from 61.4 to 66.2 Bcf/d (7.9%) (EIA 2012). This increase was exclusively from onshore, where production increased from 53.9 to 60.2 Bcf/day. Onshore oil production grew also, mainly from shale (tight oil) plays (EIA 2012) **(Figs. 1 through 3).** Shales were once discounted as reservoirs by the oil and gas industry because of the low production rates that resulted from low permeability; however, with advances in horizontal drilling and hydraulic fracturing technologies, production rates and economics of shale gas wells have significantly improved (East et al. 2004; Ketter et al. 2006).

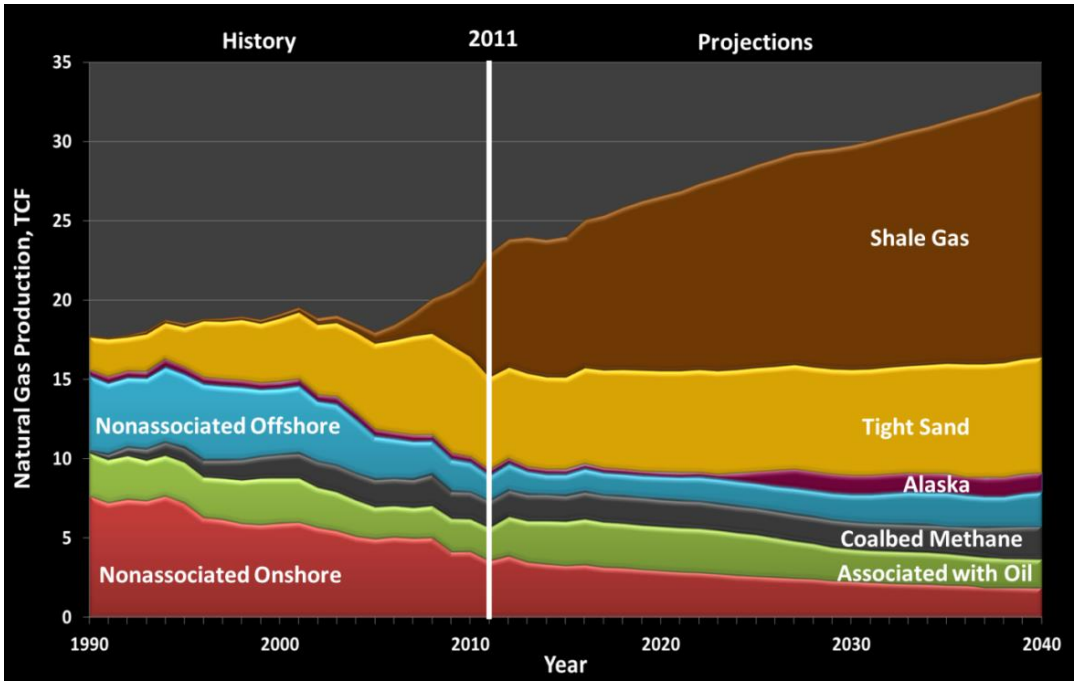

Fig. 1—US dry natural gas production by source, 1990–2040, TCF (EIA 2012a).

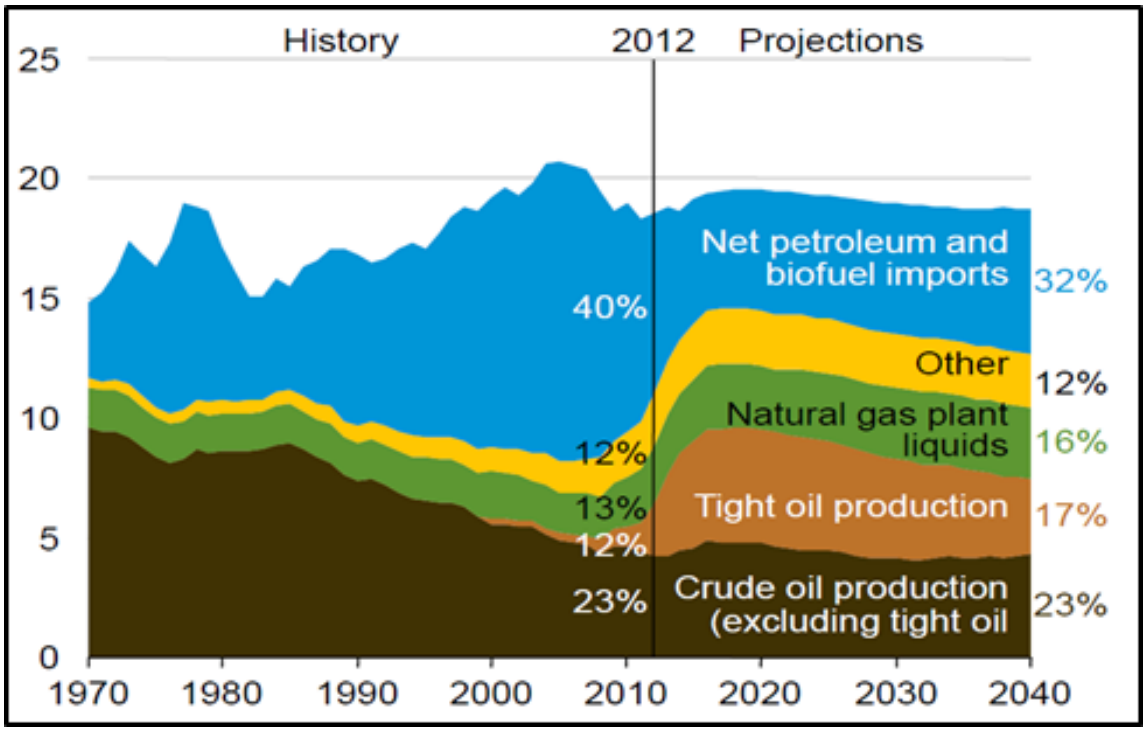

Fig. 2—Petroleum and other liquid fuels supply by source, 1970–2040 (million barrels per day) (EIA 2014).

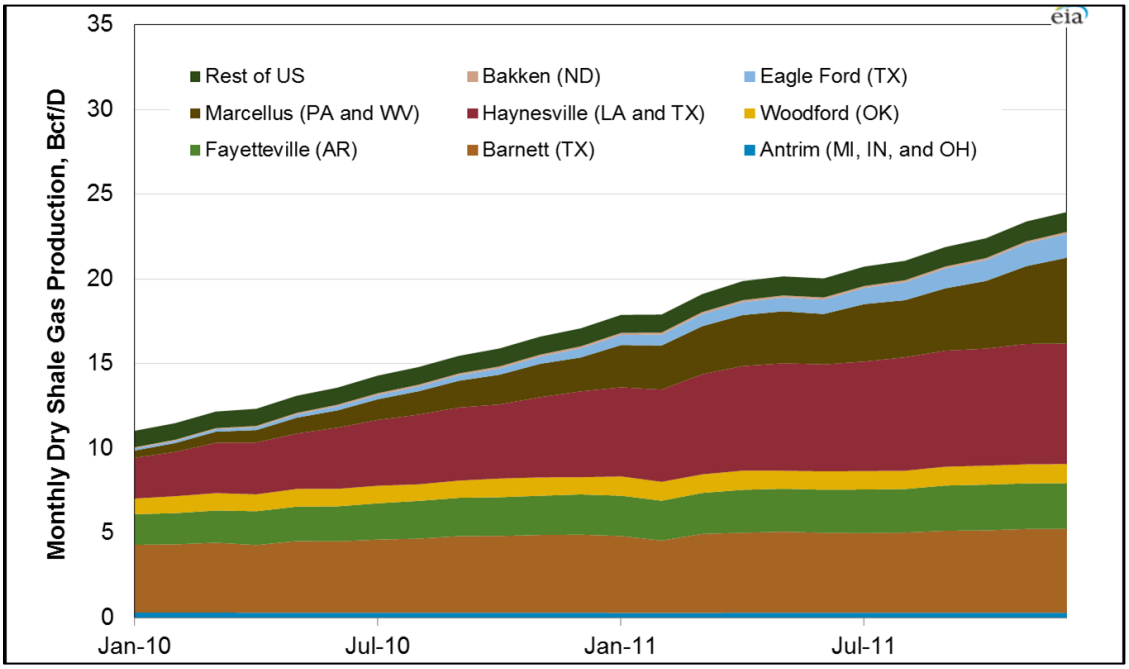

Fig. 3—Monthly dry gas production of shale plays (billion cubic feet (Bcf)/day) (EIA 2012b).

After successful development of Barnett Shale in Fort Worth Basin, Haynesville Shale in Louisiana and Texas, and the Marcellus Shale in Pennsylvania, the Eagle Ford Shale has become one of the most rapidly developing shale gas plays in the US **(Fig. 4)** (TRC 2014). In 2009, Eagle Ford Shale recoverable resources were estimated to be 21 Tcf natural gas and 3 billion barrels of shale oil **(Fig. 5)** (EIA 2011).

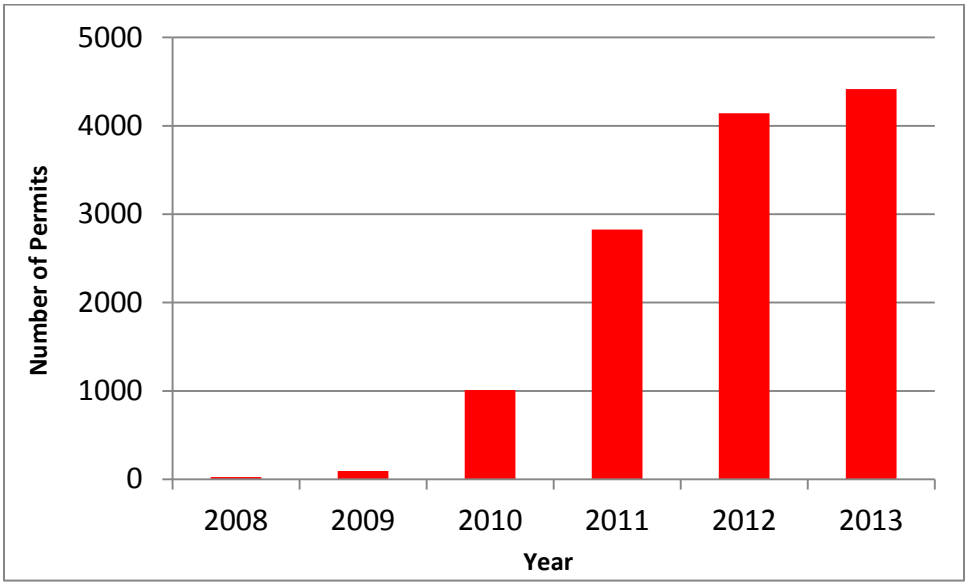

Fig. 4—Texas Eagle Ford Shale drilling permits issued 2008 through 2013 (TRC 2014).

Eagle Ford was initially developed as a shale gas play. With plummeting gas prices, Eagle Ford development shifted to the oil region **(Fig. 6)** (TRC 2013a–c). Although Eagle Ford gas production remained relatively stable from 2011 to 2012, oil production increased by nearly 300% (Fig. 6) (TRC 2013a–c). Shale gas and oil play a significant role in the US's energy independence, and they will continue to be a vital source of energy to the US and the rest of the world.

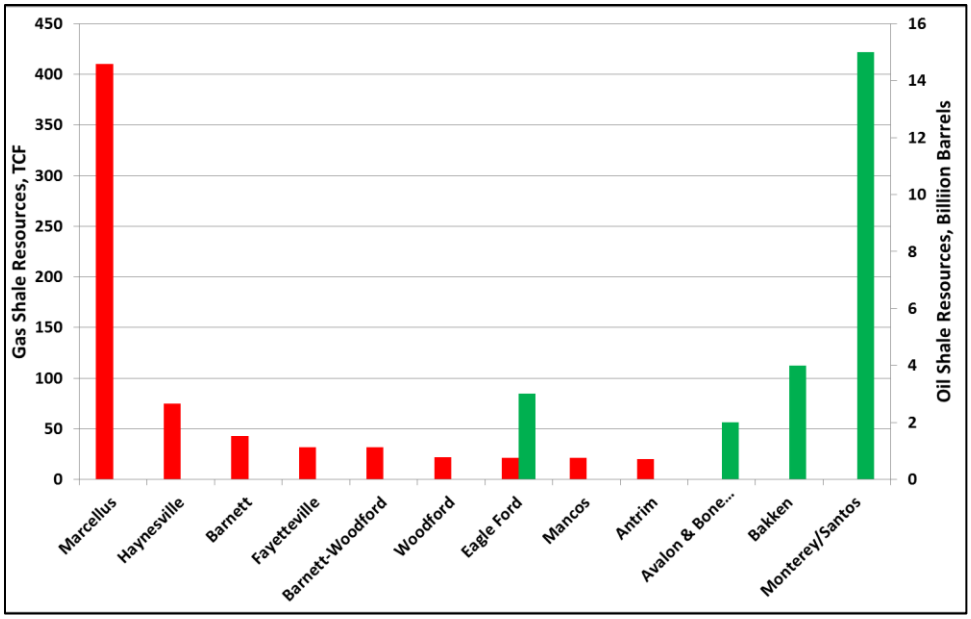

Fig. 5—Review of emerging resources: US shale gas and shale oil plays (EIA 2011).

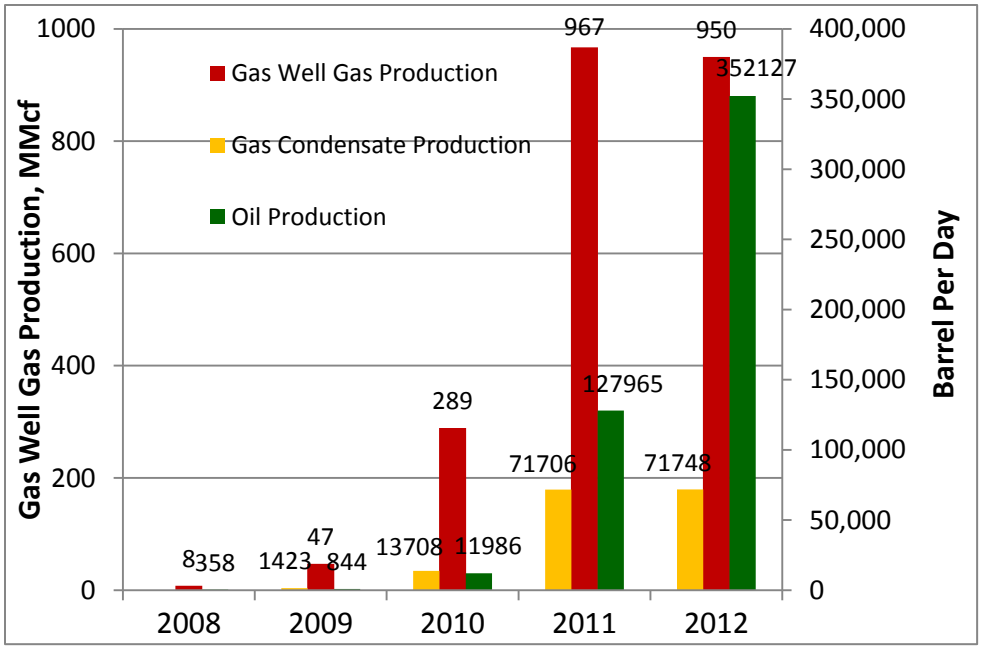

Fig. 6—Texas Eagle Ford Shale: production of oil, gas condensate, and gas wells, 2008 through 2012 (TRC 2013a – c).

The challenges of evaluating shale reservoirs lie in their extremely low porosity, low permeability, high clay content, and difficulty in calculating water saturation (Spears and Jackson 2009). Significant progress has been made to find the key controls for shale productivity and to evaluate these properties. From earlier work on the Barnett Shale, essential geochemistry factors were identified, including total organic carbon (TOC), thermal maturity, burial history, and gas content (Bowker 2003; Jarvie 2004; Montgomery et al. 2005; Pollastro et al. 2007). Common errors in interpreting these parameters were discussed in later works (Dembicki 2009). Accurate mineralogy and lithology evaluations can improve understanding of the mechanical properties of Eagle Ford Shale and assist perforation interval selection (Heidari and Torres–Verdin 2011). More recently, the typical analysis for shale reservoirs has been extended to include TOC, X-ray diffraction, absorbed and free gas, vitrinite reflectance, detailed core and thin-section descriptions, porosity, permeability, and water saturation (Passey et al. 2010; Dicman and Vernik 2012).

EAGLE FORD SHALE GEOLOGICAL FEATURES

Eagle Ford Shale extends from the Mexican border northeastward to the Texas–Louisiana border. Present exploration and production are focused on the Rio Grande Embayment of South Texas, where more than a dozen operators have Eagle Ford leases and/or vertical and horizontal production wells. The Eagle Ford Shale wells produce oil, condensate, and dry gas, depending on the geological setting.

From its outcrop, the Eagle Ford extends basinward (southeastward) to the Edwards and Sligo Reef Trends, where its depth exceeds 14,000 ft (**Fig. 7**) (Hentz and Ruppel 2010). There are several main structural features in the Gulf Province, which extends across the Texas and Louisiana boarders (Ewing 1991; Condon and Dyman 2006). Just northwest of the province boundary is the elevated Llano Uplift **(Fig. 8).** The San Marcos Arch is a subsurface extension of the Llano Uplift that extends southeastward toward the Gulf of Mexico (Fig. 8).

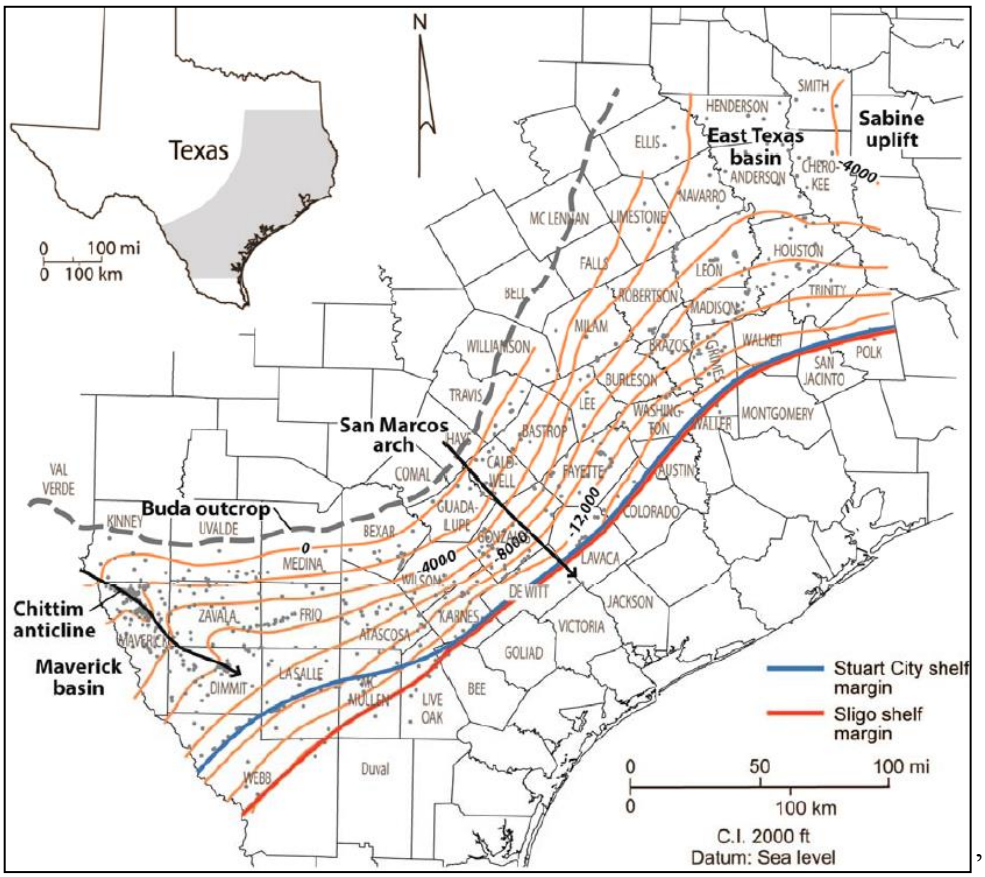

Fig. 7—Structural top of Eagle Ford Shale (Hentz and Ruppel 2010).

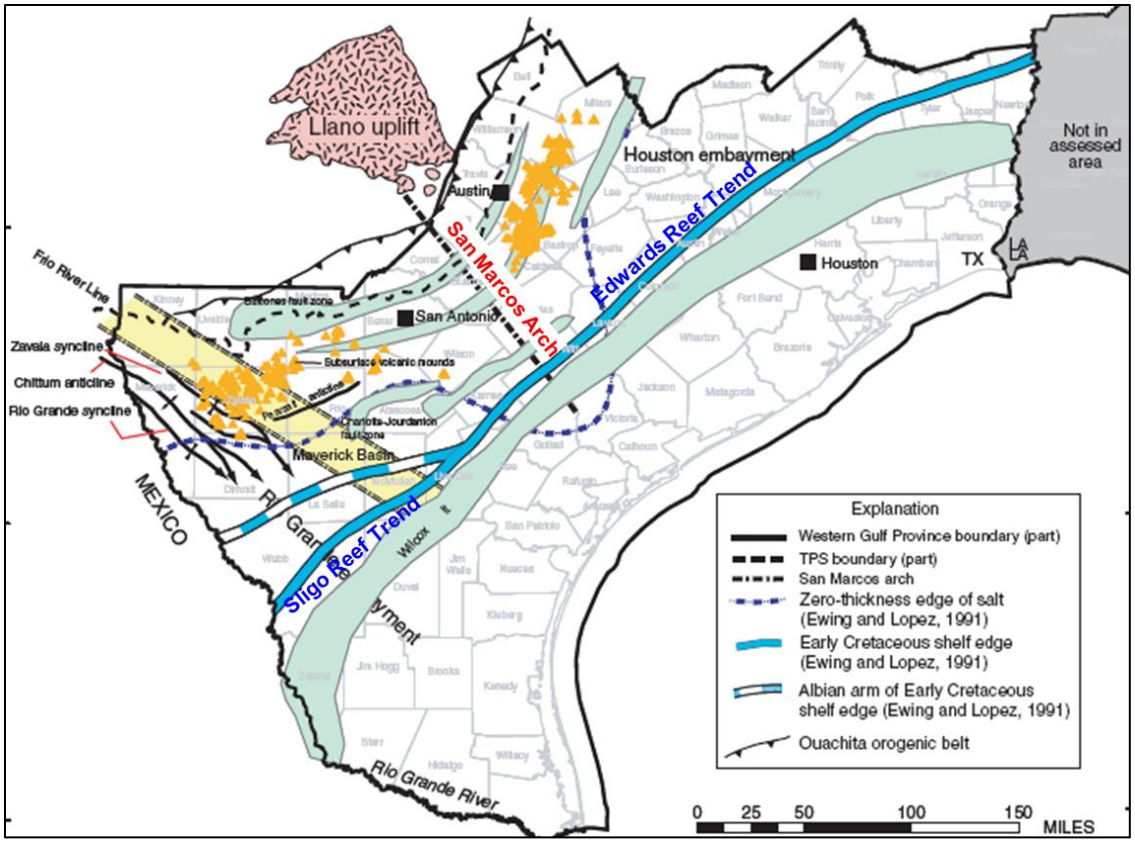

Fig. 8—Map of the western part of the Western Gulf Province showing main structural features. Modified from Condon and Dyman (2006).

The Rio Grande embayment lies southwest of the San Marcos Arch (Fig. 8) (Ewing 1991; Condon and Dyman 2006). The Edwards and Sligo Reef Trends are two prominent factors that influence the structure in the Rio Grande Embayment (Fig. 8). Most of the folds in the western part of the Maverick Basin are of Late Cretaceous to Tertiary age and are the result of Laramide compression (Ewing 1991; Condon and Dyman 2006). The main folds in the western part of the basin are the Rio Grande and Zavala synclines, separated by the southeastward-plunging Chittum anticline (Fig. 8) (Condon and Dyman 2006).

The Eagle Ford Group is of Late Cretaceous age **(Fig. 9)** (Hentz and Ruppel 2010, after Childs et al. 1988). In the Rio Grande Embayment, Eagle Ford Shale overlies the Buda formation and is overlain by the Austin Chalk. In the Houston Embayment and San Marcos Arch region, Eagle Ford Shale can be divided into Turonian Eagle Ford and Cenomanian Eagle Ford. The Cenomanian Eagle Ford unconformably overlies the Buda Limestone and is disconformably overlain by the Austin Chalk. In the East Texas Basin, only Turonian Eagle Ford is present, and it is overlain by the Austin Chalk (Fig. 9).

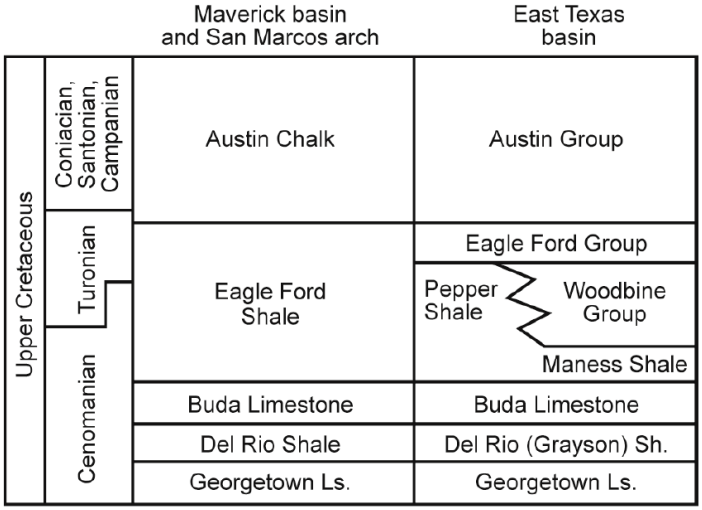

Fig. 9—Lithostratigraphy of the Eagle Ford Shale in Texas (Hentz and Ruppel 2010, after Childs et al. 1988).

From the well log responses, Eagle Ford Shale can be divided into Upper and Lower Eagle Shale. The Lower Eagle Ford Shale has high gamma ray response that indicates high shale content and a low-energy deposition environment (Liro et al. 1994; Dawson 2000; Condon and Dyman 2006). The Upper Eagle Ford Shale shows low gamma ray responses, indicating a relatively high carbonate composition and low shale content.

The total Eagle Ford Shale thins from >600 ft in the Maverick County depocenter to <50 ft to the northeast. The Lower Eagle Ford is present throughout the study area **(Fig. 10)** (Hentz and Ruppel 2010). The thickness of the Lower Eagle Ford Shale is >200 ft in western Maverick Basin depocenter (Fig. 10) (Hentz and Ruppel 2010). It thins northward to <50 ft at the updip limit of well control in Bexar County (Fig. 10) (Hentz and Ruppel 2010). The Upper Eagle Ford Shale is present in only the southwest region, and its thickness >425 ft in the Maverick County depocenter. From Frio County, the Upper Eagle Ford Shale thins northeastward and pinches out in Atascosa County **(Fig. 11)** (Hentz and Ruppel 2010).

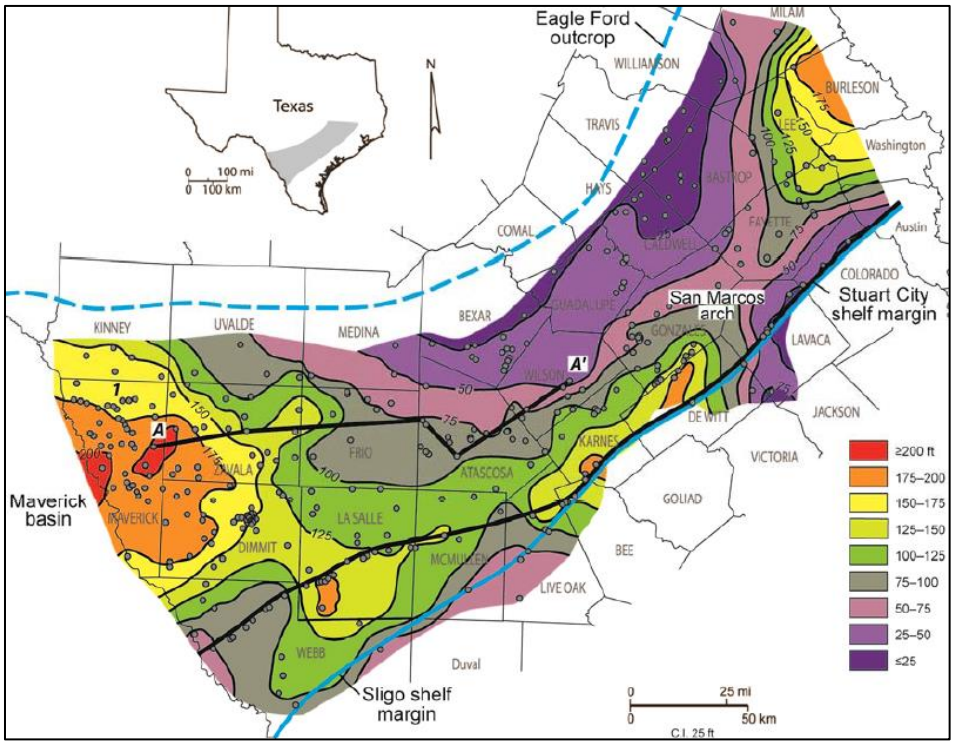

Fig. 10—Isopach map of the Lower Eagle Ford Shale (Hentz and Ruppel 2010).

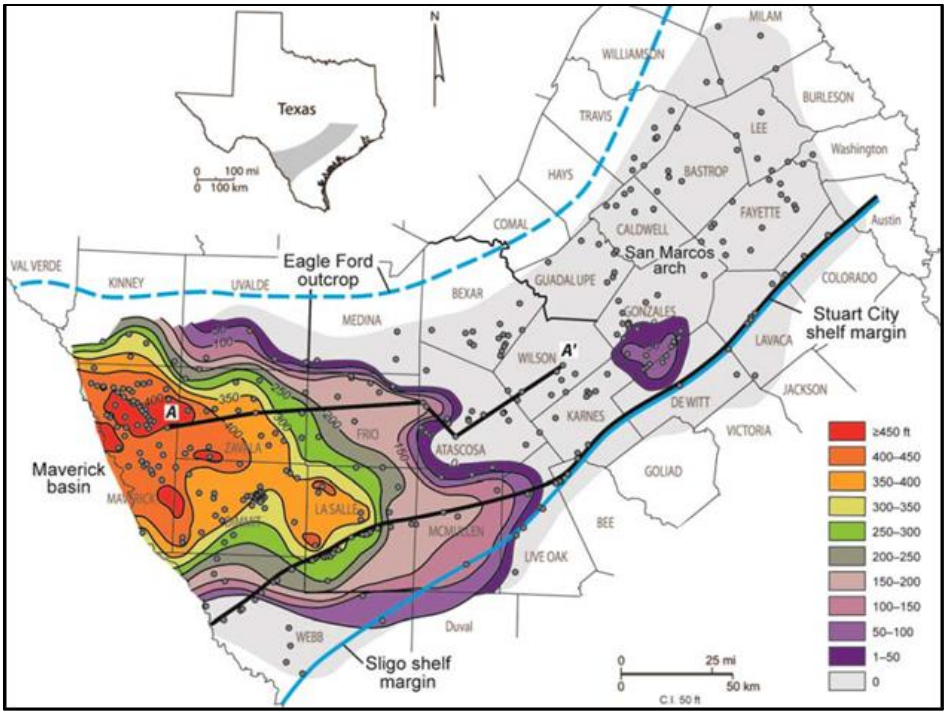

Fig. 11—Isopach map of the Upper Eagle Ford Shale (Hentz and Ruppel 2010).

RESERVOIR PROPERTIES

The Eagle Ford Shale varies significantly in reservoir properties, including thickness, mineral composition, and hydrocarbon type (Hentz and Ruppel 2010; Mullen 2010). Thermal maturity increases basinward, and the formation passes through the oil and condensate windows, and along the Edwards and Sligo Reef Trends, it is in the dry gas window (Lewan 2002).

Previous outcrop studies indicate three major lithologic units in the formation, including: (1) organic-rich, pyritic, and fossiliferous marine shales and bituminous claystone (in the lower part) that were deposited during a transgressive episode (Condon and Dyman 2006); (2) a condensed section of pyritic, phosphatic, and bentonitic shale beds (in the

middle part) (Condon and Dyman 2006); and (3) shales, limestones, and carbonaceous siltstones (in the upper part) that were laid down during a regressive highstand (Condon and Dyman 2006; Dawson 2000).

Total organic carbon content is typically 4 - 5% (Condon and Dyman 2006); kerogen composition is mixed Type 2 and Type 3 (Liro et al. 1994). Outcrop samples near Austin were reported to have average TOC contents of 5.15 weight percent in the lower Eagle Ford Shale (Dawson 2000). The Eagle Ford Shale is thermally immature at outcrop.

Eagle Ford porosity ranges from 5 to 10%; core derived permeability from samples from two wells was 1–2 microdarcies (mD) (Petrohawk 2009; TXCO 2009; Mullen 2011). In the production region, Eagle Ford Shale is predominately calcite rich (40 to 68%). Clay content averages 15%, quartz-plus-feldspar content is approximately 15%, and TOC averages 4% (Mullen et al. 2010; Mullen 2010; Quinine et al. 2013). In the downdip region, Eagle Ford formation temperatures range from 280 to 315°F, and the formation pressure gradient is 0.65 to 0.75 psi/ft (Petrohawk 2009; TXCO 2009).

PRODUCTION

Eagle Ford Shale produces oil, gas condensate, and dry gas **(Fig. 12).** There are 10 to 20 fracturing stages for both gas-rich and liquid-rich wells **(Table 1)** (Fan et al. 2010). The most productive gas wells are located in La Salle County, whereas the most productive oil wells are located in Karnes and Gonzales counties (Fan et al. 2011).

For horizontal wells, the total number of fracture stages ranges from 10 to 20 for both gas-rich and liquid-rich wells. There are also similarities are also in lateral horizontal length and cluster per stage (Table 1). However, compared to liquid-rich wells, stimulation of gas-rich wells requires more total fluid and less proppant. The average pump rate of gas-rich wells is as high as 70 bpm, whereas it is only 50 bpm for liquid-rich wells (Table 1) (Fan et al. 2011).

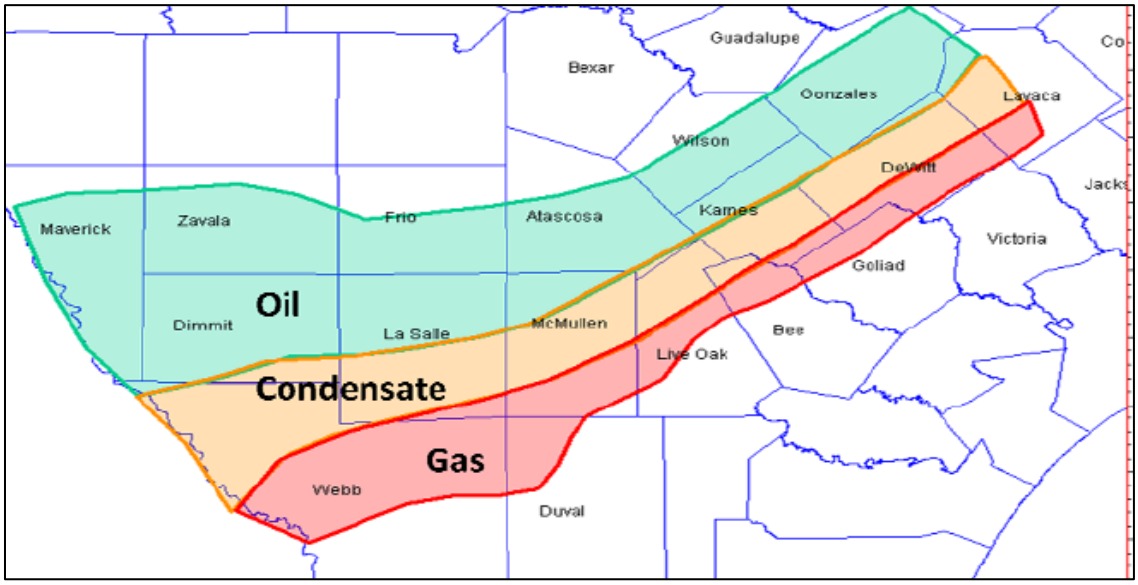

Fig. 12—Maturation window of Eagle Ford Shale hydrocarbon (Fan et al. 2011).

TABLE 1—TYPICAL COMPLETION FOR HORIZONTAL EAGLE FORD WELLS IN THE GAS AND LIQUID-RICH AREAS (FAN ET AL 2010)

	Eagle Ford Gas-Rich Area	Eagle Ford Liquid-Rich Area
Number of stages	10–20	10–20
Lateral length, ft	~4,500	~4,500
Number of clusters per stage	4–8	4–8
Stage length, ft	200–400	200–400
Distance b/w clusters, ft	30–80	30–80
Number of clusters	50–120	50–120
Fluid total, Mgal	6,112	4,032
Fluid per stage, Mgals	509	252
Fluid per cluster, Mgal	127	50
Fluid per ft, Mgal	1.4	0.8
Proppant total, Mlbs	3,432	5,120
Proppant per stage, Mlbs	246	320
Prop per cluster, Mlbs	61	64
Prop per ft, Mlbs	0.7	1
Max prop conc, ppa	1.5	4
Average pump rate, bpm	70	51
Average pump rate per cluster, bpm	17.5	10
Pump rate per perf, bpm	1.5–2.5	1.28

Stimulation design has evolved with the maturation of Eagle Shale play development. In 2009, 96% of the stimulation operations by Petrohawk were slickwater, which used linear gels or other friction reducers in the water treatment (Rushing et al. 2003), pumped at 12 stages per well (Rhein et al. 2011). The completion strategy evolved to hybrid fracture treatment with 16 stimulation stages, which captures the advantages of both conventional gel and water-frac treatments. Hybrid treatment provides only a modest improvement in production but a significant reduction of water consumption. In 2010, channel-fracturing technology was introduced in the Eagle Ford Shale, which significantly improved the completion efficiency. Channel fracturing is the hydraulic fracture technique that applies intermittent pumping of proppant laden and proppant-free

gelled fluid at high frequency, generating a heterogenious placement of proppant and open channels throughout proppant pack (Gillard et al 2010; Rhein et al. 2011). Channel fracturing improved the cumulative production and reduced the required amount of fracturing fluid and proppant (Rhein et al. 2011)

STATEMENT OF THE PROBLEM, OBJECTIVES, AND METHODS

To optimally develop the Eagle Ford Shale, several questions must be answered. Can we predict regional extents of fluid compositions and gas condensate? Can we use reservoir modeling to optimize oil production? Can the Eagle Ford Shale be subdivided into mappable stratigraphic units that are pertinent to reservoir fluid composition and engineering decisions? Successful exploration and development of the Eagle Ford Shale Play requires reservoir characterization, recognition of fluid regions, and application of optimal operational practices in all regions.

Objectives of this study were to, (1) assess the regional variations of the Eagle Ford Shale and its geologic properties, (2) to evaluate the controls that these properties exercise on Eagle Ford Shale well performance, (3) to optimize Eagle Ford well deliverability by identifying the most favorable production areas and operational parameters.

We began work on this project by identifying the Eagle Ford Shale units and building the stratigraphic model using well logs. The stratigraphic and petrophysical evaluations

of the Eagle Ford Shale provided the framework by which to assess vertical and lateral variability of reservoir and rock mechanical properties. We identified mappable stratigraphic units in regional cross sections, correlated those units throughout the study area, made the isopach maps, and evaluated key petrophysical parameters, such as mineralogy, TOC, and cyclicity of the Lower Eagle Ford. Other key reservoir parameters were also analyzed and mapped, including reservoir pressure gradient and fluid types.

Spatial statistics were used to quantitatively identify the key parameters affecting Eagle Ford production. Because of the various sources of data, there were no wells that had both production and reservoir properties. Conventional kriging and Markov Chain Monte Carlo (MCMC) were used to predict reservoir properties at Eagle Ford production well locations. Spatial linear regression was conducted to identify the relative significance among various reservoir properties to Eagle Ford Shale production.

With the framework provided by the stratigraphic and petrophysical analyses, we built reservoir models in various fluid regions and performed history matching based on available production data. Significant uncertainty was identified by obtaining multiple combinations of parameters that would result in a good history match. Well deliverability was modeled to optimize the oil production rate by designing appropriate operational parameters.

CHAPTER II

REGIONAL PRODUCTION TRENDS AND FLUID PROPERTIES*

REGIONAL PRODUCTION ANALYSIS

Eagle Ford Shale produces both oil and gas. Peak monthly well production is variable for all fluids. The production region is narrow in the northeastern area and widens to the southwest. The most productive gas wells are located south of the Stuart City Shelf Margin, where production commonly exceeds 80 MMcf/month/well (MMcf/M/W) (**Fig. 13**). Peak oil production is greatest in Karnes and Gonzales counties, where production exceeds 16,000 bbl/month/well (bbl/M/W) (**Fig. 14**).

FLUID IDENTIFICATION

The hydrocarbon types of Eagle Ford Shale were identified by average GOR from the first three months of production. Fluid types evolve basinward from black oil to volatile oil, gas condensate, and finally, to dry gas (**Fig. 15**), correlating with increasing formation depth (Fig. 7) and thermal maturity. The production and fluid type regions are wide in southwest and narrow on the northeast (Fig. 15), as a result of steeper structural dip with proximity to the San Marcos Arch (Fig. 7). Dry gas wells are mainly located south of the Stuart City Shelf Margin (Fig. 15).

---

*Part of this chapter is reprinted with permission from Tian, Y., Ayers, W.B., and McCain, W.D. Jr. 2012. The Eagle Ford Shale Play, South Texas: Regional Variations in Fluid Types, Hydrocarbon Production and Reservoir Properties. Paper presented for International Petroleum Technology Conference, Beijing, China, 26-28 March. Copyright [2013] by Society of Petroleum Engineers.

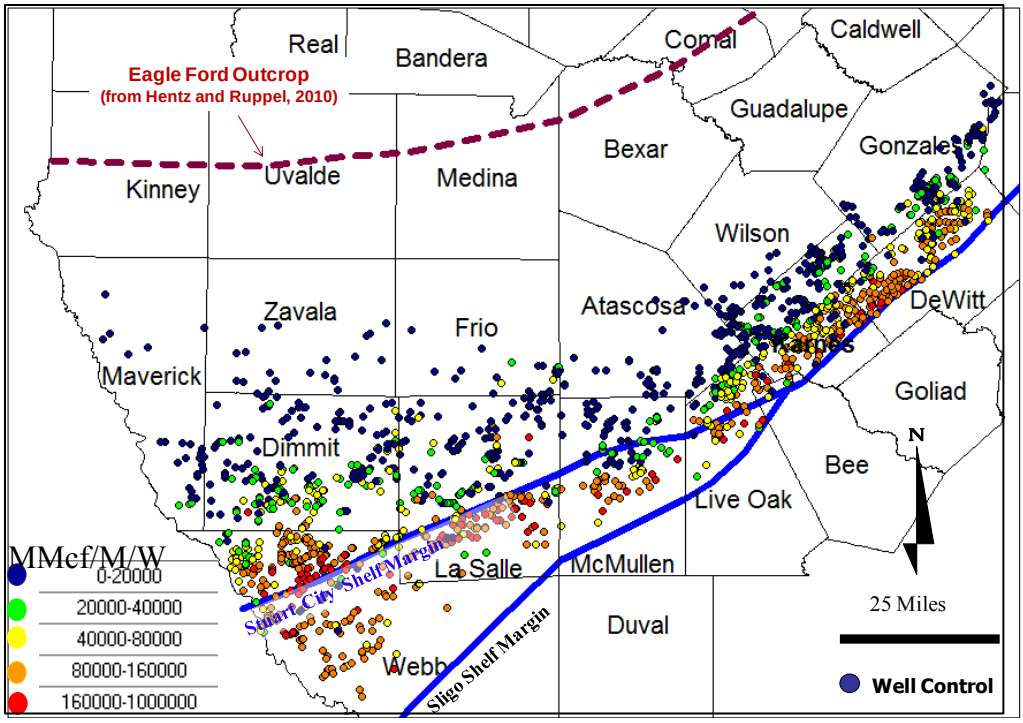

Fig. 13—Eagle Ford Shale peak monthly gas production. Data from Drillinginfo (2013).

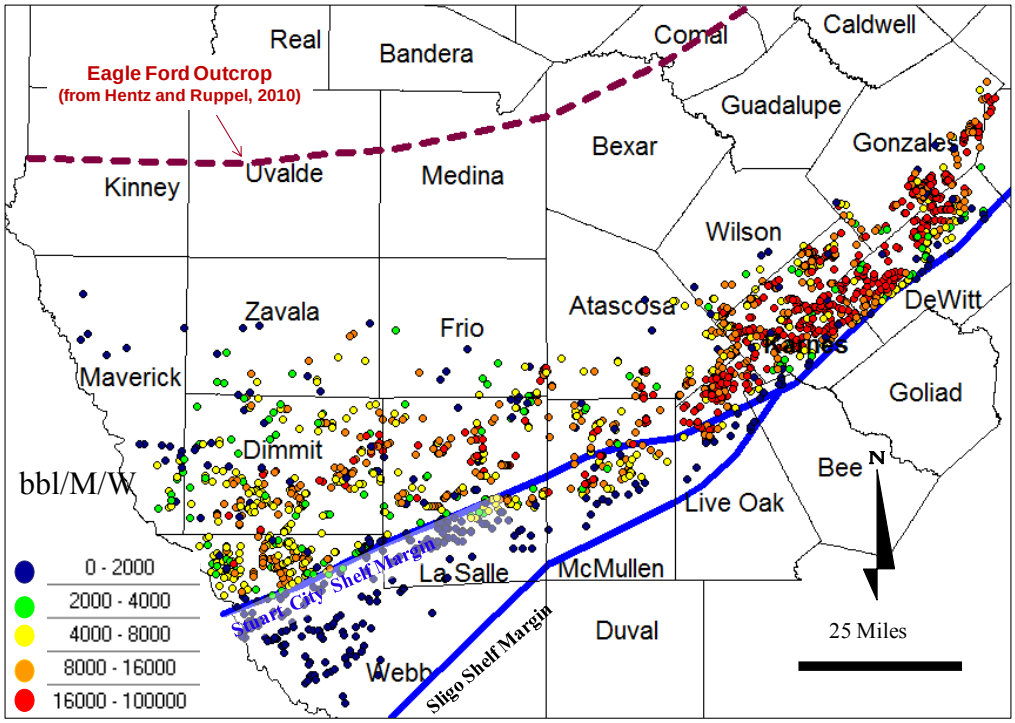

Fig. 14—Eagle Ford Shale peak monthly oil production. Data from Drillinginfo (2013).

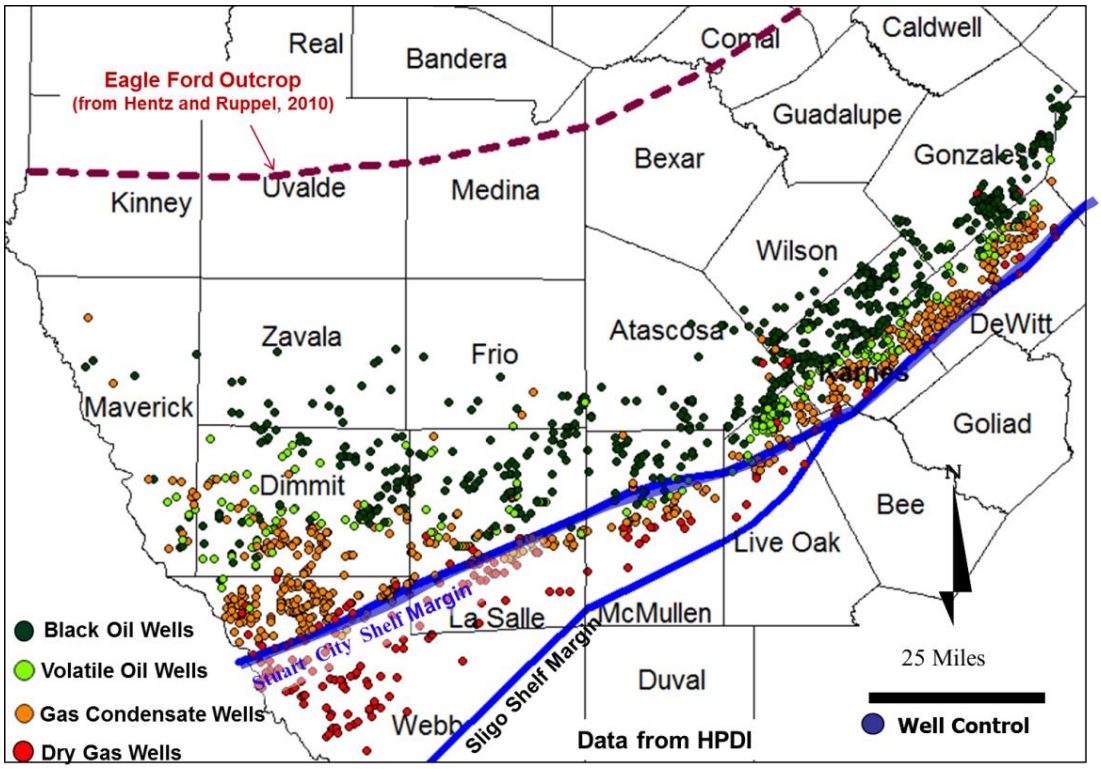

Fig. 15—Fluid types of Eagle Ford Shale identified by the average GOR from first three months. Data from Drillinginfo (2013).

Heptane-plus content can also be used to identify fluid types (**Table 2**) (McCain 1990). With the data extracted from PVT reports, we mapped the heptane plus composition of Eagle Ford Shale fluids (**Fig. 16**). The cutoff value to distinguish the volatile oil from the gas condensate region was 12.9 mole percent. The boundary identified by average GOR of the first three months is very close to 12.9% contour in north Live Oak County and central Karnes County, demonstrating consistent results from the two methods.

Table 2 Determination of Reservoir Fluid Type by Heptane Plus (McCain 1990)	
Reservoir Fluid	Composition of Heptane Plus in Initial Reservoir Fluid, mole percent
Dry Gas	$Z_{C7+}<0.5$
Wet Gas	$<0.5<Z_{C7+}<4.0$
Gas Condensate	$4<Z_{C7+}<12.9$
Volatile Oil	$12.9<Z_{C7+}<18$
Oil, type indeterminate by heptane plus	$18<Z_{C7+}<26.5$
Black Oil	$26.5<Z_{C7+}$

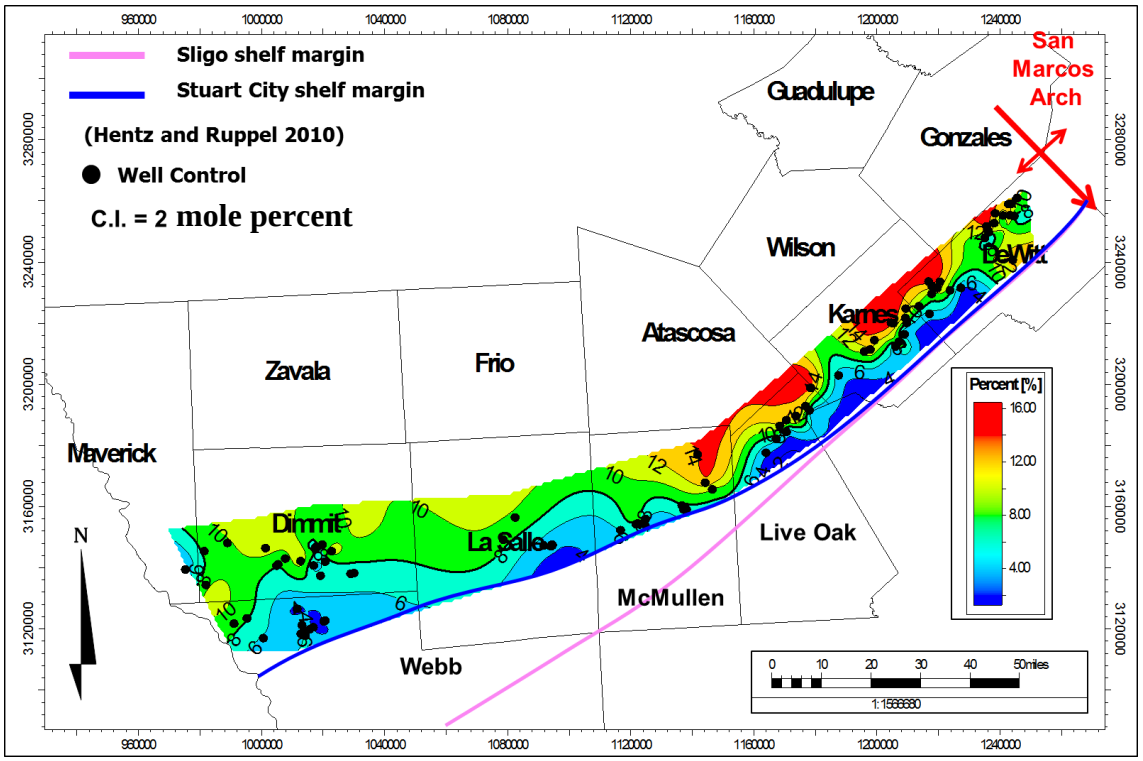

Fig. 16—Heptane-plus content map for Eagle Ford wells. Data from TRC (2013).

After identifying the fluid types and regions, we plotted the GOR vs. time for each fluid type. GOR of black oil wells generally increases in the first 3 months and plateaus afterwards at GORs ranging from 300 to 2,000 scf/bbl (standard cubic feet per barrel)

(**Fig. 17a**). The GOR of volatile oil wells remains constant at GOR between 1,000 to 10,000 scf/bbl (**Fig. 17b**). The GOR of gas condensate wells is generally constant since initial production, and it ranges from 4,000 to 20,000 scf/bbl (**Fig. 17c**).

An average GOR plot was calculated using total gas production divided total oil production (Eq.1) The average GOR of black oil increases during the first 3 months from approximately 700 to 1000 scf/bbl (Fig. 17a). The initial average GOR of volatile oil wells was 2,000 scf/bbl; average GOR of volatile oil wells increases to approximately 3000 scf/bbl during the first 5 months and remains nearly constant afterwards (Fig. 17b). The average GOR of gas condensate wells increased steadily from initial production values of less than 10,000 to more than 18,000 scf/bbl, after 36 months of production (Fig. 17c).

$$GOR_{ave,month} = \frac{\sum_1^n Q_{q,i}}{\sum_1^n Q_{o,i}} \quad \text{..... (Eq.1)}$$

OIL GRAVITY AND GAS SPECIFIC GRAVITY

Oil gravity and gas specific gravity are input parameters to reservoir models and are used in reserves estimations (McCain, 1990; Gong et al. 2013, Yu et al. 2013). However, these parameters may be mapped regionally, to better understand reservoir fluids and well production. Oil gravity increases from less than 43 API updip to more than 60 API downdip in the Webb County **(Fig. 18**).

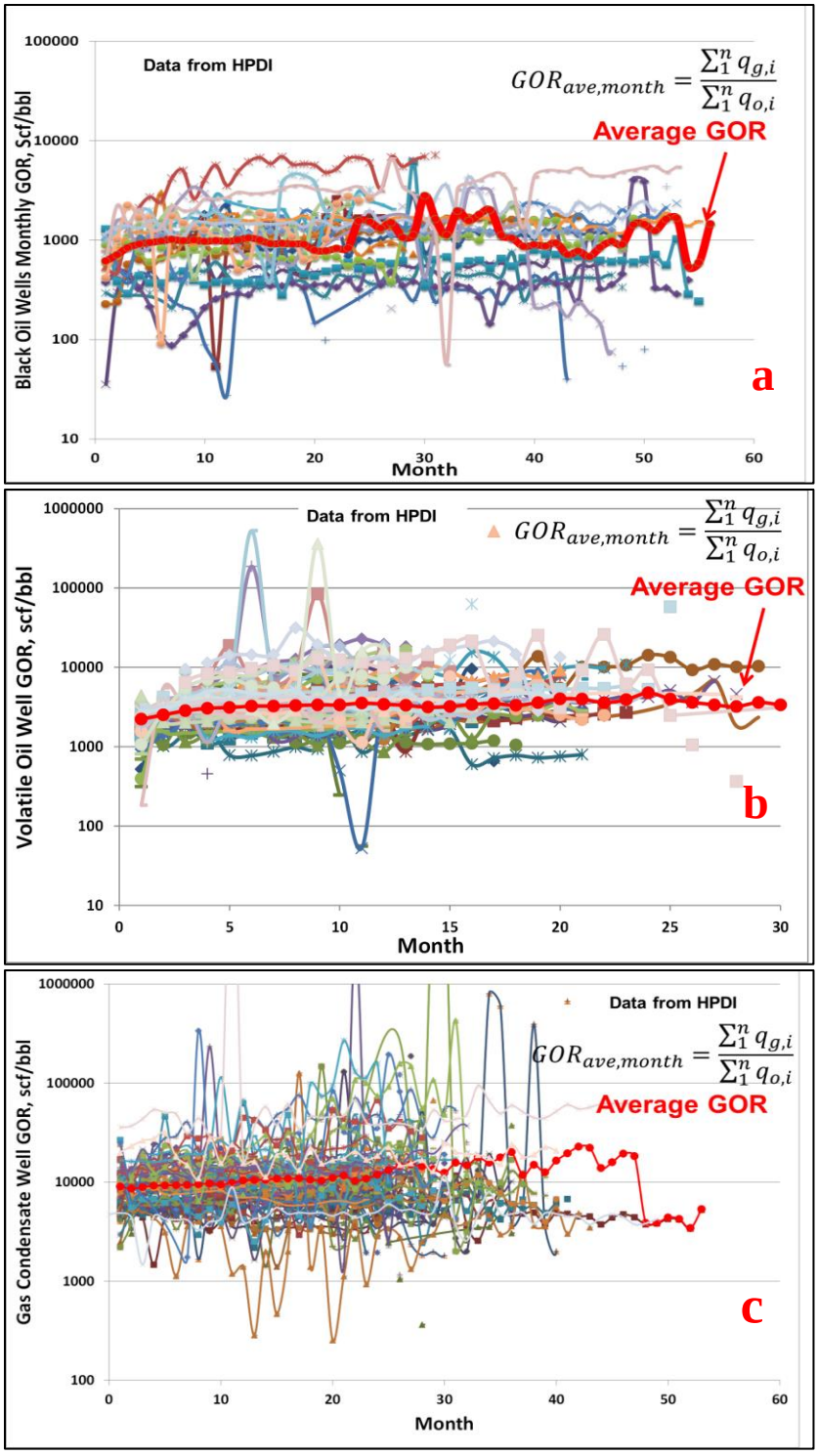

Fig. 17—GOR Profile for (a) black oil wells, (b) for volatile oil wells, and (c) gas condensate wells. The heavy red line in average GOR. Data retrieved from HPDI (2012).

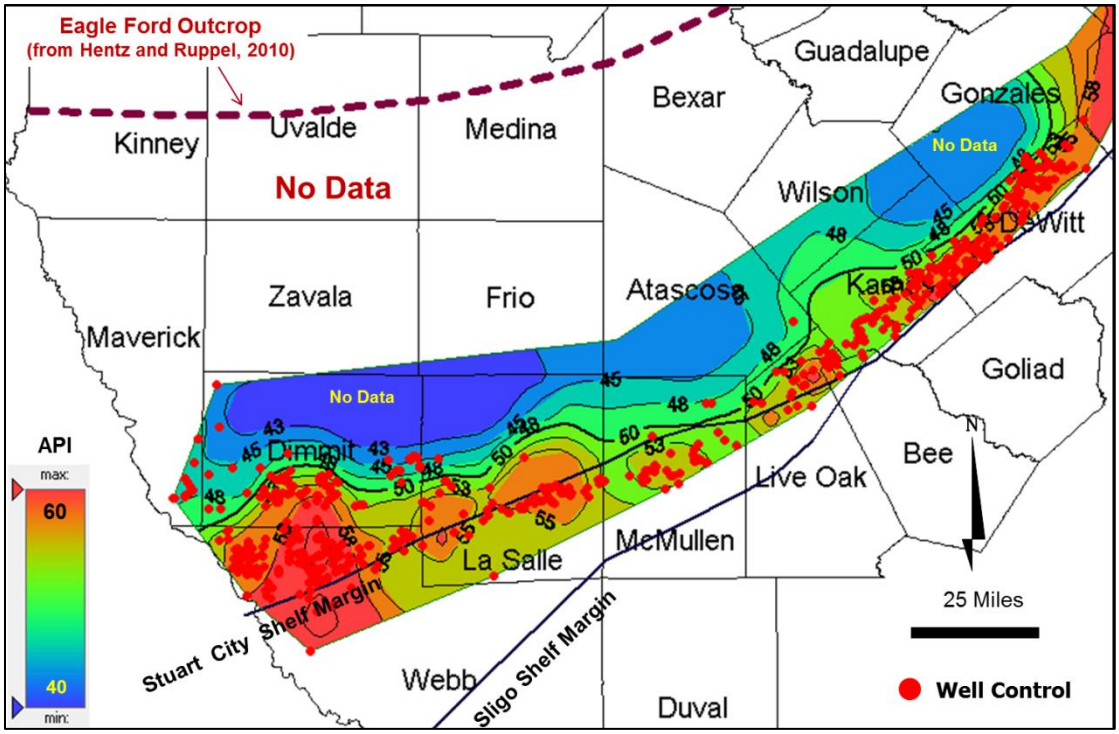

Fig. 18—Oil API gravity increases from northwest to southeast. Data from Drillinginfo (2013).

The gas specific gravity increases from approximately 0.6 in the south to more than 0.85 in the north (**Fig. 19**). Oil gravity and gas specific gravity maps demonstrate the increasing thermal maturity from northwest to southeast with increasing depth (Fig. 7, 18 and 19).The fact that the gas specific gravity in northern Webb County is as low as 0.6 suggest high composition of light hydrocarbon molecules. That is consistent with the dry gas fluid identified in previous work (Fig. 15) (Tian et al. 2012).

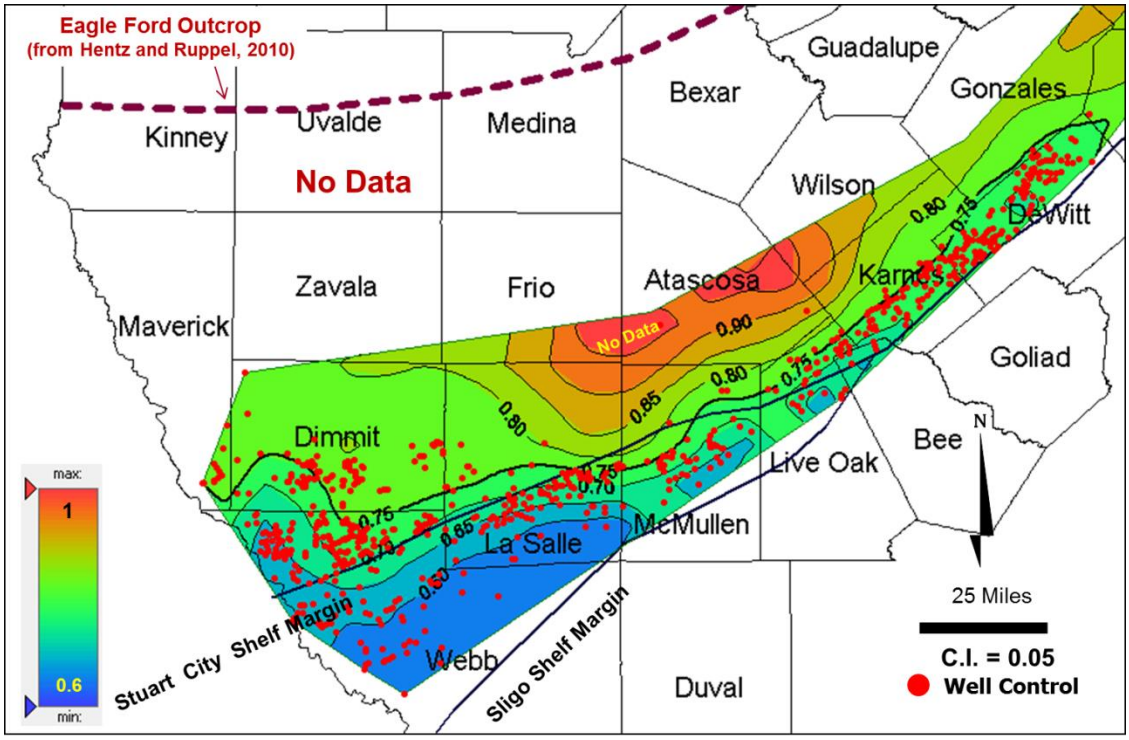

Fig. 19—Gas specific gravity increases from southeast to northwest. Data from Drillinginfo (2013).

RESERVOIR PRESSURE AND PRESSURE GRADIENT

Reservoir fluid pressure plays an important role in recovery of hydrocarbons from the Eagle Ford shale (Wan et al. 2013). To analyze the regional variation of reservoir fluid pressure, we evaluated Eagle Ford Shale PVT Reports from the Texas Railroad Commission. There were 97 Eagle Ford reports containing hydrocarbon compositional analyses, and 23 reports containing both reservoir pressure and temperature. These limited data indicate that reservoir pressure increases from less than 6,000 psi at approximately 7,500-ft depth in southern Dimmit County to more than 10,000 psi at approximately 12,000-ft depth in Karnes and DeWitt Counties in the northeast (**Fig. 20**).

Integration of reservoir pressure (Fig. 20) with structural elevation shows no obvious and consistent correlation between these two parameters. From Well A in north Live Oak County to Well B in Dewitt County (Fig. 20), the subsurface elevation (and depth) remains relatively constant (Fig. 7), whereas the reservoir pressure increases markedly (Fig. 20). The available data suggest that the reservoir pressure gradient increases to the northeast, so we calculated and mapped the reservoir pressure gradient (pressure / vertical depth).

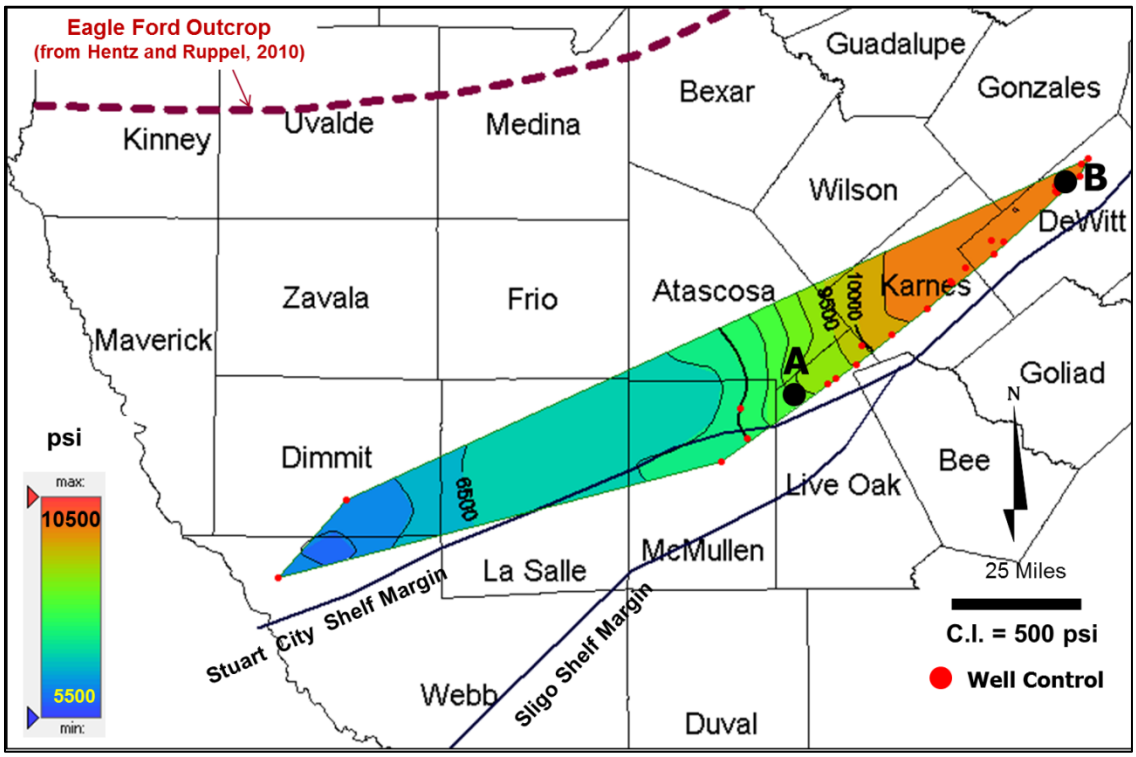

Fig. 20—Eagle Ford Shale reservoir pressure of from PVT analysis results. Data from TRC (2013).

Since there were no depth data for the wells for which we had PVT reports, another approach was used to calculate the reservoir pressure gradient. Well coordinates were

searched by well names retrieved from the PVT reports, and approximate reservoir depths were read at these well locations from the structural map (assuming that topographic variations across the region are relatively minor and insignificant to these calculations) (Fig. 7). Reservoir pressure gradients increase from less than 0.68 psi/ft. in the southeast to approximately 0.85 psi/ft in the northeastern region (**Fig. 21**).

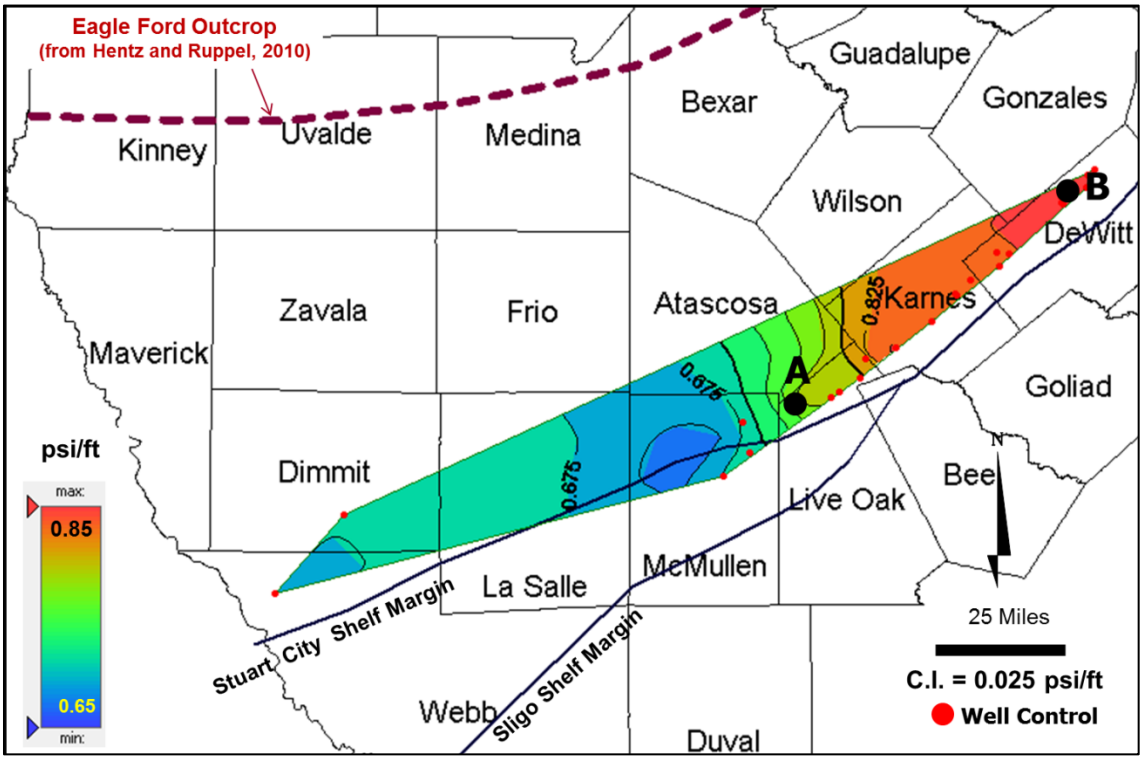

Fig. 21—Eagle Ford Shale pressure gradient. Data from TRC (2013).

STIMULATION PRACTICE IN EAGLE FORD SHALE

Well stimulation practices differ among operators concerning the number of hydraulic fracture stages (**Fig. 22**). Hundreds of completion permits were investigated to identify the most common number of fracture stages in Eagle Ford Shale. The majority of

ConocoPhillips wells were stimulated in 15 stages, whereas other companies, e.g., Marathon Oil Company, tested various numbers of stages (Fig. 22).

To investigate possible correlation between production and number of hydraulic fracture stages, crossplots were made between cumulative barrel of oil equivalent (BOE) with number of hydraulic fracture stages (**Figs. 23 through 26**). Among four operators, the production does not correlate well with number of hydraulic fracture stages. The production rates from wells with the same number of fracture stage are highly variable (Figs. 23 through 26).

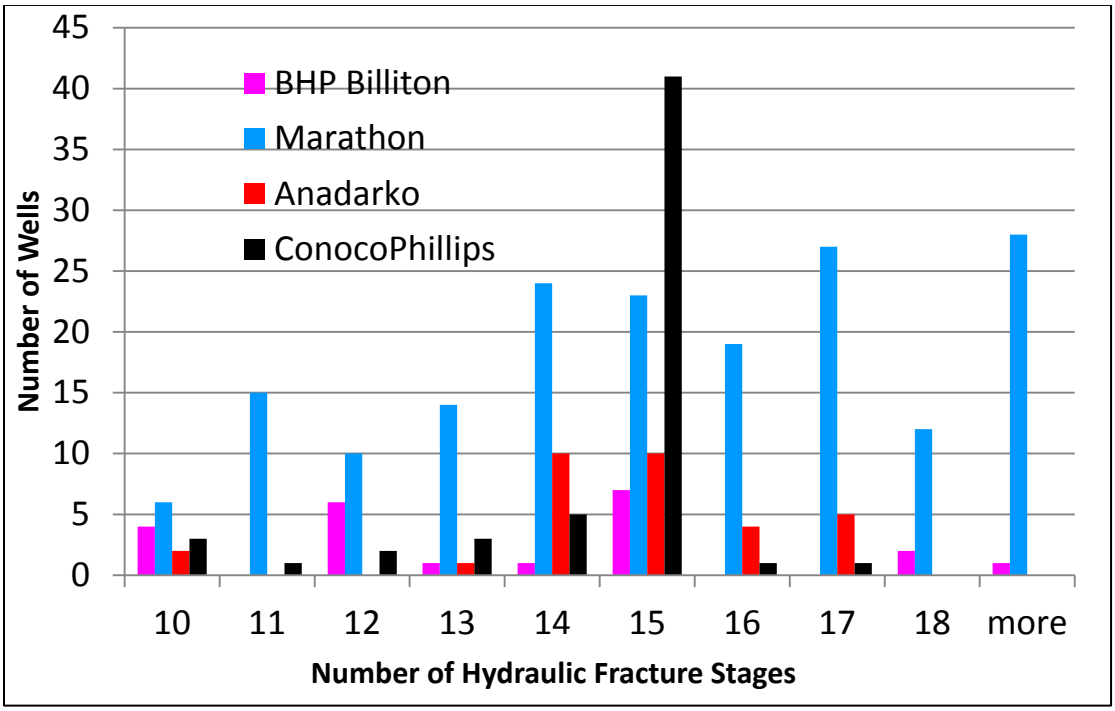

Fig. 22—Number of hydraulic fracture stages stimulated in Eagle Ford Wells, by operators. Data from Drilliginfo (2012).

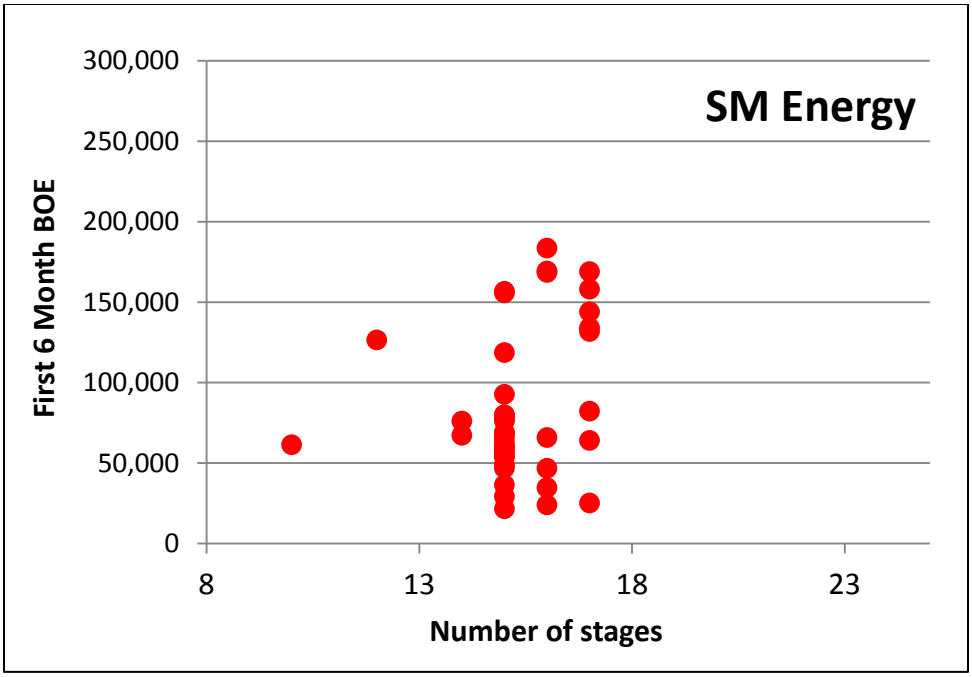

Fig. 23—Number of hydraulic fracture stages vs. first 6 month production of SM Energy wells. Data from Drillinginfo (2012).

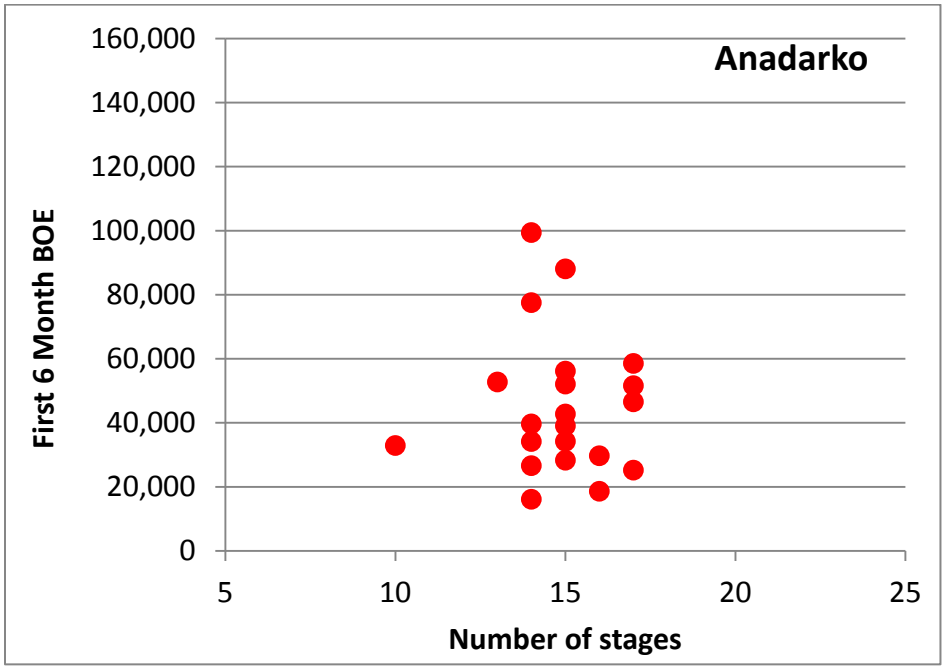

Fig. 24—Number of hydraulic fracture stages vs. first 6 months production of Anadarko wells. Data from Drillinginfo (2012).

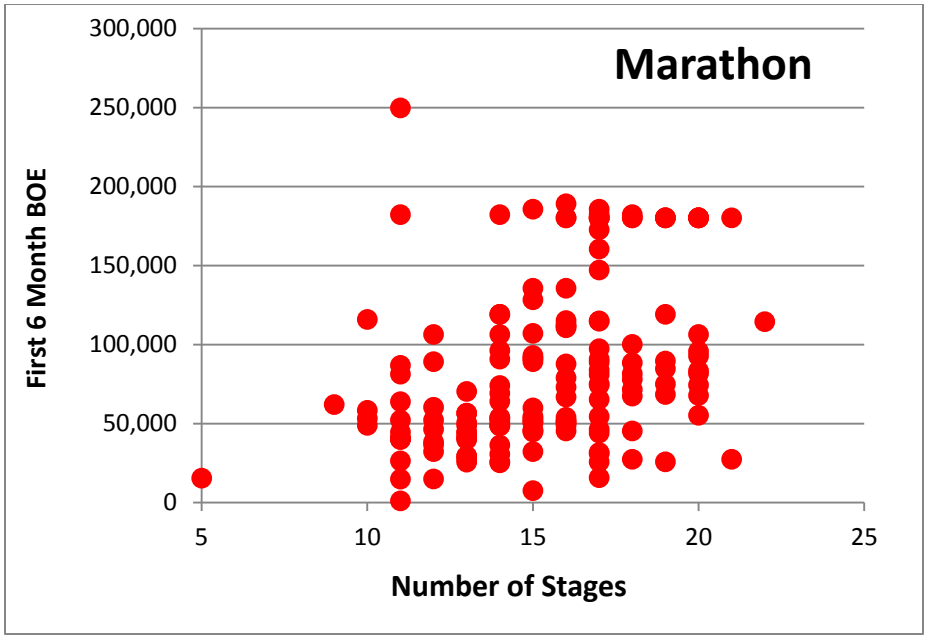

Fig. 25—Number of hydraulic fracture stages vs. first 6 month production of Marathon Oil Company wells. Data from Drillinginfo (2012).

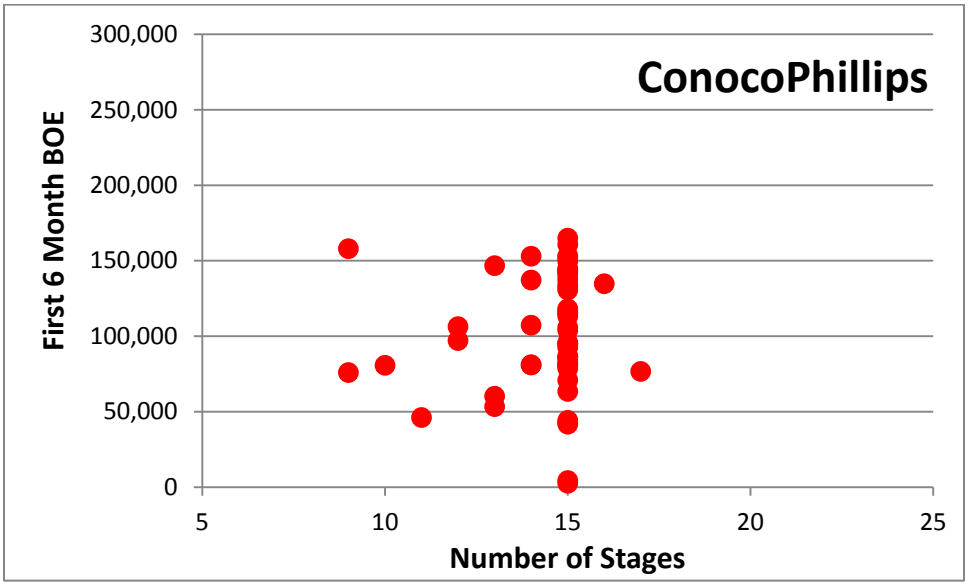

Fig. 26—Number of hydraulic fracture stages vs. first 6 month production of ConocoPhillips wells. Data from Drillinginfo (2012).

CHAPTER III

STRUCTURAL AND STRATIGRAPHIC ANALYSES*

To model well deliverability with reservoir models, we conducted stratigraphic and petrophysical evaluations of the Eagle Ford Shale. Stratigraphic analysis provided the framework to assess vertical and lateral variability of reservoir and rock mechanical properties, as well as fluid composition, much as has been done for the Barnett Shale (Tian and Ayers 2009; Tian and Ayers 2010).

METHODS

We used well logs to identify the mappable stratigraphic units in regional cross sections, correlate those units throughout the study area, make the isopach maps, and evaluate key petrophysical parameters. Approximately 600 depth-registered image and 500 digital well logs were used to analyze the structural and stratigraphic settings of the Eagle Ford Shale. From numerous regional cross sections, we analyzed stratigraphy and divided the Eagle Ford Shale into three units. Deeper formations, including Del Rio, Georgetown, and Edwards were also correlated to aid stratigraphic interpretation. We mapped structural tops of the Eagle Ford Shale and Buda Limestone, and we mapped total thicknesses of the Eagle Ford Shale and its subunits.

---

*Part of this chapter is reprinted with permission from Tian, Y., Ayers, W.B., and McCain, W.D. Jr. 2012. Regional Analysis of Stratigraphy, Reservoir Characteristics, and Fluid Phases in the Eagle Ford Shale, South Texas. Gulf Coast Association of Geological Societies Transactions, v.62, p. 471-483. Copyright [2012] by Gulf Coast Association of Geological Societies.

STRUCTURAL SETTING

From outcrop, the Eagle Ford Shale dips southeastward; its elevation is less than 14,000 ft SSL near Sligo Shelf margin (**Fig. 27**). The Chittim Anticline and associated synclines are major structural features in south Texas (Fig. 27). In the rest of the basin, the dip is gradual. Closely spaced contours near San Marcos Arch indicate steeper dip of the formation in that region (Fig. 27).

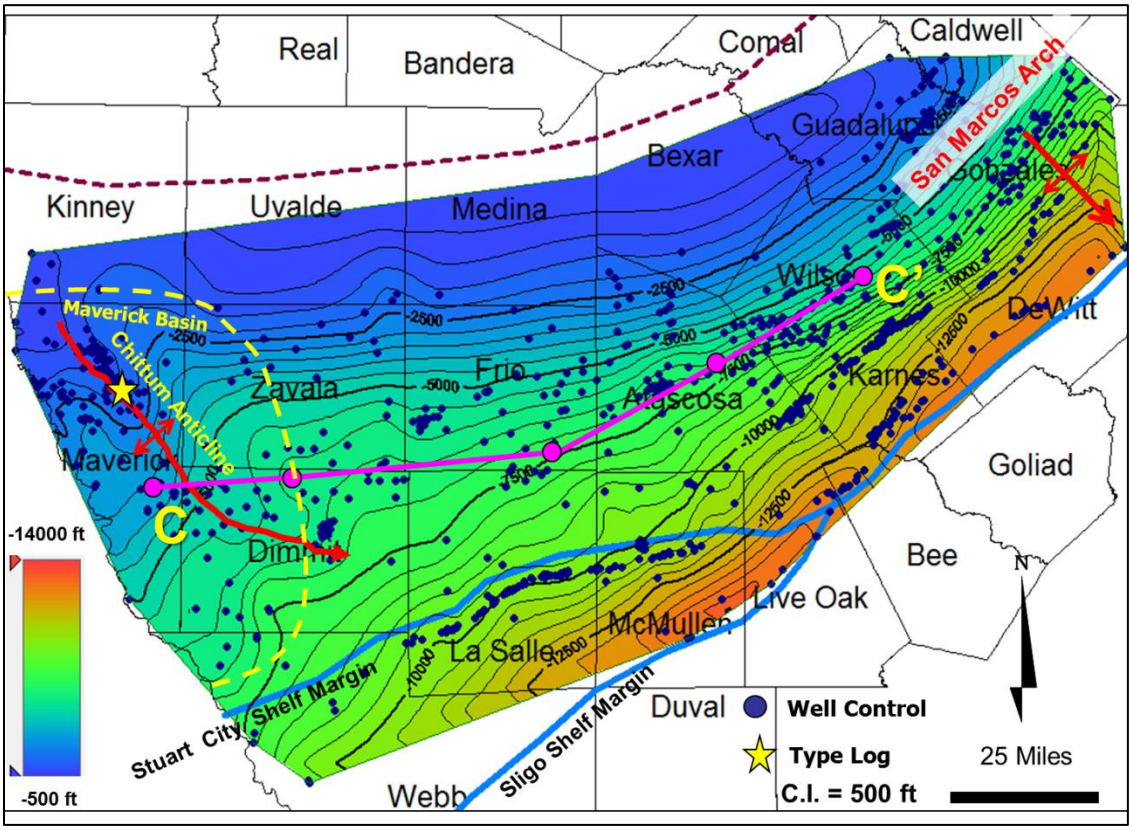

Fig. 27—Structure base of the Eagle Ford Shale.

The Eagle Ford Shale overlies Buda Limestone and is overlain by the Austin Chalk (**Fig**. 9 and**Fig**. 28). Eagle Ford Shale lithology varies vertically (Fig. 28). Hentz and Ruppel

(2010) divided Eagle Ford Shale into upper and lower units. We recognized those two units, and based on the subtle differences in gamma ray and resistivity log responses, we subdivided the Upper Eagle Ford Shale (UEF) into Lower-Upper (Lower UEF) and Upper-Upper Eagle Ford Shale (Upper UEF) units; thus, 3 units were established and mapped (Fig. 28)

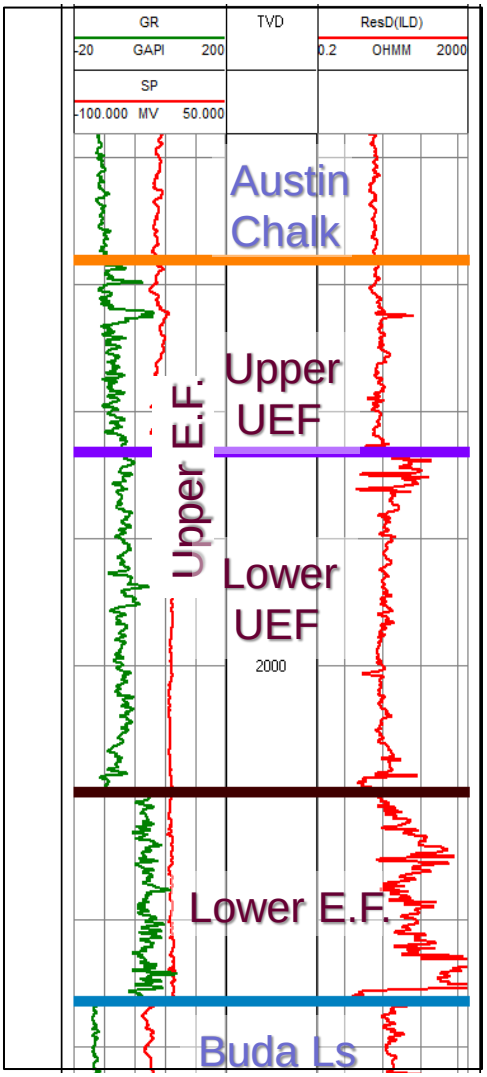

Fig. 28—Type log in Maverick County showing three units identified in the Eagle Ford Shale (The Exploration Company, Paloma E 1 53). See Fig. 27 for location.

Well log cross plots were used to differentiate among the Eagle Ford Shale units and Buda Limestone. In the neutron porosity vs. density cross plot, Buda Limestone (marly lime) plots closest to the limestone line **(Fig. 29**). Lower Eagle Ford and Lower UEF are shifted from the limestone curve toward lower right, suggesting greater shale content (Fig. 29). Upper UEF plots closer to the limestone line than do the Lower Eagle Ford Shale and Lower UEF, which suggests a higher percent of calcite in the Upper UEF.

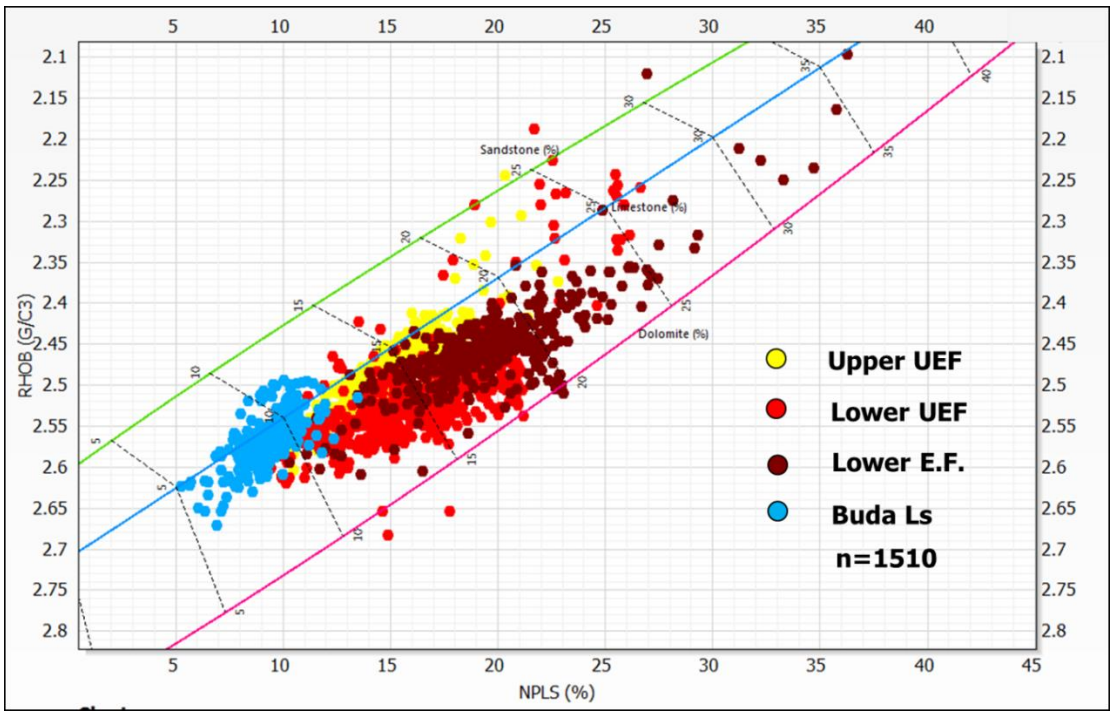

Fig. 29—Density vs. neutron porosity crossplot for Eagle Ford Shale units and Buda Limestone.

The cross plot of PEF vs. gamma ray clearly differentiates the Eagle Ford Shale units and the Buda Limestone (**Fig. 30**). Lower Eagle Ford Shale PEF ranges from 2.7 to 7.7 BE, which is slightly lower than PEF of the other units (3.1 to 5.2 in the Lower UEF and 4.2 to 5.6 in Upper UEF) (Fig. 30). The cross plot of deep resistivity vs. gamma ray

shows a wide range of deep resistivity in the Lower Eagle Ford Shale (10 to 8,000 OHM-M) (**Fig. 31**). Resistivity ranges from 1 to 100 OHM-M in the Lower UEF. The Upper UEF has the lowest resistivity (6 to 20 OHM-M) of all Eagle Ford Shale units (Fig. 31).

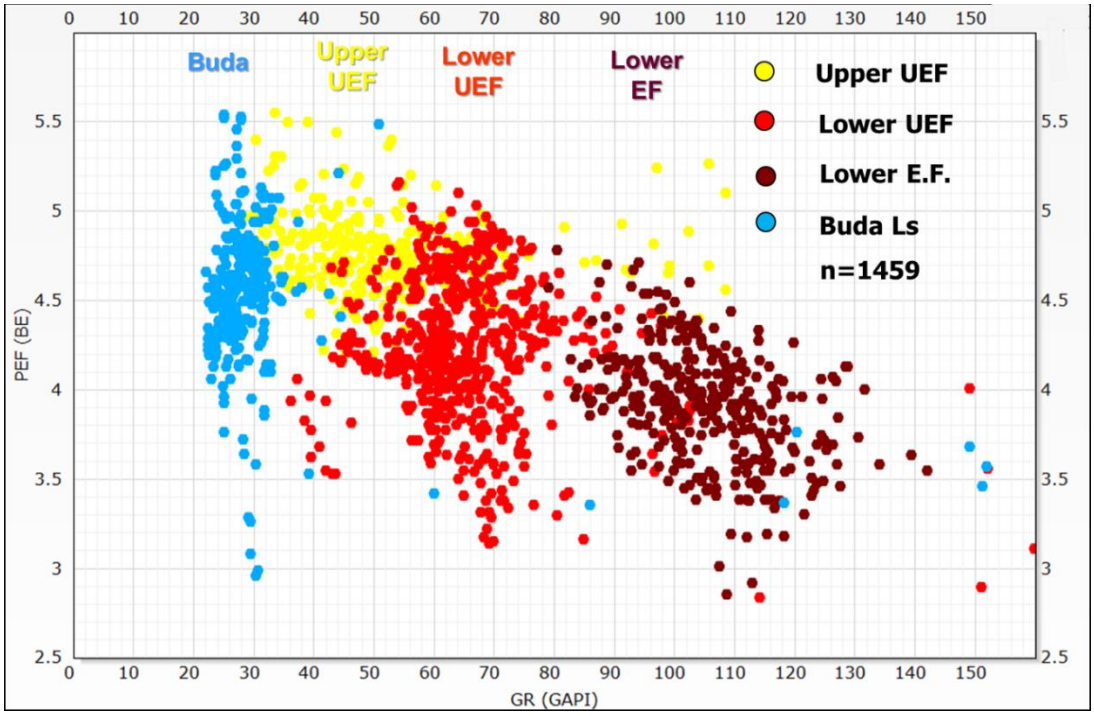

Fig. 30—PEF vs. gamma ray crossplot for Eagle Ford Shale units and Buda Limestone.

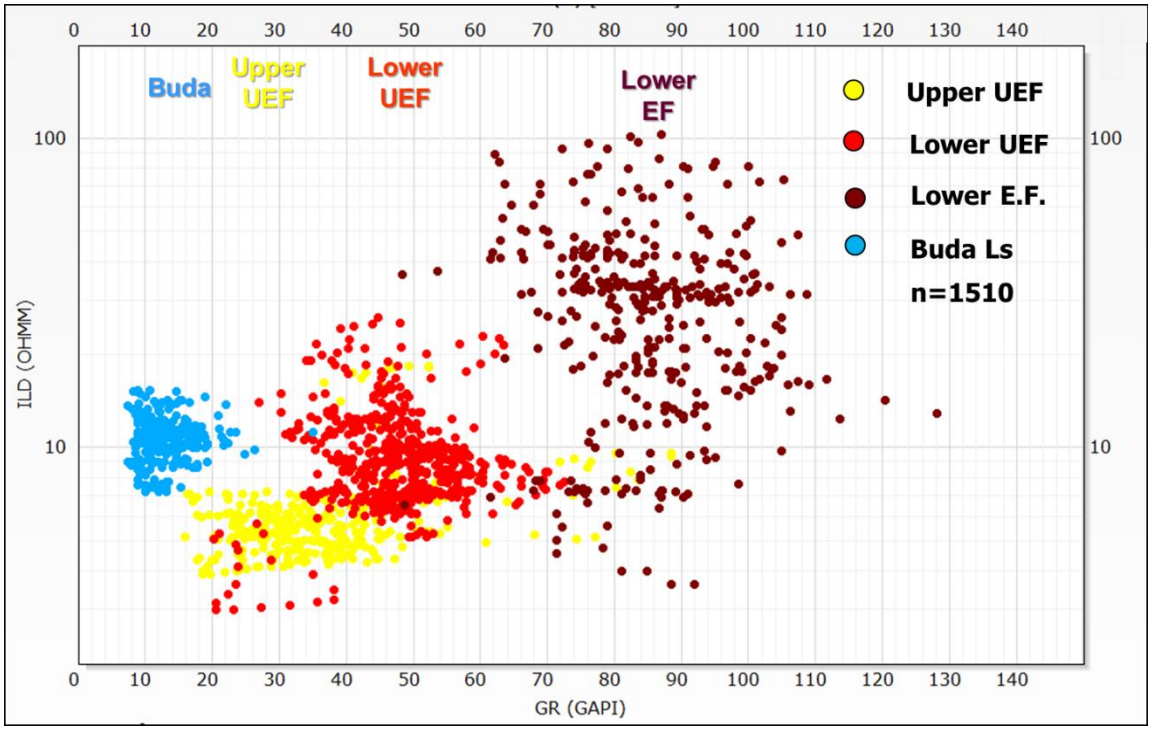

Fig. 31—Deep resistivity vs. gamma ray crossplot for Eagle Ford Shale units and Buda Limestone.

THICKNESSES OF EAGLE FORD SHALE UNITS

Thicknesses of Eagle Ford Shale units vary regionally. Cross sections were made in the dip and strike directions of the basin to study the regional variation of Eagle Ford thickness (**Fig. 32**). Total Eagle Ford shale become thinning from more than 600 ft in the Maverick County depocenter to less than 50 ft on the Northeast **(Fig. 33**).

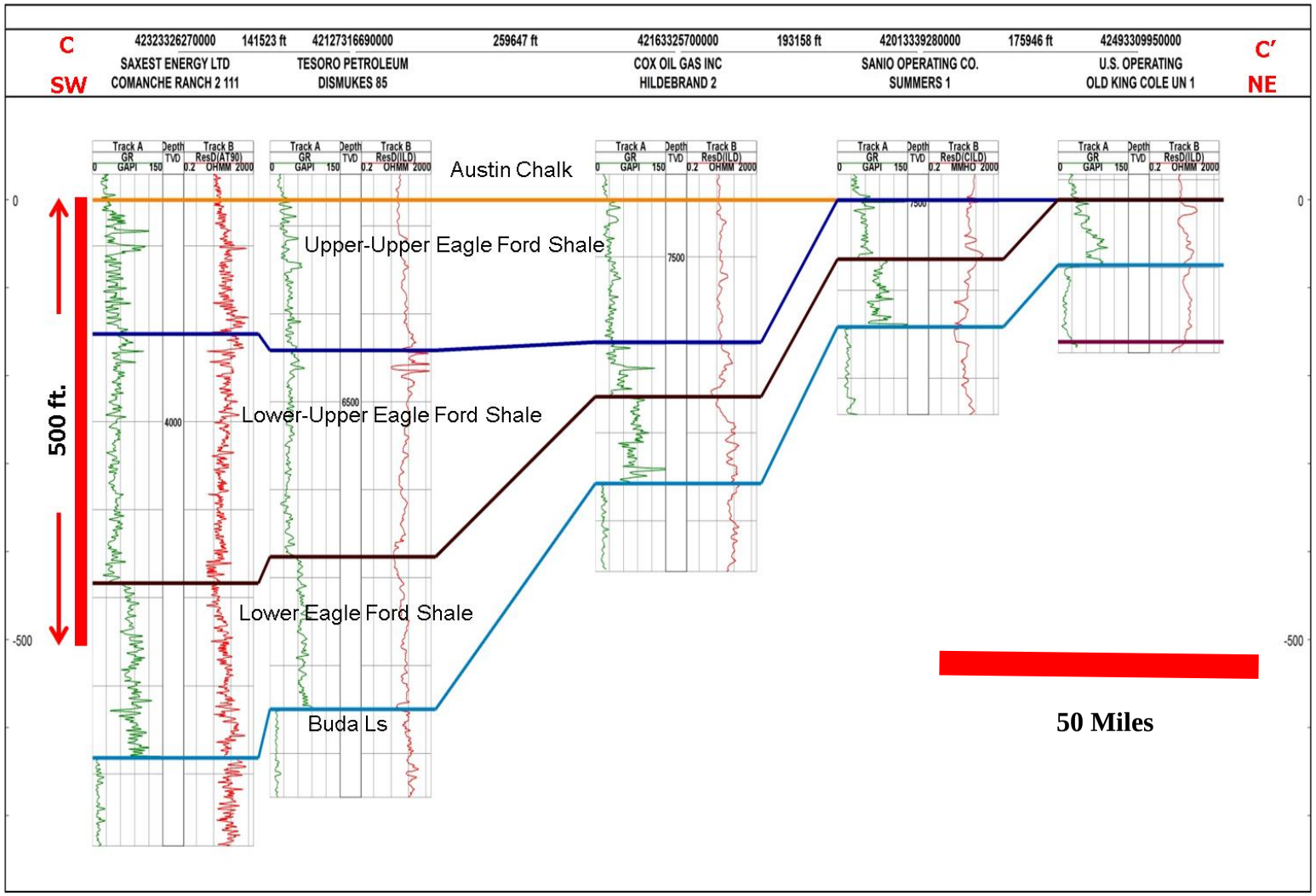

Fig. 32— Cross section of Eagle Ford Shale showing the three stratigraphic subdivisions. See Figure 27 for location.

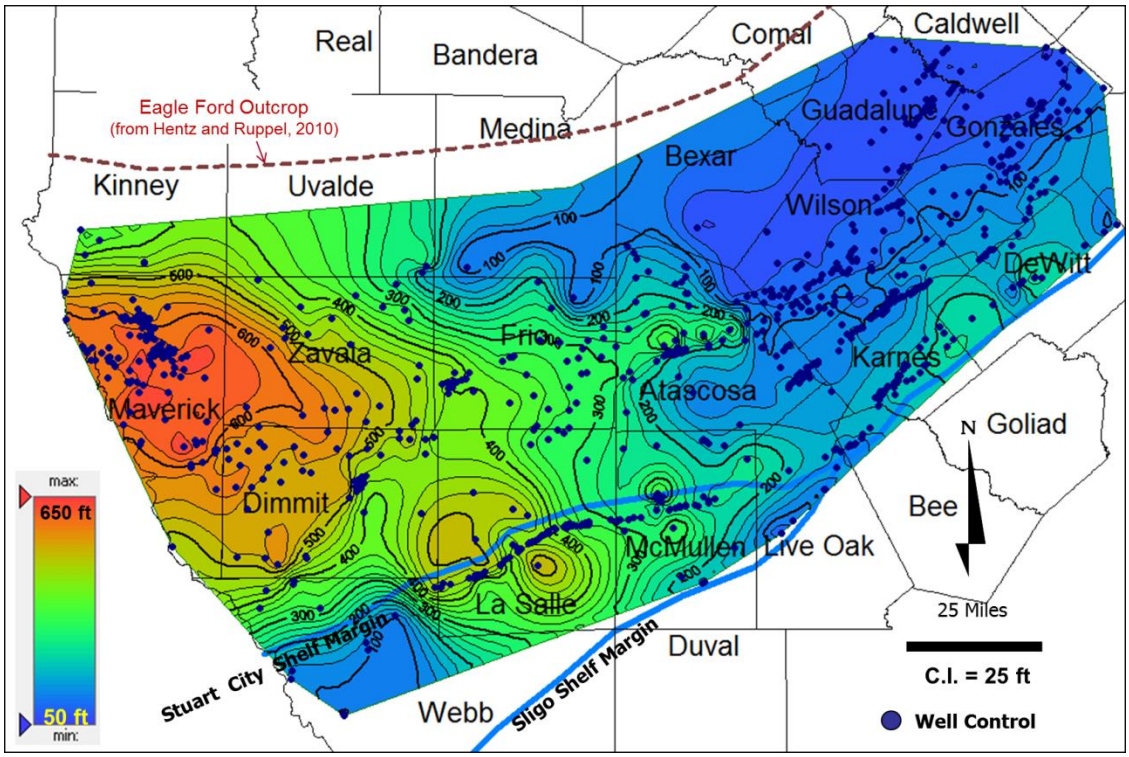

Fig. 33—Thickness of total Eagle Ford Shale.

The thickness of Lower Eagle Ford Shale exceeds 200 ft in the western Maverick Basin (**Fig. 34**) depocenter. It thins northeastward to less than 50 ft thick at the updip limit of well control in Bexar County (Fig. 34). Outside the Maverick Basin depo center, local buildups of thickness are present in both La Salle and Karnes Counties (Fig. 34), which are the most productive gas and oil regions (Fig. 13 andFig. 14).

The Upper Eagle Ford Shale is restricted to the Maverick Basin depocenter, where maximum thickness exceeds 425 ft (**Fig. 35)**. It thins and pinches out to the northeast (Fig. 35). The Eagle Shale depocenter shifted from Lower UEF to Upper UEF deposition (**Figs. 36 and 37**). In the Maverick Basin depocenter, the thickness of the Lower UEF

exceeds 275 ft (Fig. 36), and it extends further to the northeast than the Upper UEF (Figs. 36 and 37). The Upper UEF depocenter is in LaSalle County, where the unit exceeds 350 ft thick. The Upper UEF pinches out abruptly to the northeast (Fig. 37).

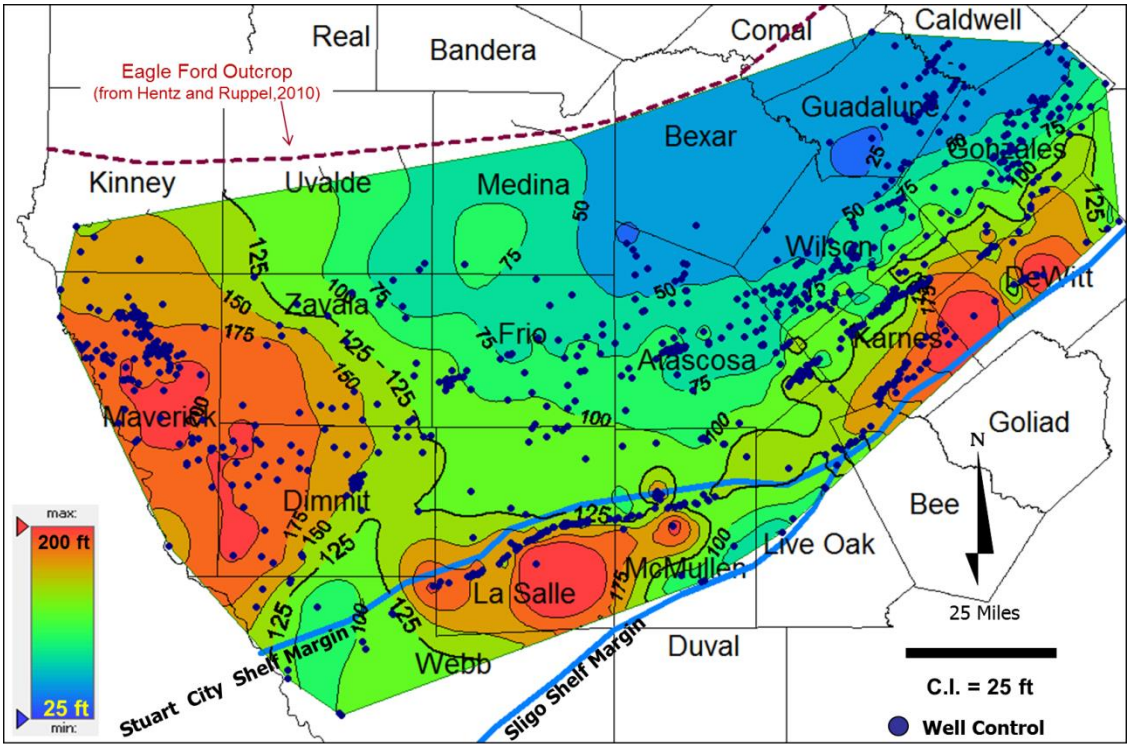

Fig. 34—Thickness of Lower Eagle Ford Shale.

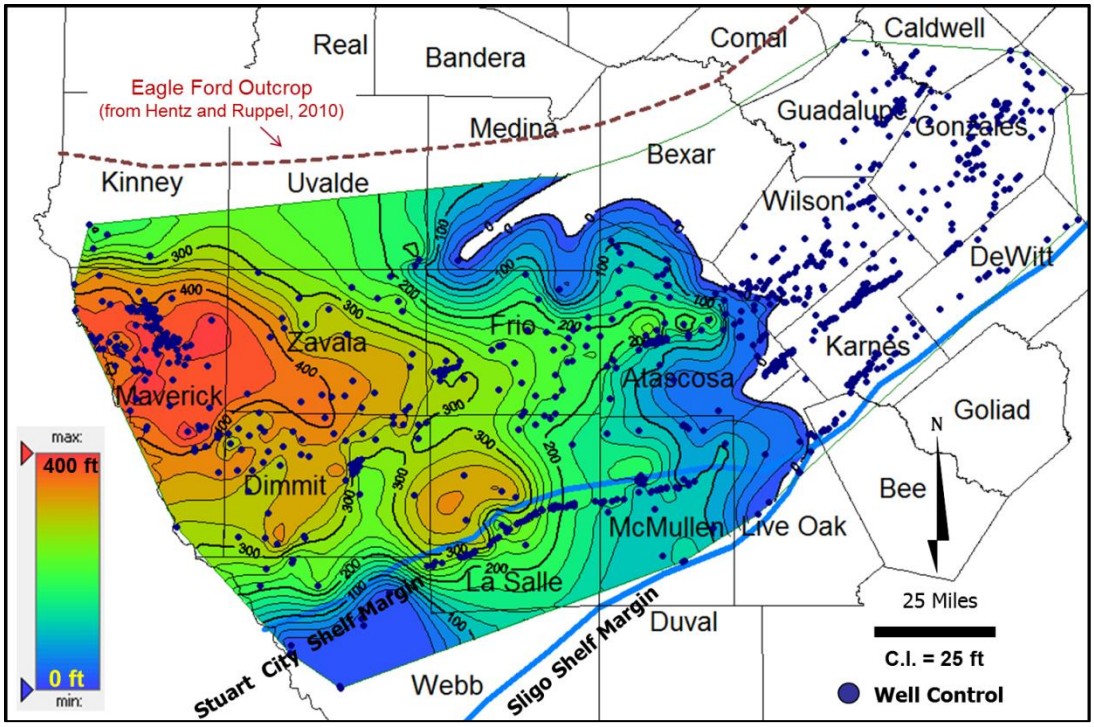

Fig. 35—Thickness of total Upper Eagle Ford Shale.

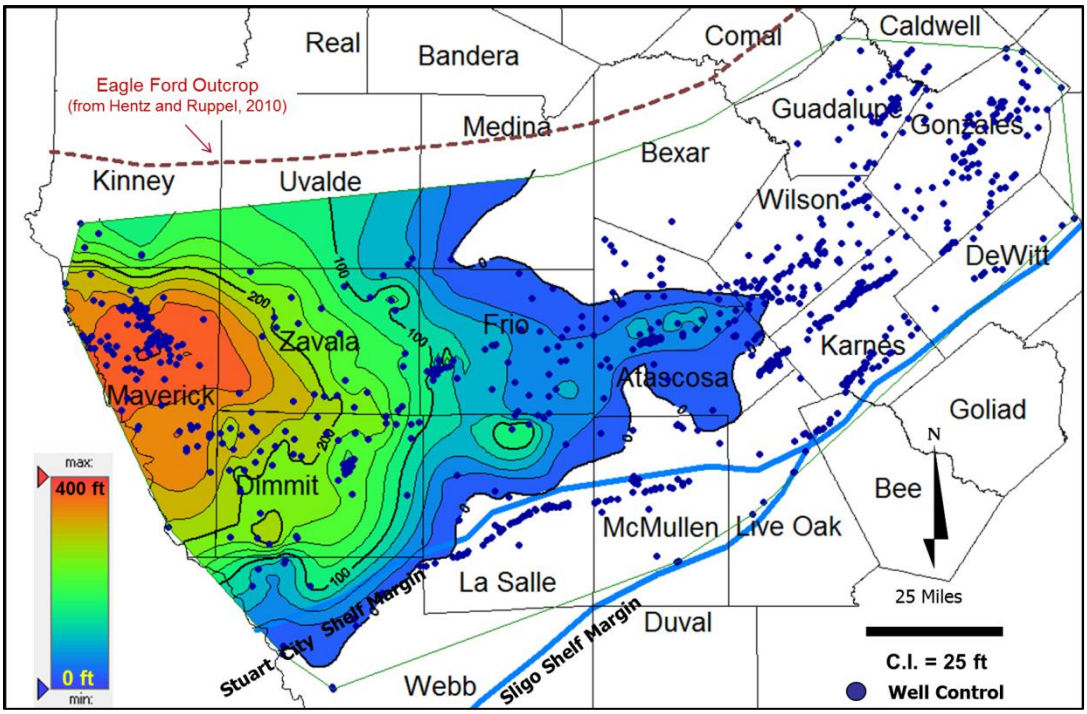

Fig. 36—Thickness of lower unit of Upper Eagle Ford Shale.

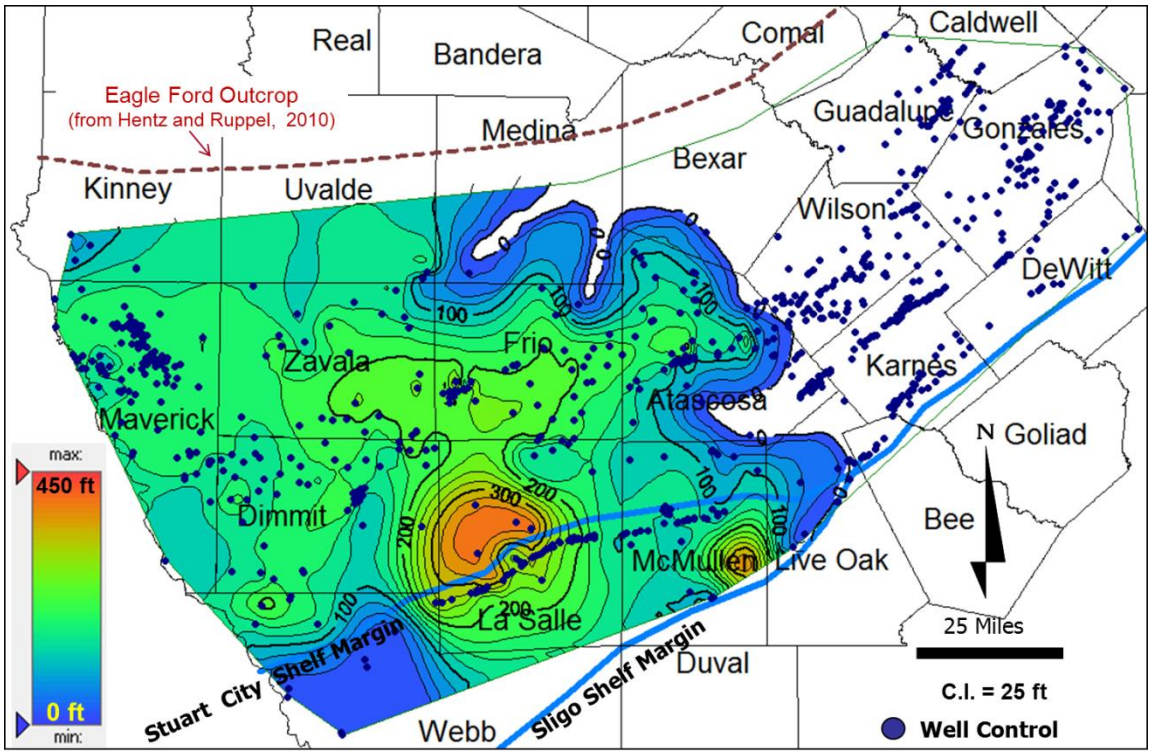

Fig. 37—Thickness of upper unit of Upper Eagle Ford Shale.

CHAPTER IV

PETROPHYSICAL EVALUATION OF KEY RESERVOIR PARAMETERS*

Eagle Ford Shale reservoir fluids, TOC, and lithologic cyclicity vary across the Rio Grande Embayment of South Texas. It is necessary to understand these regional variations to assess controls on Eagle Ford Shale hydrocarbon production, determine the technical and economic risks, and evaluate potential success of the unconventional resource play. Regional variations of the frequency (cyclicity) and thickness of organic-rich marl and limestone interbeds influence well completion design, and these variations may be related to well production performance. To analyze the TOC and lithologic cyclicity of the Lower Eagle Ford Shale in south Texas, we used typical triple-combo logs commonly run by the oil and gas industry.

TOC ANALYSES BY WELL LOGS

TOC of Eagle Ford Shale varies stratigraphically and regionally. TOC was evaluated to assess the quantity of hydrocarbon that may have been generated and the amount that may be stored in the adsorbed state (Montgomery et al. 2005; Spears and Jackson 2009). Early studies of TOC used several types of logs and indirectly and qualitatively indicate the magnitude of TOC. These approaches used gamma ray, bulk density, and uranium

*Part of this chapter is reprinted with permission from Tian, Y., Ayers, W.B. and McCain, W.D. Jr. 2014. Regional Impacts of Lithologic Cyclicity and Reservoir and Fluid Properties on Eagle Ford Shale Well Performance. Paper 169007 presented for SPE Unconventional Resources Conference in the Woodlands, TX, 1-4 April. Copyright [2014] by Society of Petroleum Engineers.

logs. More quantitative TOC assessment was developed by Passey et al. (1990; 2010).

Bulk Density and Gamma Ray—Qualitatively Assessment of TOC

There are limitations of using gamma ray and bulk density to quantify organic material (Passey et al. 1990), but analyses of these two logs may suggest presence of organic material. It is well documented that organic material impacts both gamma ray and density log responses (Spears and Jackson 2009). Gamma ray response is high and bulk density is low in the presence of organic material. However, clay minerals may also result in similar responses. In this research, we assumed that high gamma ray and low bulk density responses suggest high clay content, high TOC, or both. Commonly, TOC is in high in clay-rich sediment; both are deposited in low-energy depositional settings. Relative abundances of clay and organic material may vary regionally, owing to changes of depositional settings. Regional mapping of clay abundance requires multiple single-well lithologic analyses in South Texas, which was beyond the scope of this study. There is a strike-elongate trend of high gamma ray response (greater than 80 API units) from north Maverick to Caldwell County (**Fig. 38**). The average gamma ray response decreases from northwest to southeast in the study area. The average bulk density of Lower Eagle Ford (**Fig. 39**) is related inversely to the gamma ray trend. A strike-elongate, high-density trend is present updip and parallel to the Sligo Shelf Margin. Generally, bulk density increases from northwest to southeast. Together, the average gamma ray and bulk density maps suggest that TOC in the lower Eagle Ford Shale is greatest in the Maverick-Caldwell County trend; we will quantify these results using

Passey's equations (1990; 2010) after further evaluation of clay vs. TOC abundance in two wells using spectral gamma ray logs.

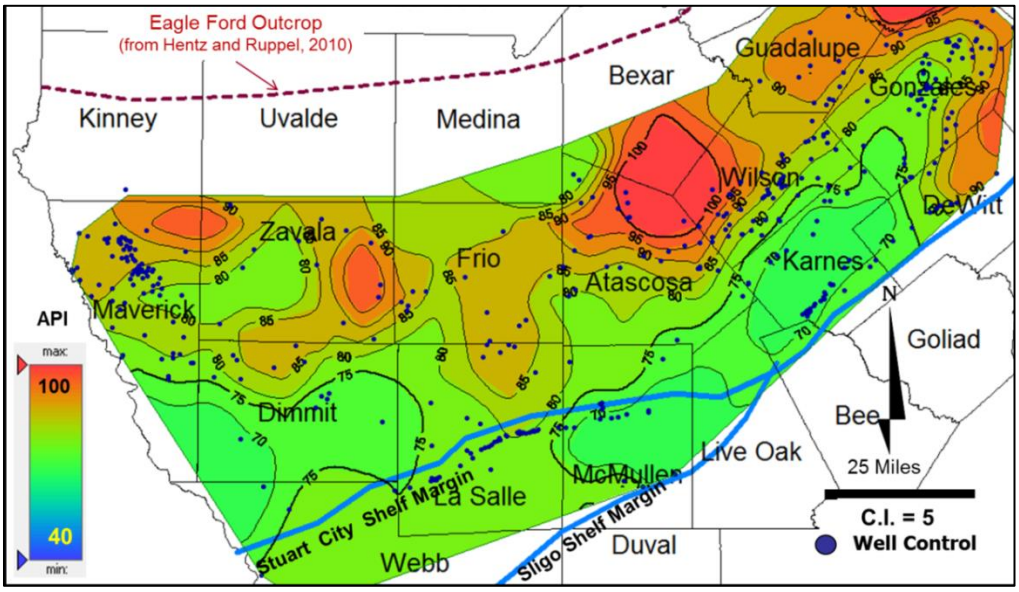

Fig. 38—Average gamma ray response of the Lower Eagle Ford Shale, with more than 500 wells.

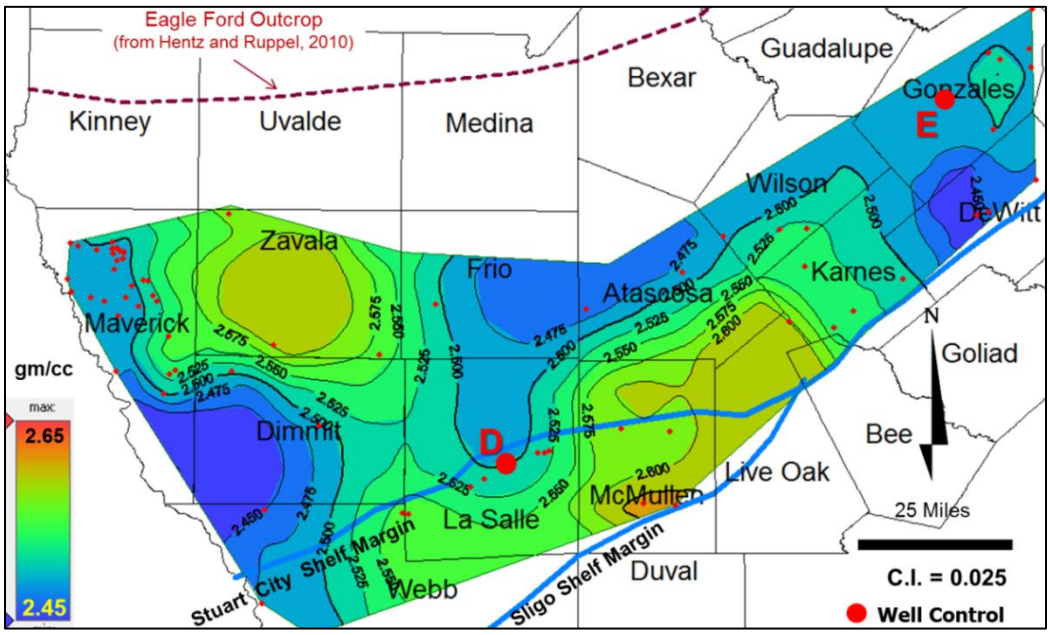

Fig. 39—Average of bulk density of Lower Eagle Ford Shale.

Spectral Gamma Ray Analysis—Qualitative Assessment of TOC

Spectral gamma ray logs were used in two single well analyses to evaluate (1) the contribution of organic (uranium) and clays (thorium and potassium) to gamma ray responses and (2) the vertical and lateral variability of clay content and TOC (**Figs. 40 through 42**). In LaSalle County Well D, we selected two intervals with similar high gamma ray responses; one interval is located in Lower Eagle Ford Shale, and the other interval is in Upper Eagle Ford Shale (lower interval "a" and upper interval "b") (Fig. 40). Evaluation of the spectral gamma ray logs indicated that the contributing factors for high gamma ray responses differed between the two intervals (Fig. 40).

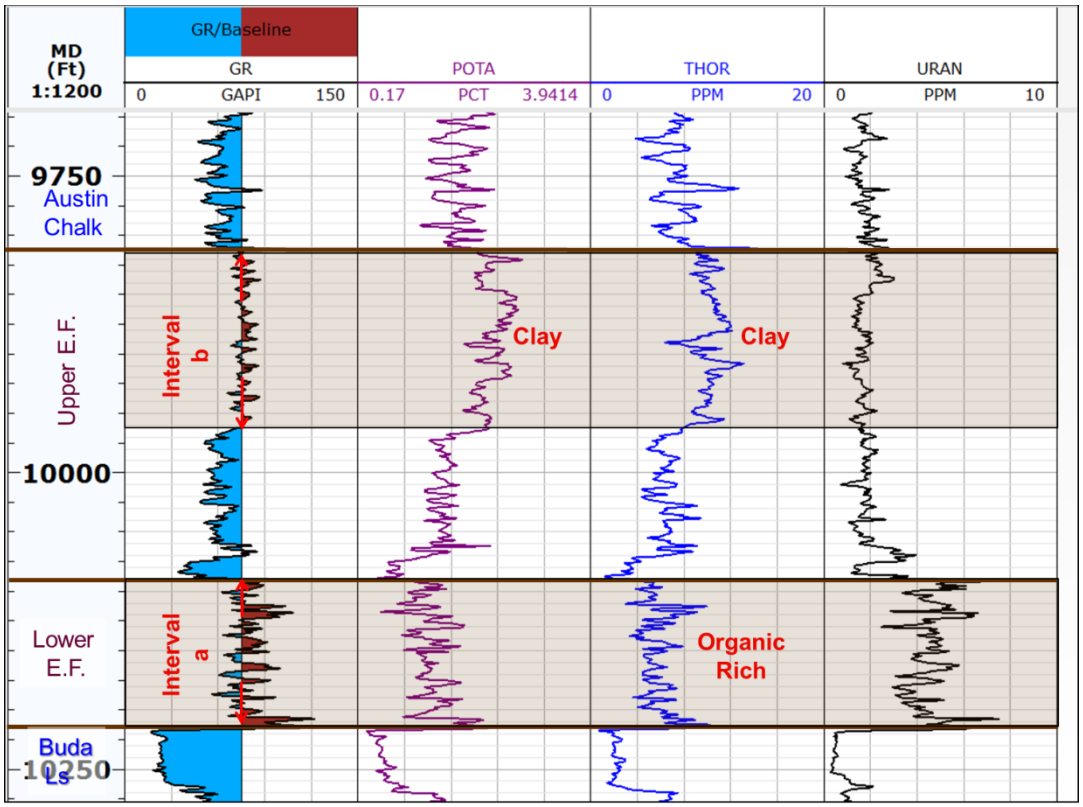

Fig. 40—Spectral gamma ray analysis of Eagle Ford Shale, Well D, Harle 1, LaSalle County. See Figure 39 for well location.

Interval “a” has low-to-medium potassium and thorium responses, which indicate low-to-medium clay content. In contrast, interval “b” has much higher potassium and thorium responses, which suggest high clay content (Fig. 40). Interval “a” has significantly higher uranium response, which suggests higher TOC concentration, whereas interval “b” has the lowest uranium response in comparison to adjacent intervals. This suggests a low TOC in interval “b” (Fig. 40). Therefore, spectral gamma ray logs effectively demonstrate the variable reservoir lithology and TOC of two intervals that have similar total gamma ray response.

Regression analysis in Techlog shows similar composition as the spectral gamma ray analysis (Fig. 41). Organic material (OM) is mainly present in interval a, Lower Eagle Ford, contributing to high gamma ray response, whereas in interval b, Upper Eagle Ford Shale, high illite content is the reason for higher gamma ray response. Also, K-feldspar is present in Upper Eagle Ford Shale, which increases gamma ray response.

In Gonzales County, where only Lower Eagle Ford Shale is present, Well E has a high gamma ray response, medium thorium and potassium responses, and high uranium responses, compared to Austin chalk and Buda Limestone (Fig. 42). Therefore, in Gonzales County, Lower Eagle Ford Shale has relatively high TOC (Fig. 42).

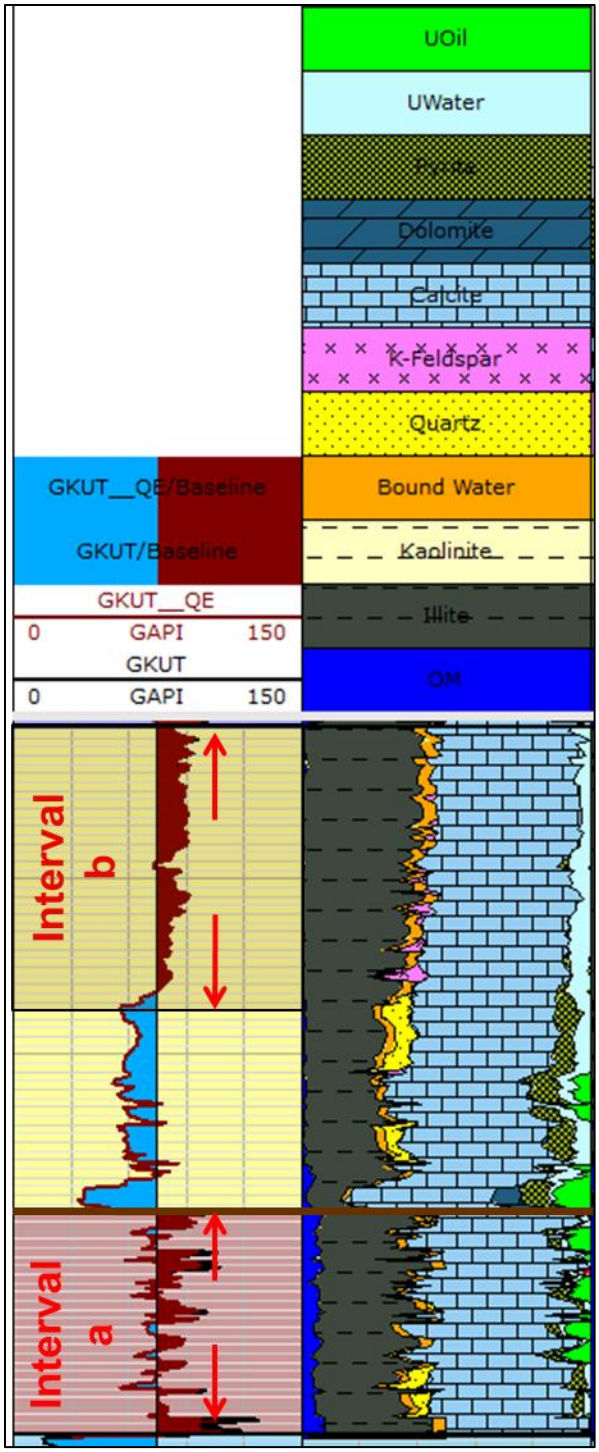

Fig. 41—Lithologic analyses of Eagle Ford Shale. Well D, Harle 1, LaSalle County. See Figure 39 for well location.

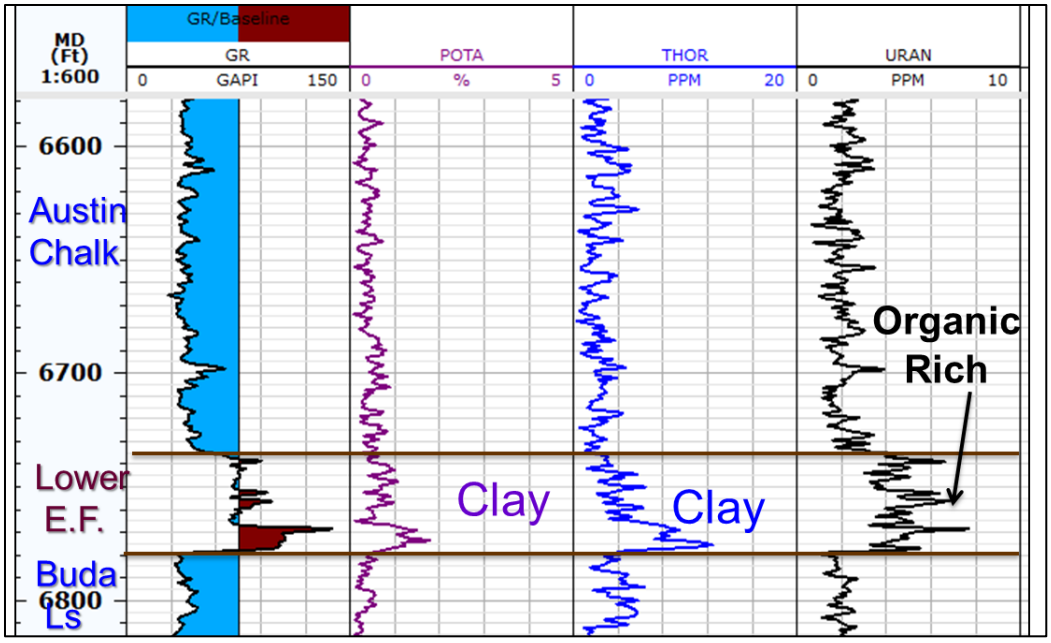

Fig. 42—Spectral gamma ray analysis of Eagle Ford Shale, Well E, Pruski Henry 1, Gonzales County. See Figure 39 for well location.

Passey's ΔR Methods—Quantitative Assessment of TOC

To quantitatively assess regional variations of TOC, we mapped the average TOC for the Lower Eagle Ford, Lower-Upper and Upper-Upper Eagle Ford Shale units using Passey's Delta Log R methods (Passey et al. 1990; Passey et al. 2010). The first Passey method of TOC determination utilized bulk density and deep resistivity logs (Eq. 2). The second method employed sonic and deep resistivity logs (Eq. 3). With the$\Delta logR$ and LOM, TOC can be calculated (Eq. 4).

$$Equation\ 2\text{: } \Delta logR_{den} = log_{10}(R/R_{baseline}) - 2.5 \times (\rho_b - \rho_{baseline}) \quad \text{(Eq. 2)}$$

$$Equation\ 3\text{: } \Delta logR_{sonic} = log_{10}(R/R_{baseline}) + 0.02 \times (\Delta t - \Delta t_{baseline}) \quad \text{(Eq. 3)}$$

$$Equation\ 4\text{: } TOC = \Delta logR \times 10^{(2.297 - 0.1688 \times LOM)} \quad \text{(Eq. 4)}$$

It is critical to obtain the proper well log baseline values of bulk density ($\rho_{baseline}$), sonic ($\Delta t_{baseline}$), and deep resistivity ($R_{baseline}$) for TOC calculations. Due to the regional variability of reservoir properties, it would be inaccurate to apply universal baseline values of bulk density, sonic, or deep resistivity to the entire database. Differences between baseline values from distant wells should be expected. Therefore, the first step of TOC analysis was to determine baseline values for individual well logs (Passey 1990).

The level of maturity (LOM) was required for the TOC calculations (Eq. 4). Eagle Ford LOM values from a contour map (Cardneaux 2012) were used to assign LOM values at individual well locations, by interpolation (**Fig. 43**). By integrating the LOM values from previous work (Cardneaux 2012) (**Fig. 44**), we were able to calculate and map TOC for the Eagle Ford Shale units using equations 1 and 2, as well as the average of these two equations (**Figs. 45 through 49**).

Using bulk density and deep resistivity (Eq. 2), the average TOC of Lower Eagle Ford Shale increases from southeast to northwest (Fig. 45). TOC is lowest (2%) in a strike-elongate trend from Webb County northeastward through McMullen County, approximately between the Stuart City and Sligo Shelf Margins (Fig. 45). Average TOC of Lower Eagle Ford Shale is greatest in Zavala and Frio Counties (more than 10%) (Fig. 45).

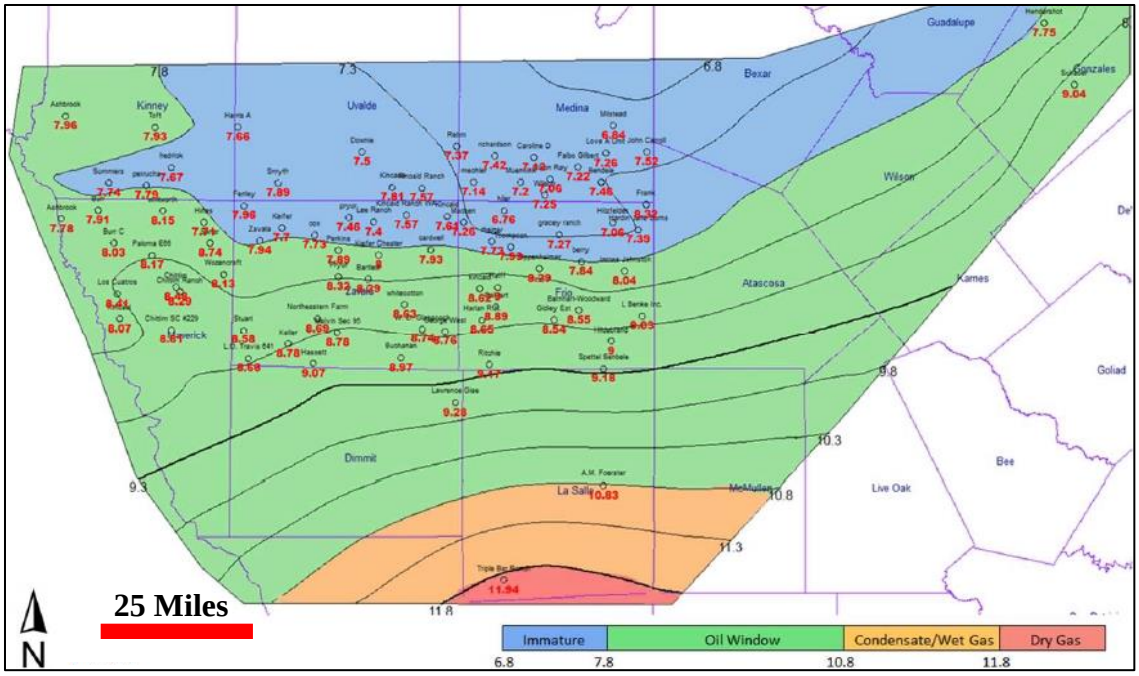

Fig. 43—Lower Eagle Ford LOM map. Contour interval is 0.5 LOM units. (Cardneaux 2012)

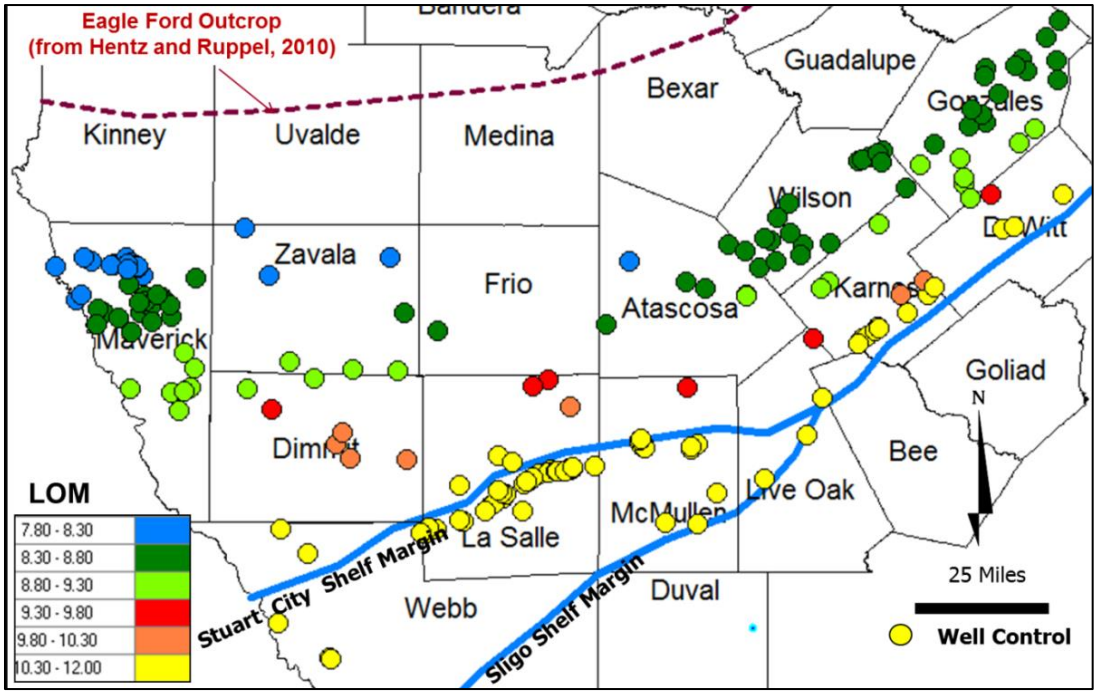

Fig. 44—Level of maturity of Lower Eagle Ford Shale, (interpreted from map by Cardneaux 2012)

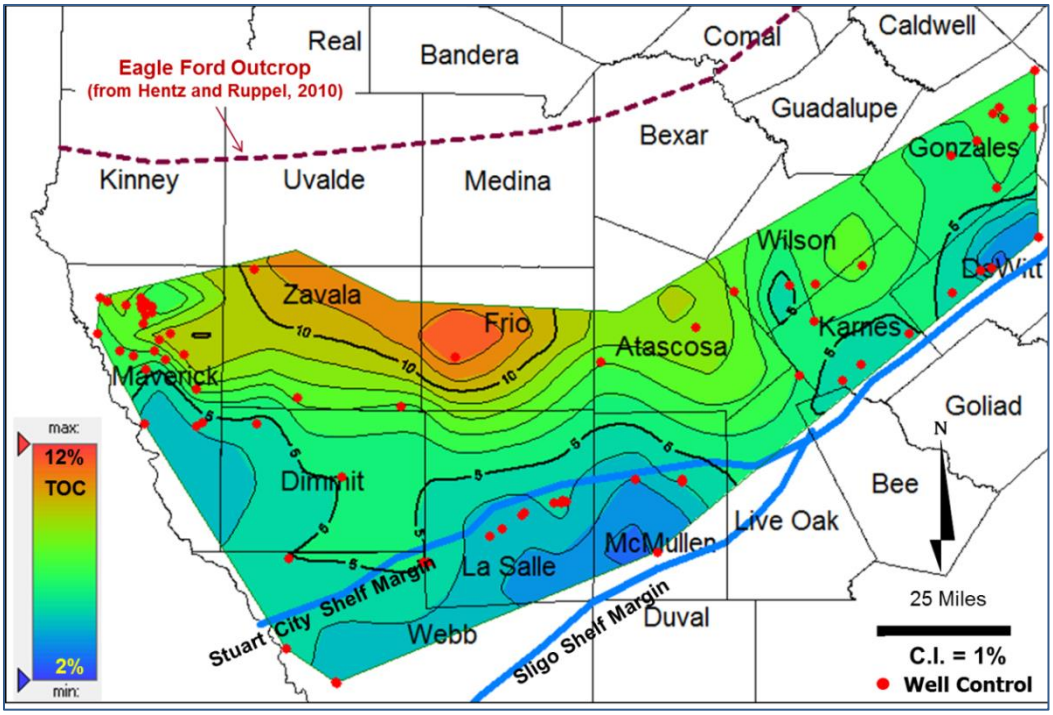

Fig. 45—TOC of Lower Eagle Ford, determined using resistivity and bulk density logs (Eq. 2).

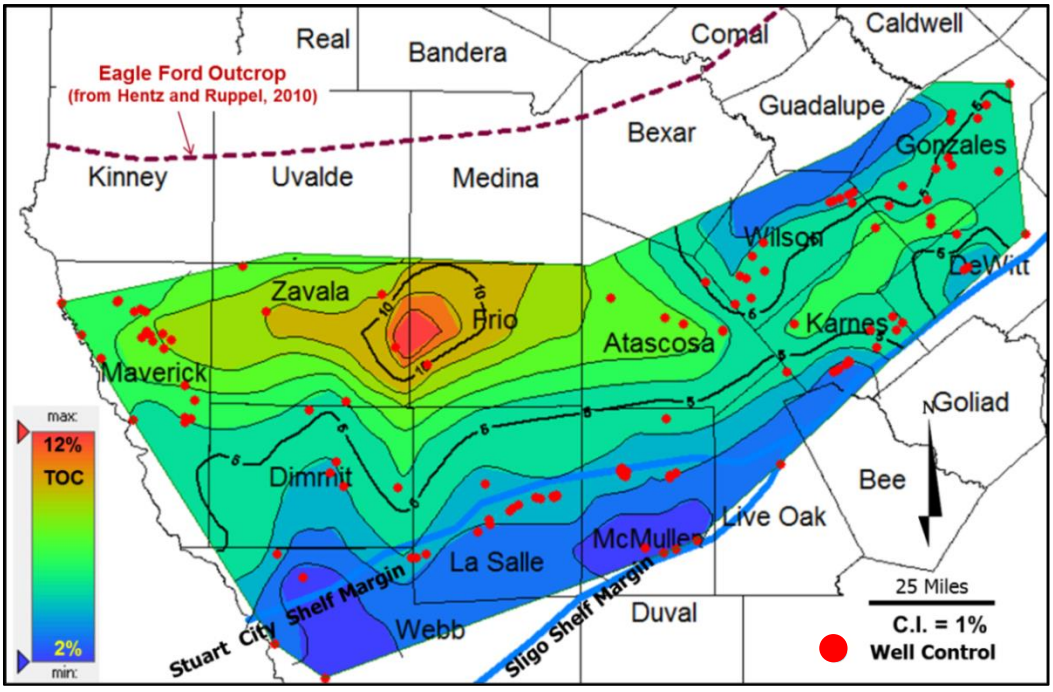

Fig. 46—TOC of Lower Eagle Ford, determined using resistivity and sonic logs (Eq. 3).

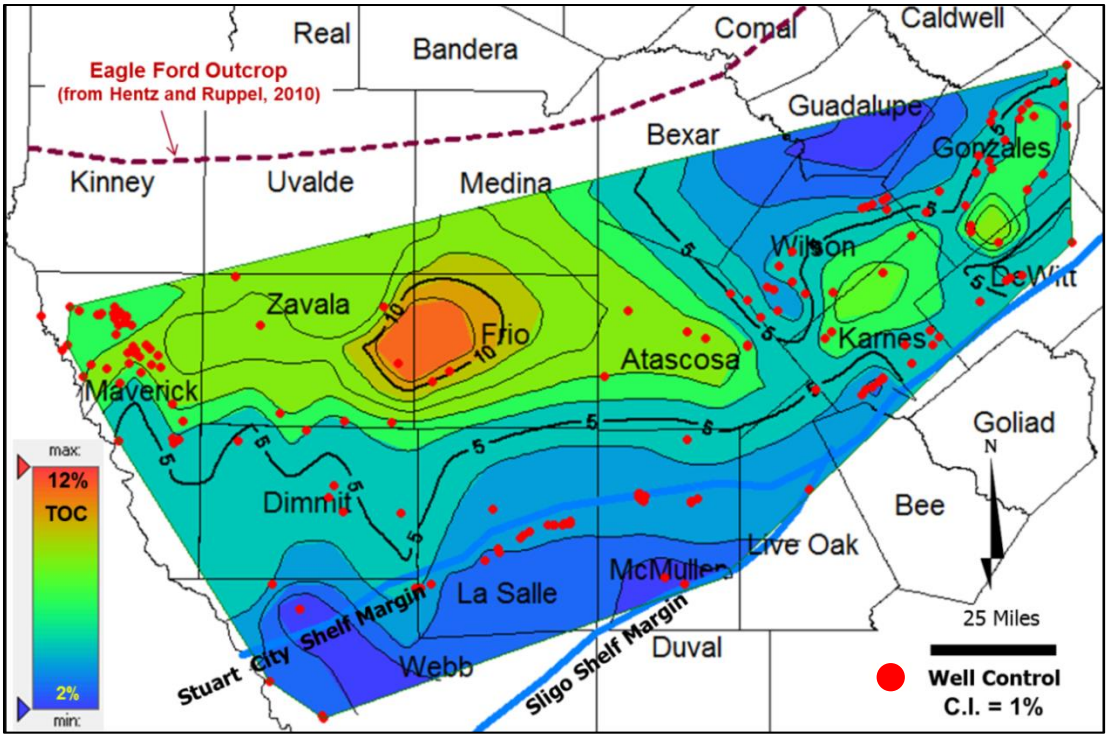

Fig. 47—Average TOC of Lower Eagle Ford Shale, determined by using Eqs. 2 and 3.

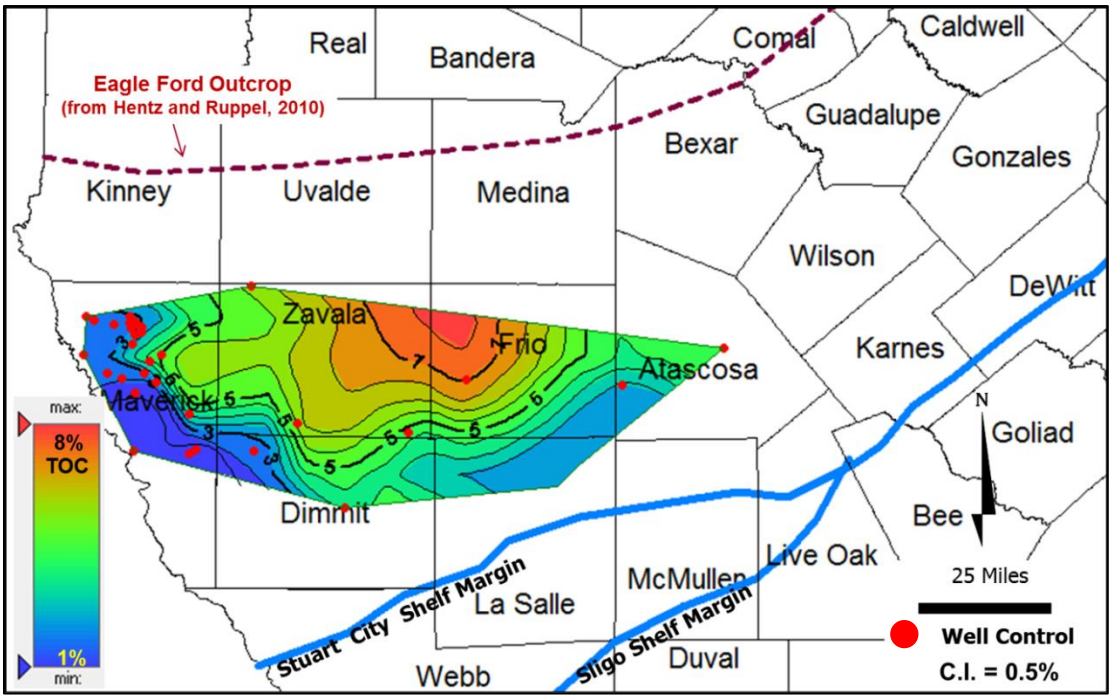

Fig. 48—Average TOC of Lower-Upper Eagle Ford Shale, determined using Eqs. 2 and 3.

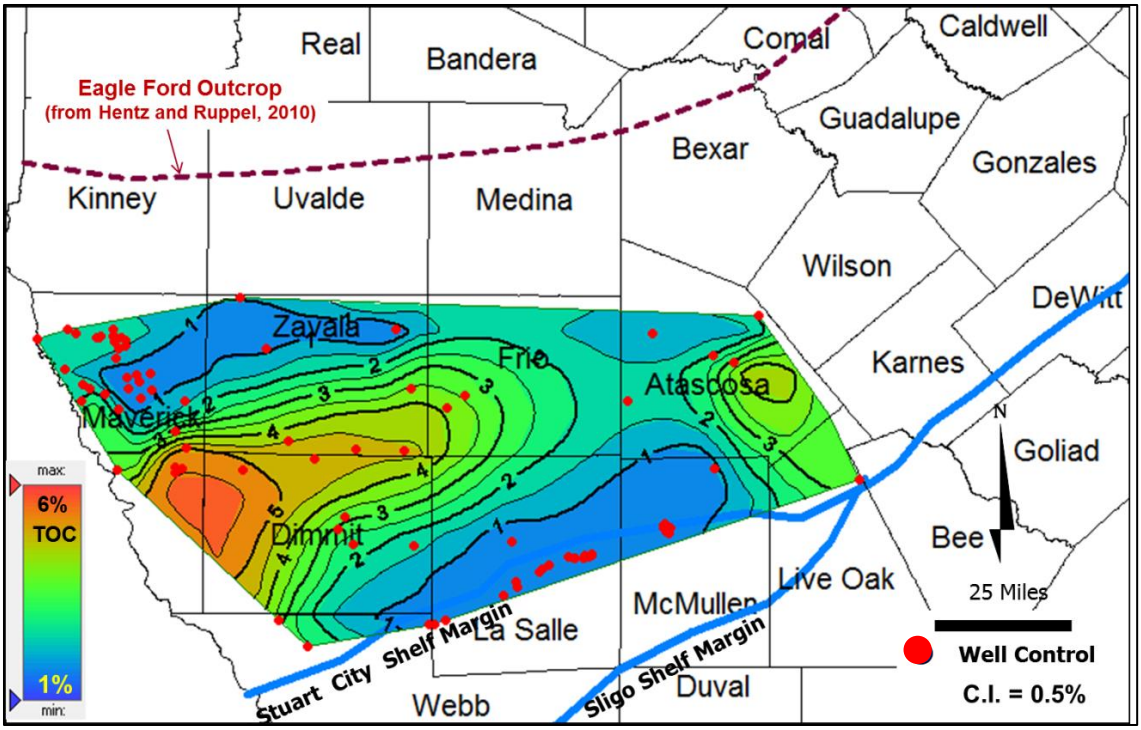

Fig. 49—Average TOC of Upper-Upper Eagle Ford Shale determined using Eqs. 2 and 3.

Using sonic density and deep resistivity (Eq. 3), the average TOC of Lower Eagle Ford Shale (Fig. 46) shows similar regional trends to those calculated from bulk density and deep resistivity (Fig. 45). TOC increases from southeast to northwest. The minimum average TOC of the Lower Eagle Ford Shale is approximately 2% in a strike-elongate trend from Webb through McMullen Counties. TOC is highest (>8%) in Zavala and Frio Counties (Fig. 46).

To improve well control for the Lower Eagle Ford Shale, we combined the TOC results from both methods (Eqs. 2 and 3). The regional southwest to northeast trend of

increasing TOC is better defined (Fig. 47). Local areas of high TOC are present in the eastern part of the study area, in Karnes and Gonzales Counties (Fig. 47).

There are a strike-elongate trend of low TOC values present from Webb to DeWitt Counties from both methods, and a strike-elongate trend of high TOC in the north (Figs. 45 through 47). These trends might be caused by depositional setting, thermal maturity, or both. With increasing depth and thermal maturity, organic material matures and is transformed into hydrocarbon; therefore, TOC decreases. The high TOC trend in the north suggests a quiet water depositional environment and/or low thermal maturity, whereas the low TOC trend suggests either a higher depositional energy environment in the south, near the shelf margins, and/or higher thermal maturity.

Vertically, the maximum average TOC of the Eagle Ford Shale is greater (10%) in the Lower Eagle Ford Shale than in the upper units (5-7%) (Figs. 47 through 49). The maximum TOC of Lower Upper Eagle Ford Shale is approximately 7% in Zavala and Frio Counties (Fig. 48). Regionally, TOC of the Lower Upper Eagle Ford Shale increases from south to north (Fig. 48). The TOC of the Upper Upper Eagle Ford Shale (Fig. 49) differs from other Eagle Ford Shale units; it is greatest (5%) in south Maverick County.

CYCLICITY

Regional variations of the frequency (cyclicity) and thickness of ductile organic-rich marl and brittle limestone interbeds influence well completion design, and these variations may be related to well production performance. Understanding these relations in the Lower Eagle Ford Shale should assist with optimizing completion design and stimulation strategies.

Cyclicity of sedimentary strata results from repetitive process of varying complexity and origin, including sea level changes, variations of sediment input, and climate fluctuations (Blatt et al. 1991; Wells 1990; Rivera et al. 2004). The presence of cyclicity greatly impacts geological interpretation and petrophysical evaluation (Rivera et al. 2004), and vertical or areal changes of cyclicity result in variations of reservoir properties and, therefore, changing hydrocarbon productivity (Rivera et al. 2004). Methods of identifying and quantifying cyclicity and sedimentary characteristics are well documented in previous works (Rivera et al. 2004; Tanyel 2006; Labrecque et al. 2011).

Gamma ray logs, which provide a visual representation of the cyclic patterns, are commonly examined for cyclicity interpretation (Rivera et al. 2004). Three methods: autocorrelation analysis; Fourier transform; and continuous wavelet transform are commonly used to evaluate lithological cyclicity (Lau and Weng 1995; Gilbert et al. 1998; Rivera et al. 2004; Tanyel 2006; Labrecque et al. 2011). These methods have

provided considerable insights to reservoir characterization, facies definition, and stratigraphic interpretations (Rivera et al. 2004; Tanyel 2006; Labrecque et al. 2011).

Regionally, the Eagle Ford Shale is composed of 3 units. The Lower Eagle Ford consists of cyclic, interbedded organic-rich marl and limestone. Gamma ray logs of the Lower Eagle Ford Shale show two distinct log responses. Low gamma ray intervals are calcite-rich, brittle rock (limestone), whereas high gamma ray intervals are organic-rich marl (ORM) ductile rocks that have carbonate and high clay content, or carbonate and high clay and TOC content (**Fig. 50**). The critical parameters controlling good shale source rocks are TOC, maturity, and kerogen type (Passey et al. 2010). Thus, the high gamma ray interval is regarded as good source rock and, potentially, good reservoir rock.

However, successful development of shale reservoirs also requires effective completions and fracturing stimulation (Rickman et al. 2008; Cipolla et al. 2011; Wan et al. 2013), for which rock brittleness is a key factor (Rickman et al. 2008). Thus, low gamma ray (brittle carbonate) intervals are better completion targets than high gamma ray (more ductile marl and shale) intervals. Fortuitously, the Lower Eagle Ford Shale has cyclic, interbedded organic-rich marl (source rock) and brittle limestone (reservoir completion targets). However, the lithologic thickness and cyclicity of the Lower Eagle Ford Shale vary greatly in South Texas (Fig. 50), and these variations impact the overall reservoir quality. Therefore, we mapped the regional variations of Lower Eagle Ford Shale cyclicity.

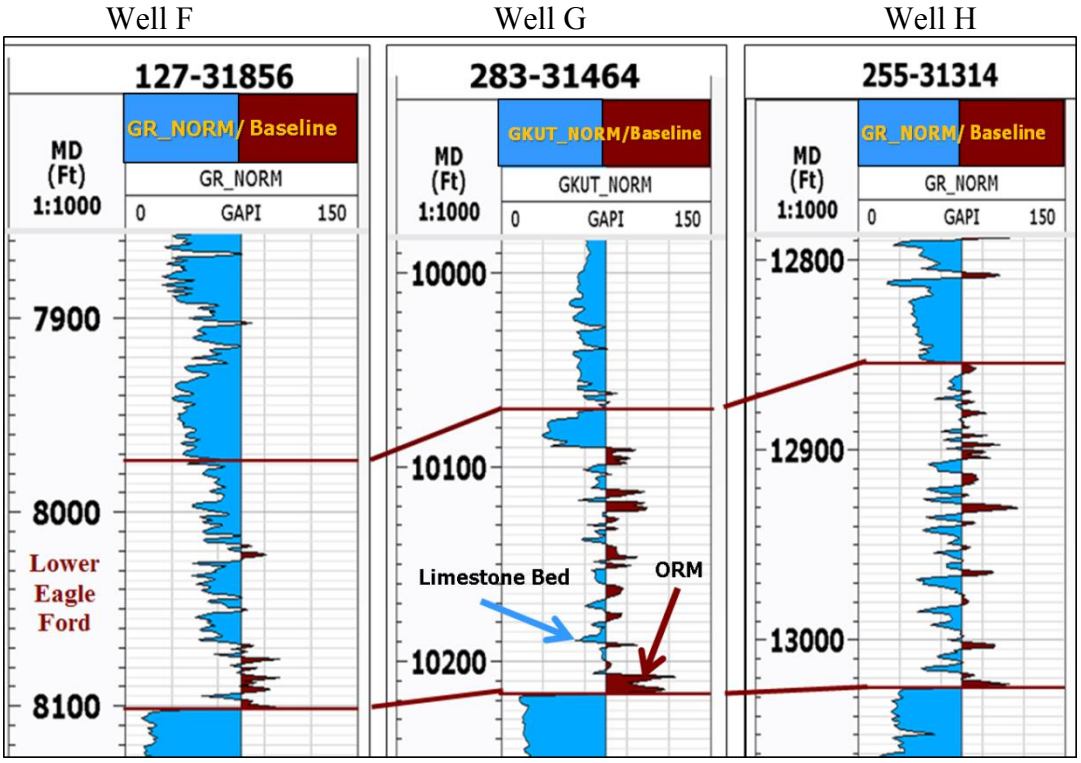

Fig. 50—Lower Eagle Ford ORM and limestone interbeds. See Fig. 52 for well locations.

To analyze lithologic cyclicity of the Lower Eagle Ford Shale in South Texas, We evaluated gamma ray logs from more than 500 vertical wells. A Matlab script was developed to count the numbers of organic-rich marl and limestone interbeds. Average bed thickness was calculated at each well and was mapped regionally.

Recognizing the advance in understanding of sedimentary strata and their reservoir characteristics gained from the above methods of cyclicity assessment, we proposed another method that uses the abundant gamma ray logs available to assess both vertical and areal cyclicity of the Eagle Ford Shale. We imposed two cutoff values and developed a Matlab script to count the numbers of limestone and ORM intervals in

gamma ray logs of Lower Eagle Ford Shale (**Fig. 51**). Limestone intervals were defined as having gamma ray responses lower than 70 API Units, whereas shale-rich intervals those having gamma ray responses greater than 80 API Units. Two cutoff values instead of one (75 API units) were used to avoid ambiguous gamma ray responses (Tian et al 2014).

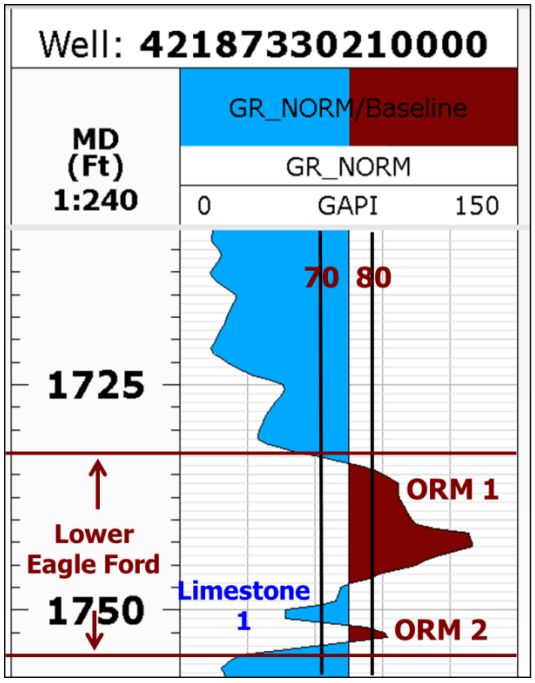

Fig. 51—Schematic showing gamma ray cutoffs used to count the numbers of Lower Eagle Ford Shale limestone and ORM beds.

The numbers of limestone beds in the Lower Eagle Ford increases from fewer than 2 in the northwest to more than 26 on the southeast near the Sligo and Stuart City Shelf Margins and on the southwest in the Maverick Basin (**Fig. 52**). The number and occurrence of ORM beds in the Lower Eagle Ford (**Fig. 53**) are similar to those of limestone (Fig. 52). ORM increases from fewer than 2 beds in the northwest to more

than 20 on the southeast and in the Maverick Basin depocenter (Fig. 53**)** (Tian et al 2014).

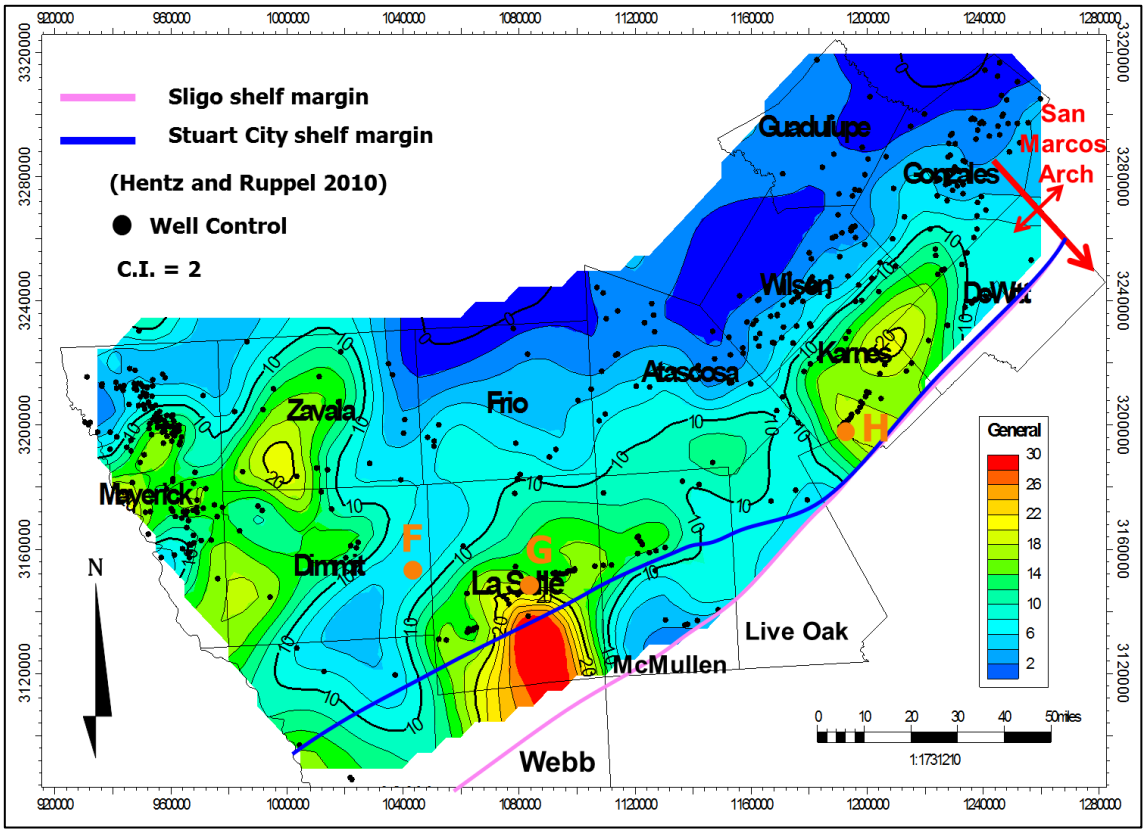

Fig. 52—Number of limestone bed of Lower Eagle Ford Shale.

Increased numbers of both limestone and ORM beds coincide with the greater thickness of Lower Eagle Ford Shale (Fig. 34, 52 and 53). To further investigate lithologic variability of the Lower Eagle Ford, we calculated the average bed thickness, by dividing the total thickness from the isopach map (Fig. 34) by the number of limestone plus ORM beds. The average bed thickness is low (< 5 ft) (**Fig. 54**) in La Salle, Karnes,

DeWitt and southern Gonzales Counties. Average bed thickness is greater than 12 ft in Maverick and northern Wilson and Gonzales Counties (Tian et al 2014).

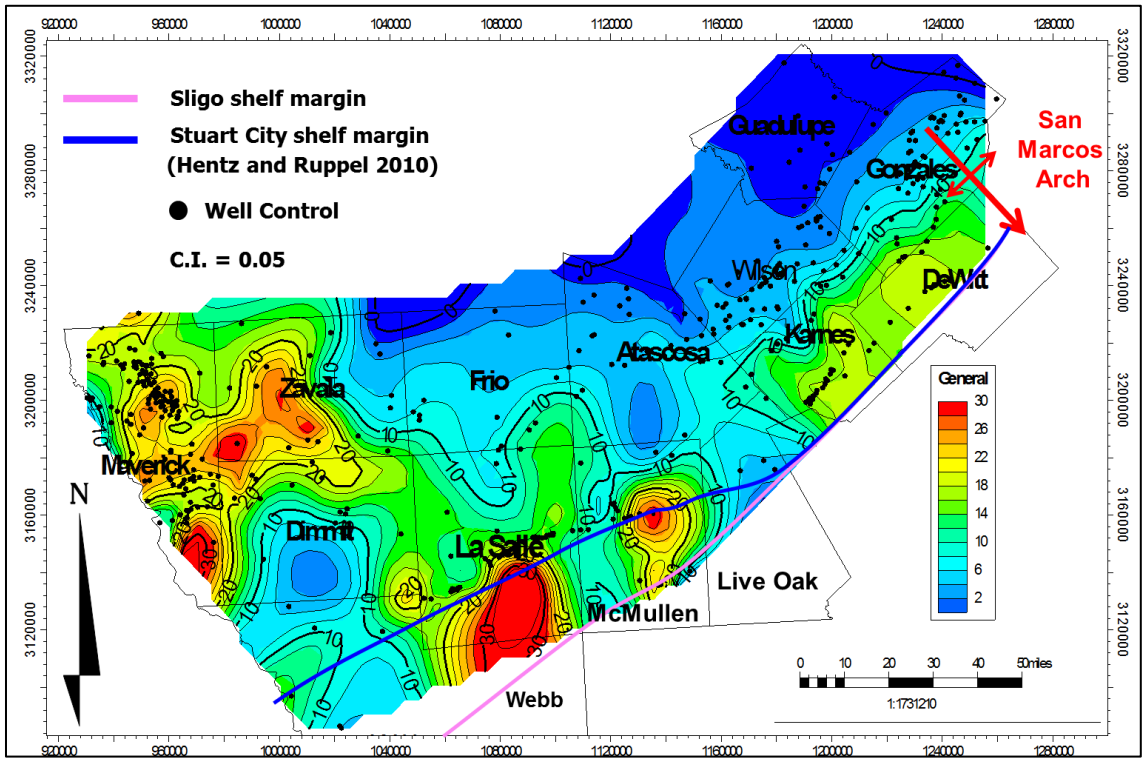

Fig. 53—Number of ORM bed in the Lower Eagle Ford Shale.

The Maverick basin, which is the depocenter of the Lower Eagle Ford Shale, has the greatest numbers of Lower Eagle Ford limestone and ORM interbeds, and greatest average bed thickness (Figs. 34, and 52 through 54). The greater total Lower Eagle Ford Shale thickness in the Maverick basin suggests more potential reservoir and source rock. Average bed thickness in Maverick County ranges from less than 5 ft to more than 13 ft, which is relatively thick compared to the other locations with the same number of

interbeds (Fig. 54). Therefore, the mechanical properties of the Eagle Ford Shale in this region are different than those of others areas (Tian et al 2014).

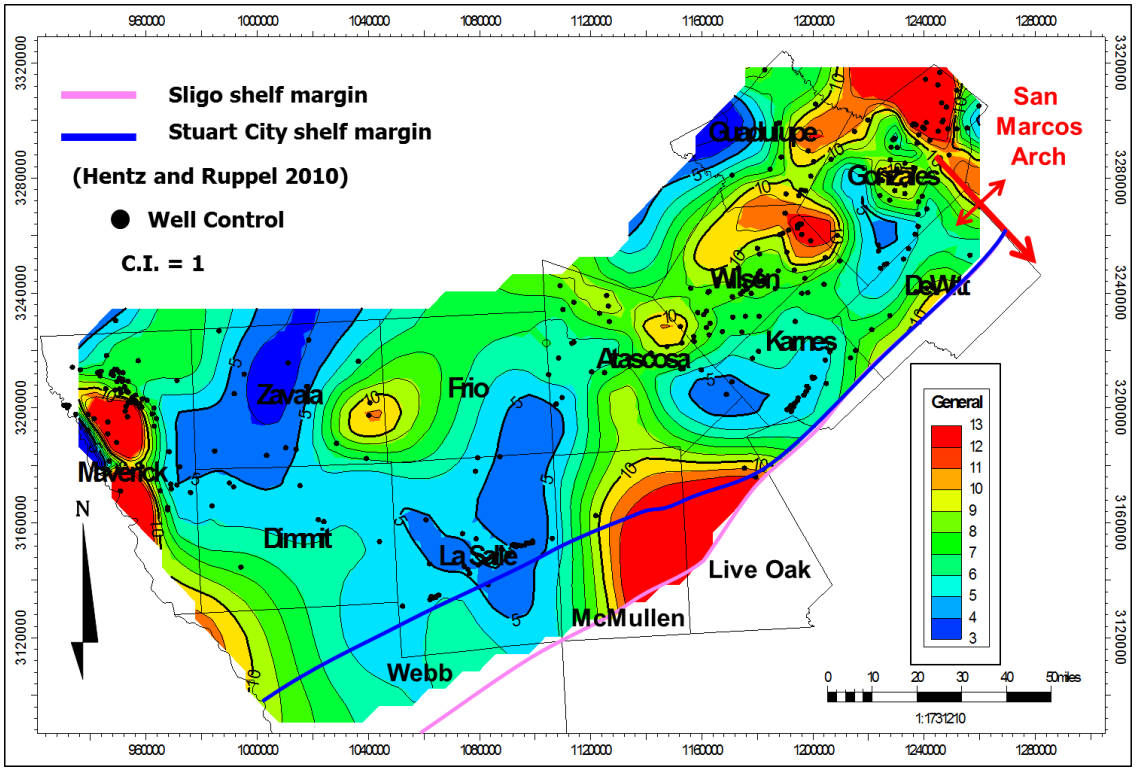

Fig. 54—Average bed thickness of Lower Eagle Ford Shale.

A strike-elongate trend of high numbers of limestone and ORM beds, and low average bed thickness, extends from La Salle County northeastward through DeWitt County, immediately updip of either the Stuart City or Sligo Shelf Margins (Figs. 52 through 54). This trend coincides with a northeast-trending region of anomalously thick Lower Eagle Ford Shale (Fig. 34). Updip of this area, a strike-elongate trend of low numbers of limestone and ORM beds having high average bed thickness extends from eastern Zavala County northeastward through Guadalupe County (Figs.52 through 54), and

coincides with low values of total Lower Eagle Ford Shale thickness (Fig. 34). While there is a direct relation between total Lower Eagle Ford thickness and average interbed thickness in the Maverick Basin depocenter, there is an inverse relation between total thickness and average interbed thickness in the La Salle – DeWitt County trend (Tian et al 2014).

CHAPTER V

QUANTITATIVE EVALUATION OF KEY RESERVOIR PARAMETERS

We evaluated the depth, pressure, thickness, TOC, distribution of limestone and ORM beds, and thickness of the Lower Eagle Ford Shale to assess the geological control on Eagle Ford Shale production.

Having characterized these key geological parameters that may affect Eagle Ford production, we were faced with the question "Is there a quantitative relation between production and the above parameters?" And if so, which geological parameter has the dominant control on production.

A difficulty of relating geological parameters to production stems from the fact that no wells in our data base had both production and geological parameters. The wells used to calculate geological parameters are vertical wells that were drilled for reservoirs below the Eagle Ford Shale. However, production wells are horizontal wells. Therefore, we cannot directly relate production to geological parameters at individual well locations.

In this chapter, we quantify the correlations between geological parameters from vertical wells and production from horizontal wells with spatial statistics, and we investigate the primary controls on production by analyzing the coefficients and *p*-values of the generalized linear regression results.

METHODS

To determine the parameters affecting production, we need both the production and geological data for a common location. This involves predictions from both the vertical well locations and the horizontal well locations. For prediction, a correct covariance function is crucial to achieving an accurate result, and understanding the distribution pattern is the key to selecting the correct method to fit the covariance function. The following workflow was designed to capture the differences among various data sets.

Data Preparation

Distribution Pattern Identification

A histogram and Q-Q plot (Q stands for quantile) were used to determine the distribution type. Data following Gaussian distribution were further analyzed regarding skewness, and Poisson distribution was analyzed with MCMC (**Fig. 55**).

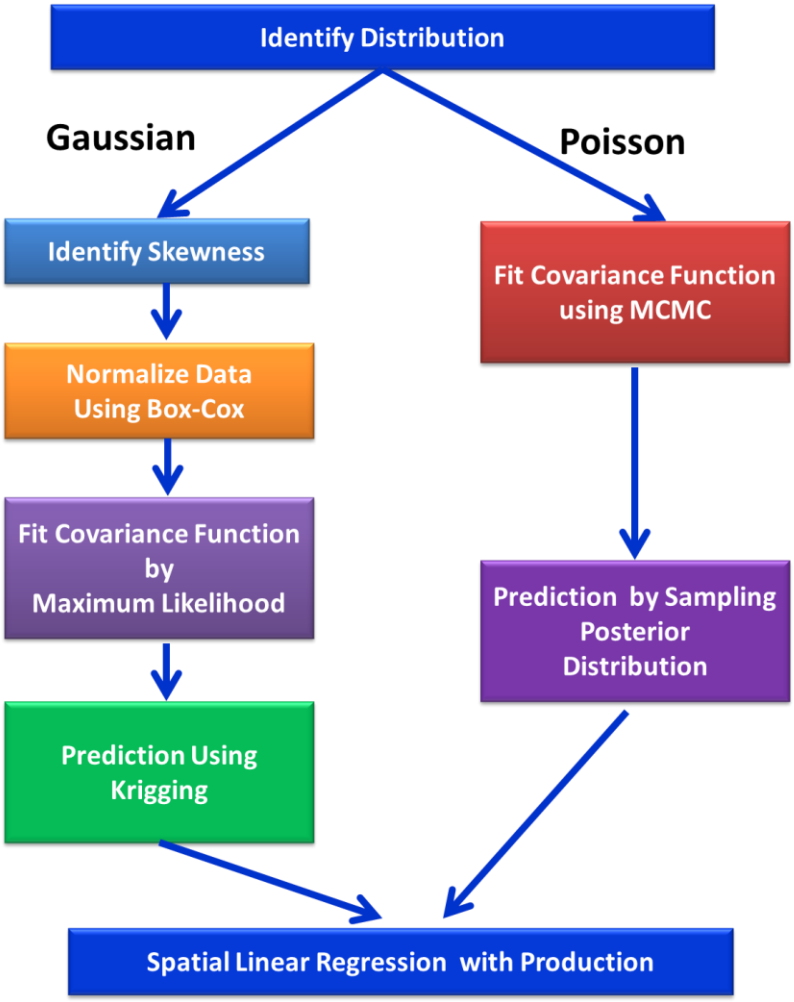

Fig. 55—Schematic workflow for quantifying influences on production from various geological parameters.

Skewness Identification

A Q-Q plot is a graphical diagnostic tool used to analyze the shape of the distribution and skewness of the data by comparing the quantiles of two different distributions (Gnanadesikan 1968). We plotted the geological parameters against randomly generated normal distribution data. If the distributions are similar, then a unit slope results (**Fig. 56**

(a)). A curved pattern on the Q-Q plot suggests the distribution is skewed and requires normalization (**Fig. 56 (b)**) (Gnanadesikan 1968).

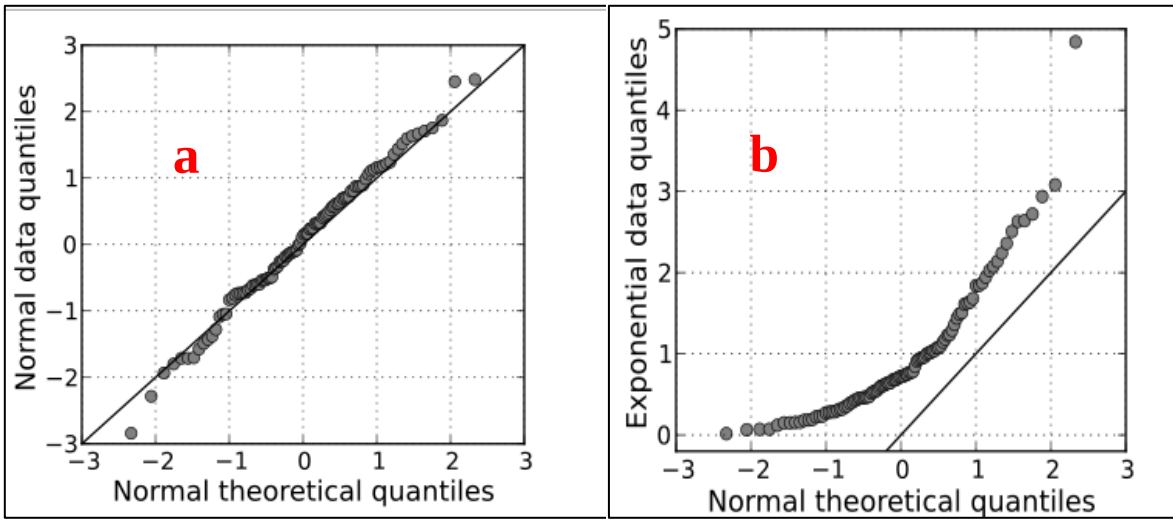

Fig. 56—(a) Unit slope on Q-Q plot for Gaussian distribution; (b) Curved pattern on Q-Q plot, suggesting skewness (Skbkekas 2009).

Transformation to Normality

Once skewness is identified by the Q-Q plot, a Box-Cox conversion is required to transform the data set into perfect Gaussian distribution. A Box-Cox transformation is defined as a continuous function with the power parameter λ, which can transform the original data into Gaussian distribution (Eq. 5) (Box and Cox 1964). By generating a list of power parameter λ and a computed profiled log-likehood vector, the most likely λ can be determined by the maximum correlation coefficient (**Fig. 57**) (Box and Cox 1964; Scott 2008). When power parameter λ is close to 1, it suggests Gaussian distribution and does not require the data to be transformed. If λ from Box-Cox analysis is close to zero, then log transformation will modify the data into Gaussian distribution.

$$y_i^{(\lambda)} = \begin{cases} \frac{y_i^{\lambda}-1}{\lambda}, if\ \lambda \neq 0 \\ \log(y_i), if \lambda = 0 \end{cases} \quad \text{..... (5)}$$

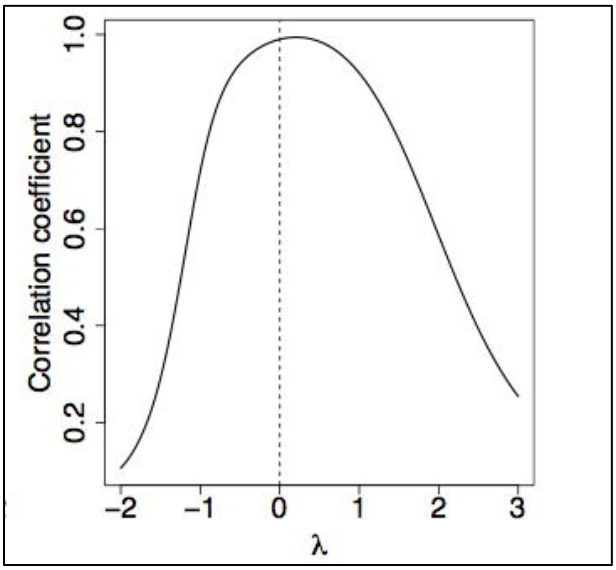

Fig. 57—Log transformation with λ being zero (Scott and Lane 2008).

Covariance Function Fitting

After fitting Eagle Ford sets into perfect Gaussian distributions, we used maximum likelihood estimation to fit the covariance models. A Gaussian data set can be written as Eq. 6, as follows.

$$Y(x) = \mu(x) + S(x) + e \quad \text{..... (6)}$$

x defines a spatial location; $\mu(x)$ is the mean value of the data set; $Y(x)$ is the observed geological data; $S(x)$ is the Gaussian process function with variance sill, range parameter, and smoothness parameter; and e is the error term with parameter τ^2. The covariance function involves three constants: sill, spatial range, and smoothness parameter (Eq. 7).

$$K(x) = \alpha \left(\frac{x}{\beta}\right)^{\nu} \kappa_{\nu}(\frac{x}{\beta}) \quad \text{..... (7)}$$

α is the sill; β is the spatial range, and ν is the smoothness parameter. By running the observed data, when the likelihood reaches its maximum value, the most likely Gaussian distribution [$S(x)$] can be estimated with sill, range parameter, and smoothness parameter. With the fitting results of sill, range, and smoothness parameter, the covariance function is known for its specific data set.

Gaussian Distribution Data Prediction

Kriging, the best linear unbiased prediction for spatial statistics, is widely applied in the oil and gas industry in building approximations of certain attributes from known points to wider areas. For the Gaussian distribution data set, we used the conventional kriging to predict the geological data for the production well locations.

The covariance function was fitted, and key parameters were exported into the kriging model. With the covariance function estimated, we performed spatial prediction of the thickness by conventional kriging from the thickness controls of stratigraphic analysis to the new locations of the production data at horizontal wells.

Poisson Distribution Data Prediction

Thus far, we have estimated covariance function using the maximum likelihood for Gaussian data. However, the number of limestone beds is discreet and should be described using Poisson distribution. For non-Gaussian distribution, a hierarchical model

was employed to predict the number of limestone beds for the new locations. The hierarchical model transforms the non-Gaussian data [$\lambda(s_i)$] at specific site S_i to a Gaussian process [$\eta(s_i)$] plus a variable (β).

$$\log[\lambda(s_i)] = \beta + \eta(s_i) \quad \text{..... (8)}$$

$$\eta(s_i) \sim N[0;\ \sigma^2 R(\phi)] \quad \text{..... (9)}$$

$\eta(s_i)$ is a Gaussian process with a mean of zero, a variance of σ^2, and a spatial range of ϕ. We used the Bayesian method for the hierarchical model to estimate the parameters and make predictions. The Bayesian method does not directly predict values for other points; rather, it simulates the distributions of parameters β, σ^2, and ϕ. The Bayesian method for the hierarchical model must proceed using Monte Carlo methods. Three chains of data with different starting values were generated. The SPGLM function was employed in software R for the MCMC process since it simulates the three variables. The function SPpredict was used to predict the number of limestone beds for new locations using the variables β, σ^2, and ϕ, exported from SPGLM.

PREDICTION RESULTS

The primary production data set is the barrel of oil equivalent (BOE) production of the first six months since initial production, including approximately 3,000 wells in 13 counties (**Fig. 58**). There is a northeast to southwest trend of production. Maximum production is in the central area of the production belt.

Five geological parameters were evaluated: structural depth (Fig. 27); thickness (Fig. 34); number of limestone beds (Fig. 52); average bed thickness (Fig. 54); and TOC (Fig. 47). The geological parameters can be divided into two types of distributions: Gaussian distributions and Poisson distributions. Depth, thickness, average layer thickness, and TOC follow Gaussian distribution, whereas the number of limestone beds follows Poisson distribution.

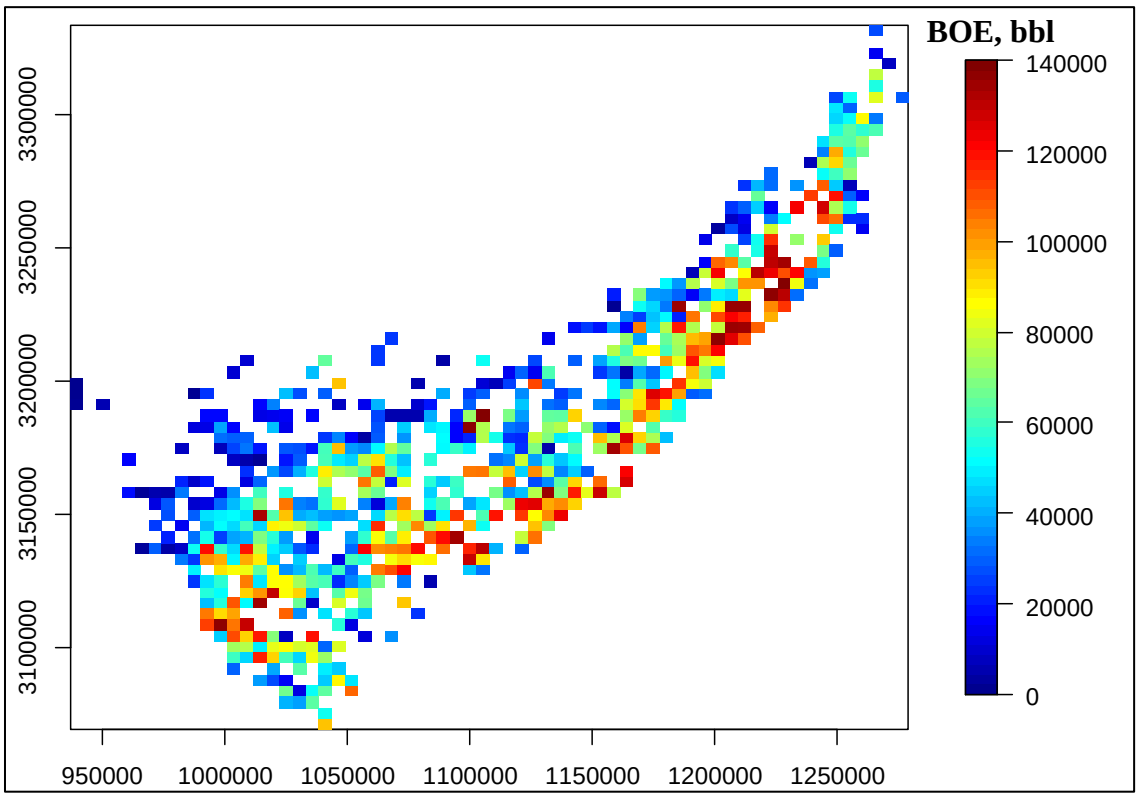

Fig. 58—Spatial map of first 6 month barrel of oil equivalent production of Eagle Ford Shale in South Texas. Coordinates uses North American Datum 1927 (NAD27) in meters.

Gaussian Data Group Prediction

The histogram and Q-Q plot show that depth data generally follow Gaussian distribution. (**Fig. 59**). Box-Cox analyses show that λ is approximately 0.93, which suggests that original depth data closely follow Gaussian distribution.

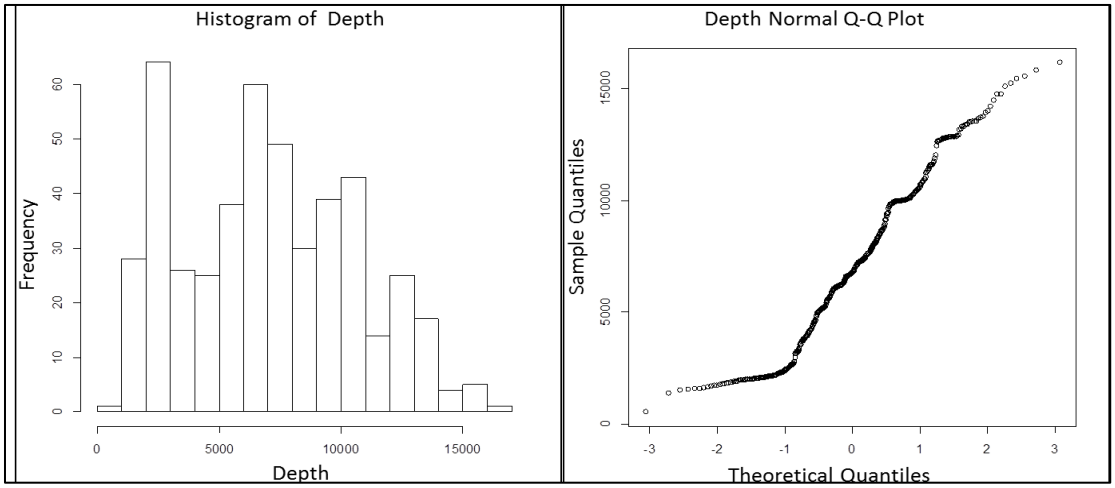

Fig. 59—Histogram and Q-Q plot of depth data.

The histogram and Q-Q plot show that thicknesses, TOC, and average bed thickness of the Lower Eagle Ford generally follow Gaussian distribution (**Fig. 60 and 61**). Box-Cox analyses show that the λ of thickness is approximately 0.2, which suggests that log transformation of the original thickness can effectively eliminate the skewness, thereby following Gaussian distribution (Fig. 60). The unit slope of the Q-Q plot after the transformation indicates a successful transformation (Fig. 60). Both TOC and average bed thickness show skewness on the Q-Q plots (Fig. 61). The skewness shown by average bed thickness was eliminated by power transformation using 0.75, whereas TOC was transformed by log transformation (Fig. 61).

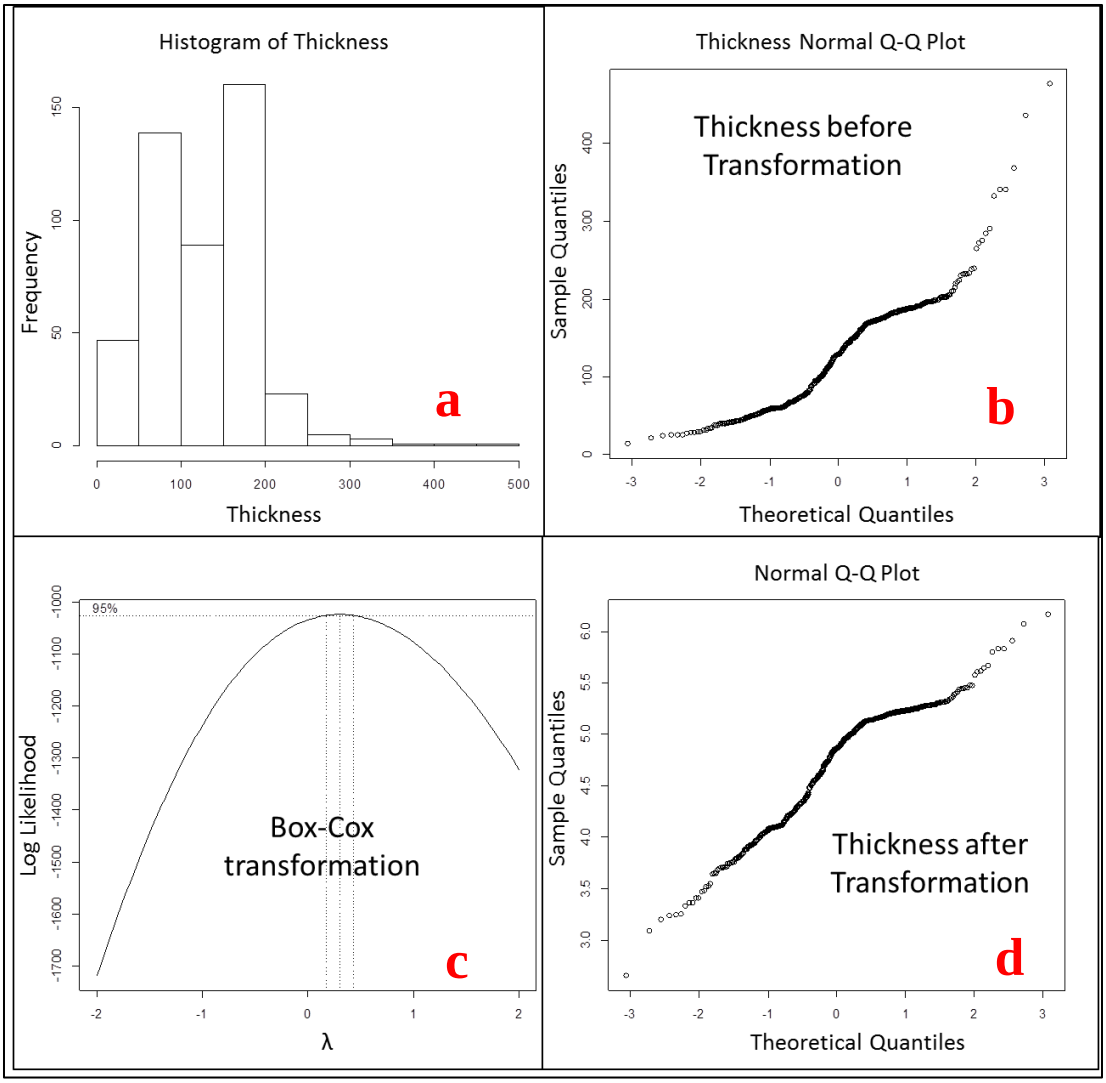

Fig. 60—(a) Histogram of thickness of Lower Eagle Ford Shale, (b) Q-Q plot of thickness, (c) Box-Cox transformation result, and (d) Q-Q plot of thickness data after Box-Cox transformation.

After transforming the data to Gaussian distribution without skewness, we used the likfit function in software R to fit the covariance function. The results of sill, spatial range, and smoothness parameter were used to predict the depth, thickness, average bed thickness, and TOC of the vertical well locations for the Eagle Ford horizontal wells (**Figs. 62 through 69**).

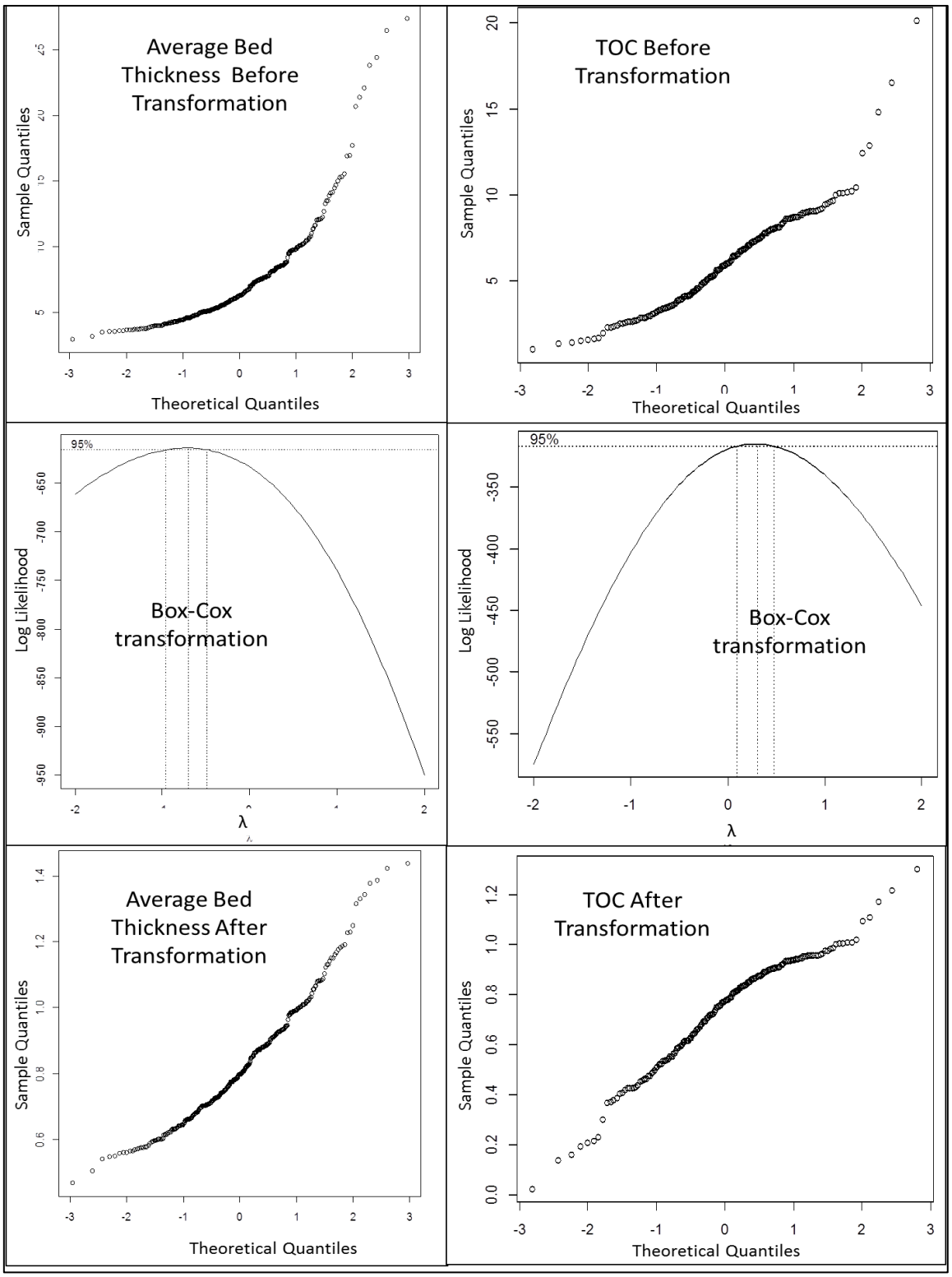

Fig. 61—Skewness elimination workflow by Q-Q plots and Box-Cox transformation.

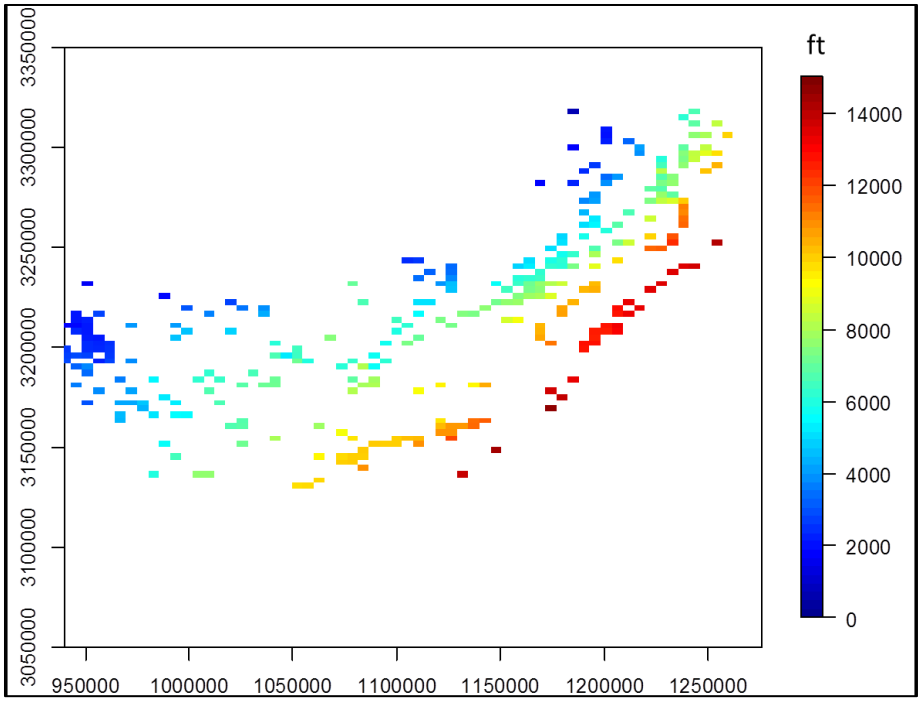

Fig. 62—Depth of Lower Eagle Ford Shale by stratigraphic analyses on vertical wells. Coordinates uses NAD27 system in meters.

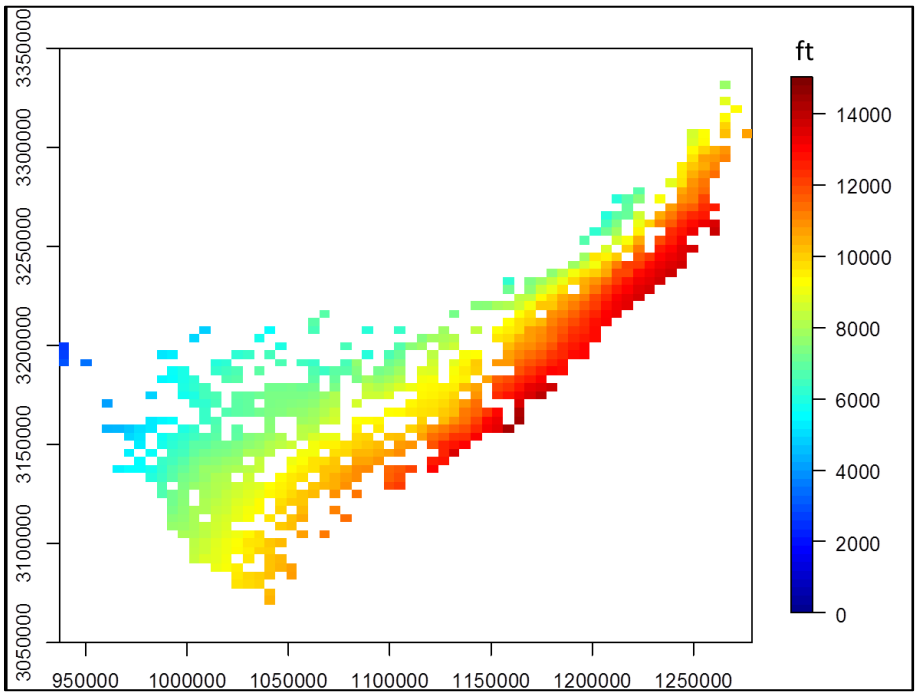

Fig. 63—Depth of Lower Eagle Ford Shale predicted for Eagle Ford production wells locations by kriging. Coordinates uses NAD27 system in meters.

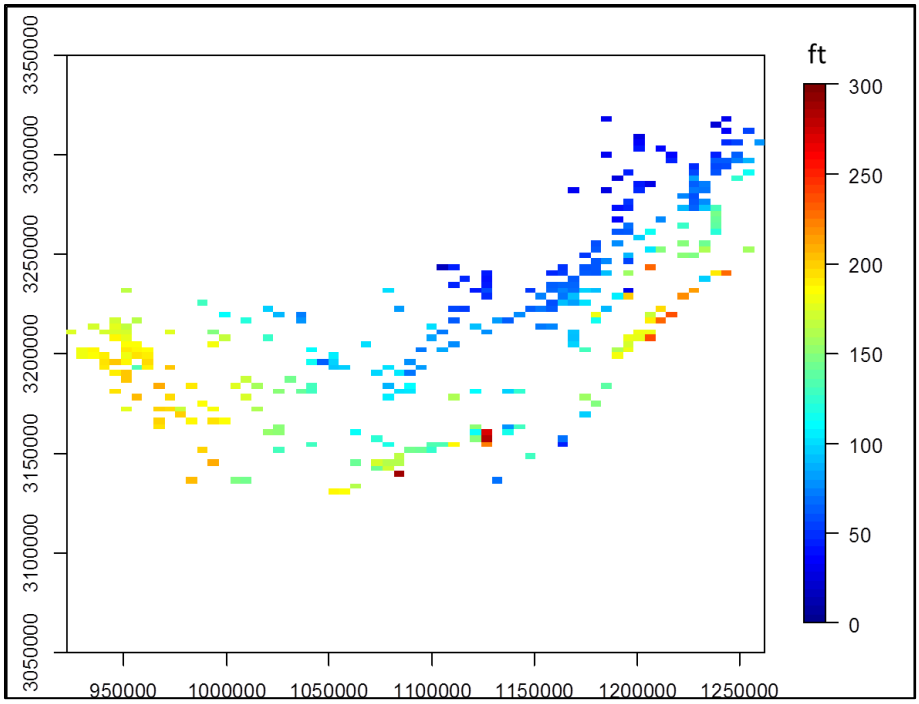

Fig. 64—Thickness of Lower Eagle Ford Shale by stratigraphic analyses on vertical wells. Coordinates uses NAD27 system in meters.

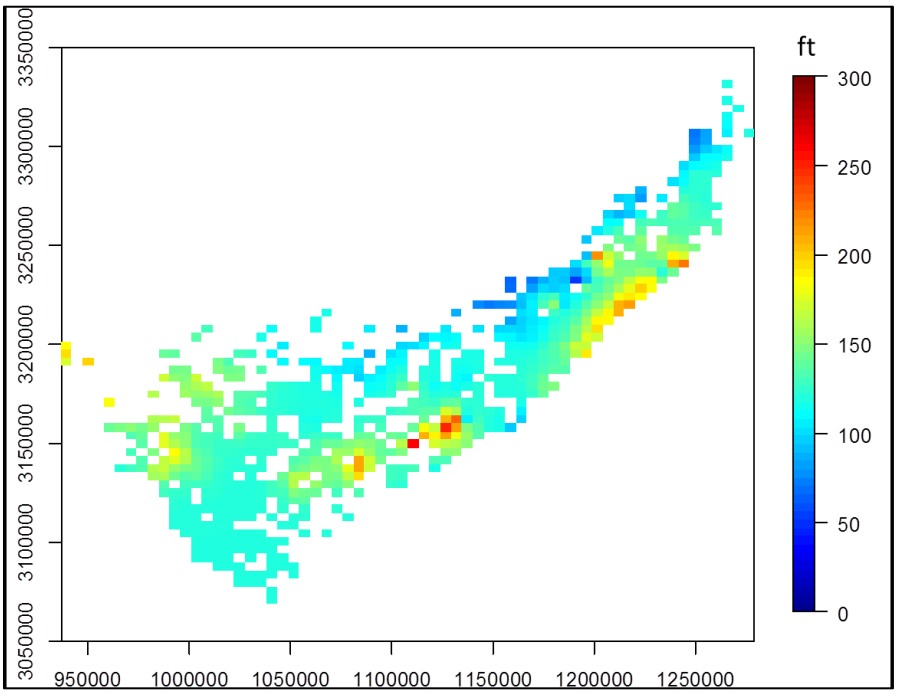

Fig. 65—Thickness of Lower Eagle Ford Shale predicted for Eagle Ford production well locations by kriging. Coordinates uses NAD27 system in meters.

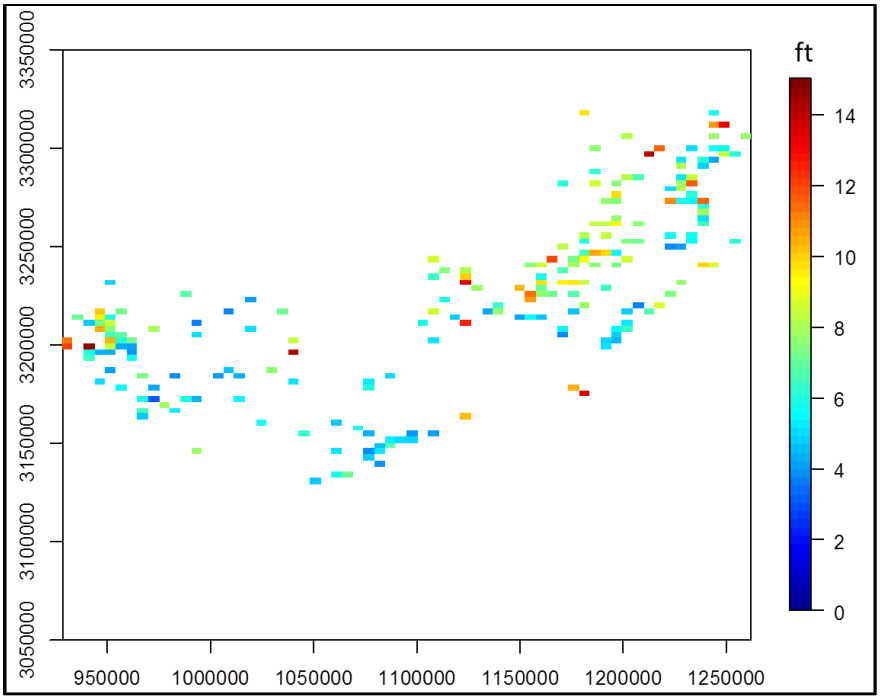

Fig. 66—Average bed thickness of Lower Eagle Ford Shale calculated at vertical wells. Coordinates uses NAD27 system in meters.

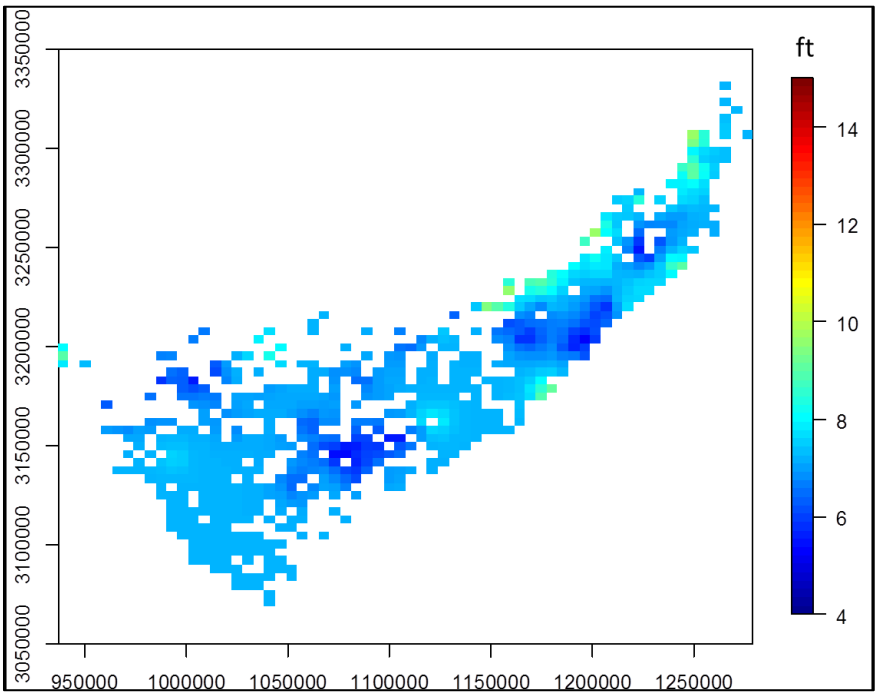

Fig. 67—Average bed thickness of Lower Eagle Ford Shale predicted for Eagle Ford production well locations by kriging. Coordinates uses NAD27 system in meters.

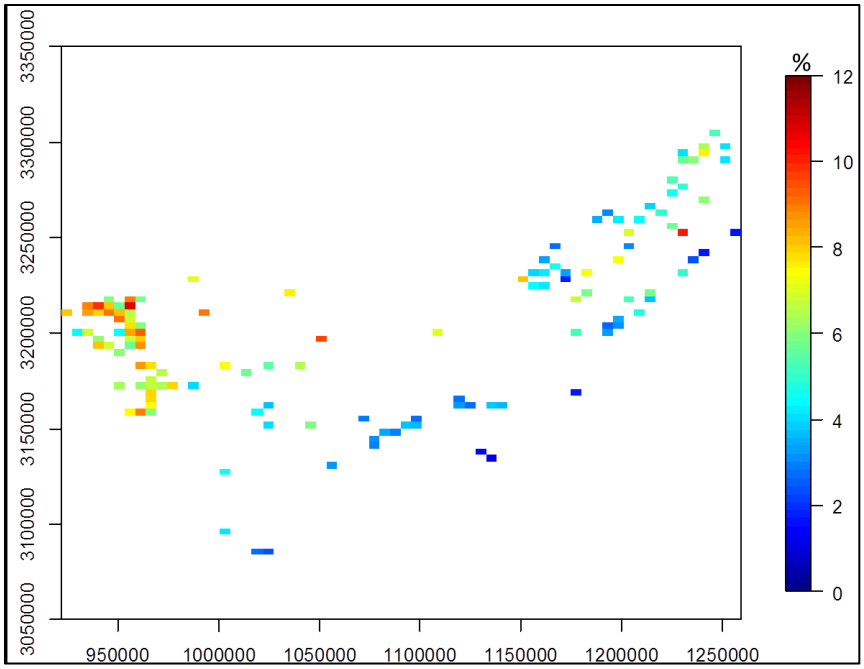

Fig. 68—TOC calculated at vertical wells by petrophysical analyses. Coordinates uses NAD27 system in meters.

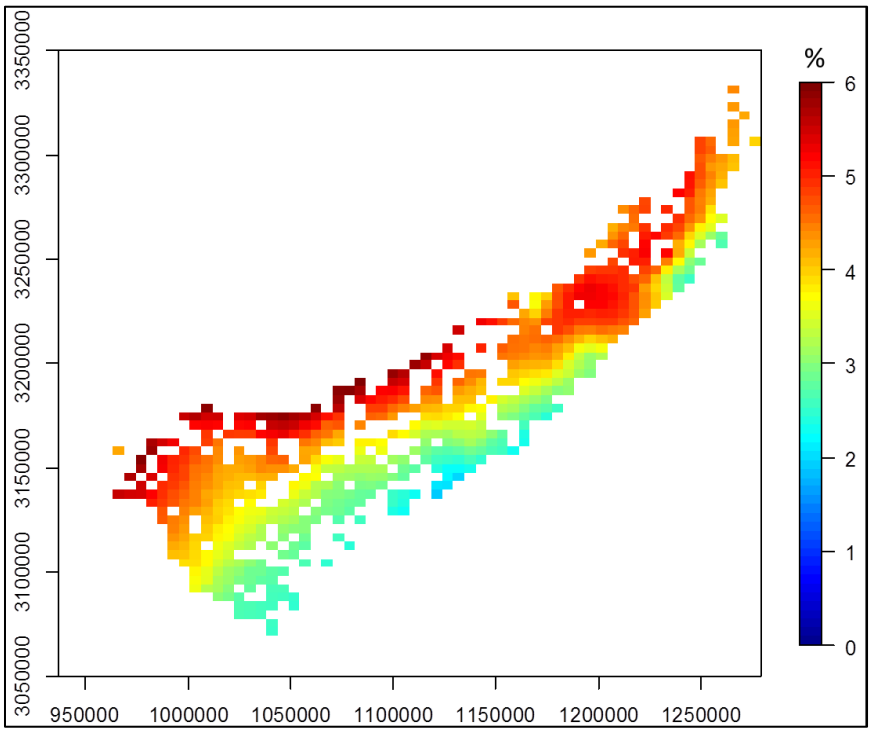

Fig. 69—TOC predicted for Eagle Ford production well locations by kriging. Coordinates uses NAD27 system in meters.

Poisson Distribution Prediction

The Q-Q plot of the number of limestone beds indicates the discontinuous character of limestone beds (**Fig. 70**). By adjusting the starting points, we achieved a model with good convergence in the MCMC model (**Fig. 71**). With the MCMC results, we predicted the number of limestone beds from vertical wells for Eagle Ford production wells (**Fig. 72 and 73**).

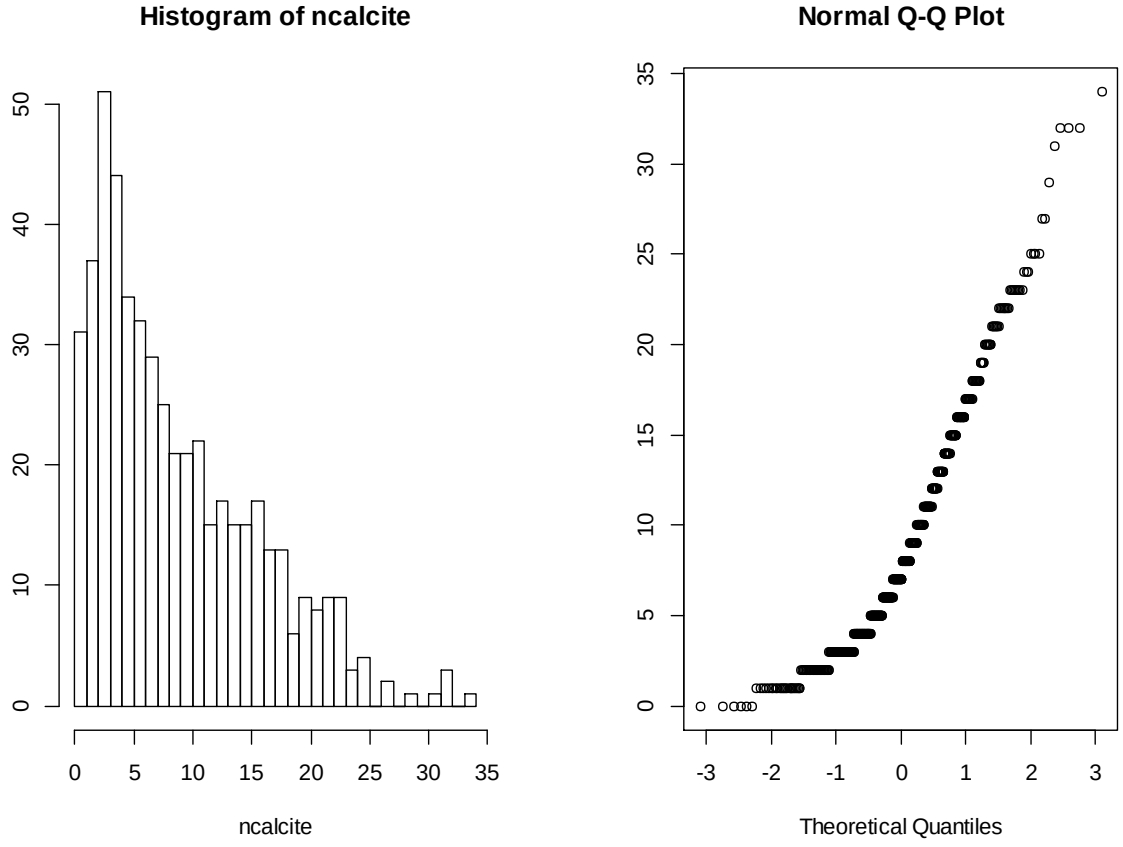

Fig. 70—Histogram and Q-Q plot of number of limestone beds.

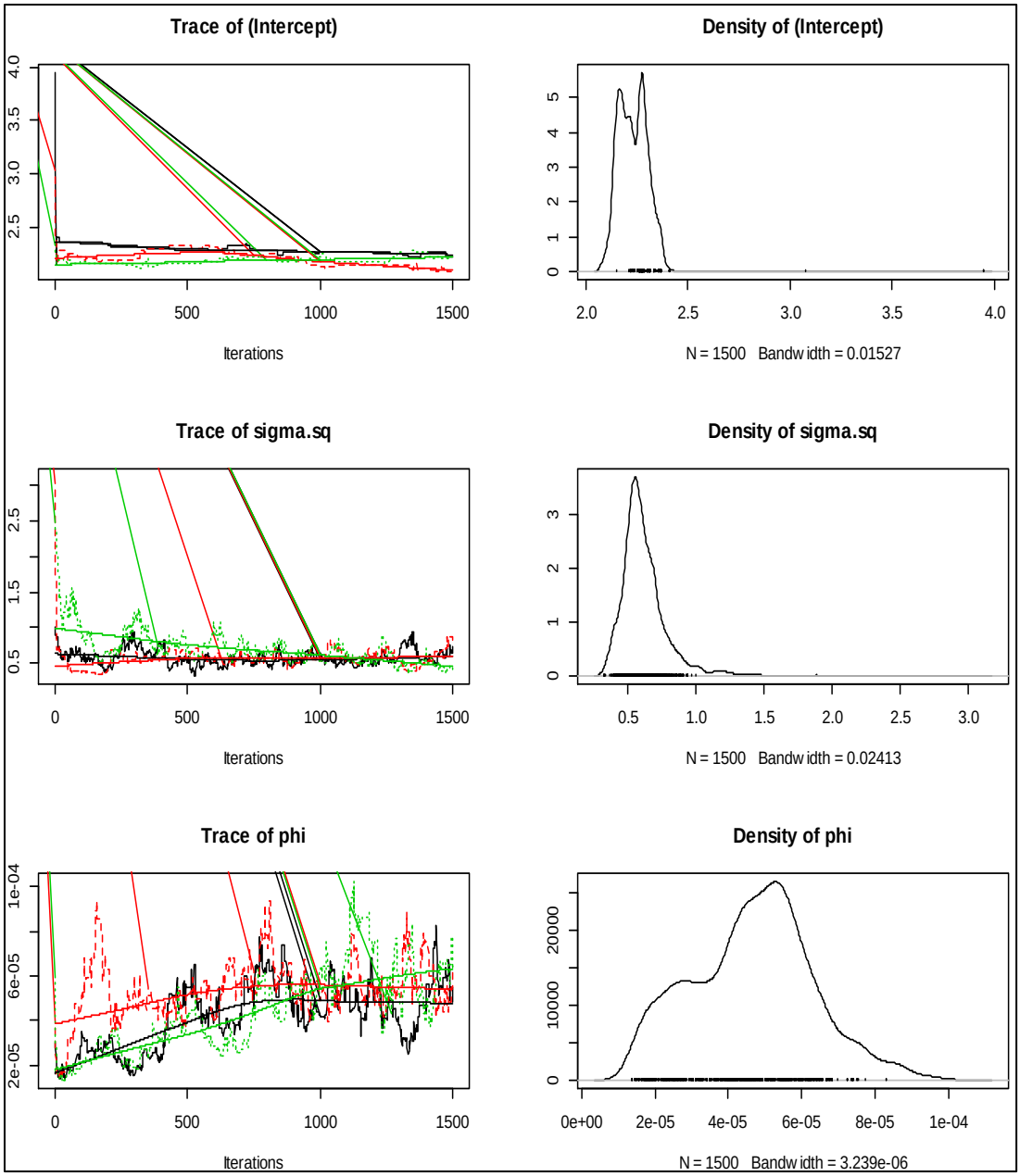

Fig. 71—MCMC sampling of intercept (β), variance (σ^2), and spatial range (ϕ) for the number of limestone beds.

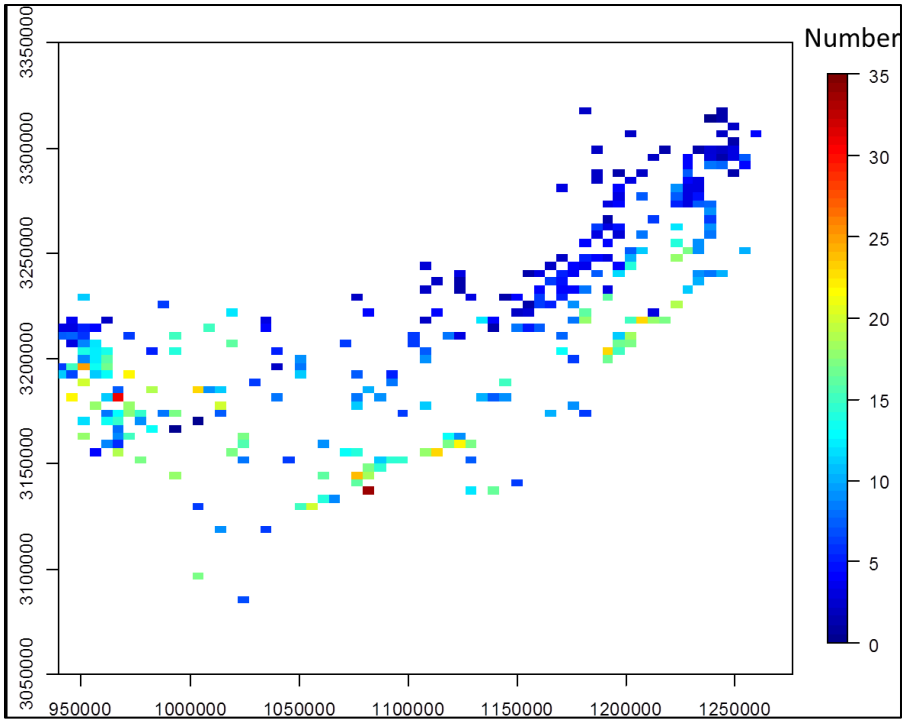

Fig. 72—Number of limestone beds at vertical wells. Coordinates uses NAD27 system in meters.

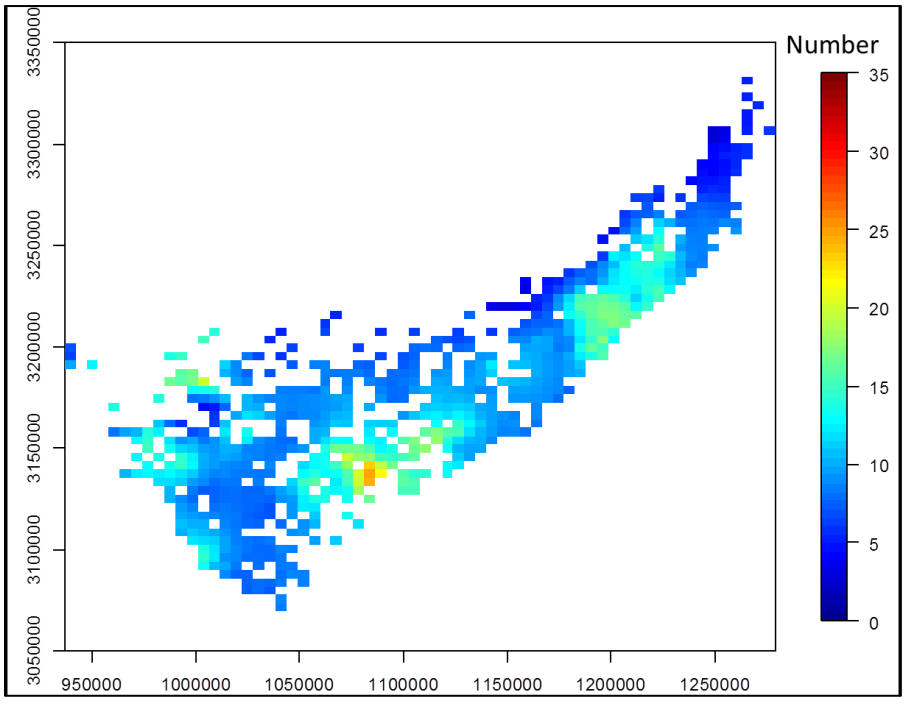

Fig. 73—Number of limestone beds predicted for Eagle Ford production well locations by Bayesian prediction. Coordinates uses NAD27 system in meters.

FITTING REGRESSION MODELS

With the results from the previous steps, we have both the production and geological data for the Eagle Ford horizontal well locations (Fig. 58, 63, 65, 67, 69, and 73). Next, we fitted the regression model and quantified the linear relation between production and other parameters. Although several models were tested, a linear regression model was used to quantitatively evaluate the relations between geological parameters and production. Latitude (X coordinate) and longitude (Y coordinate) were built into the model to characterize the spatial variations.

Step 1. Polynomial Model: In the first model, there is a second-order relation. This is especially true between production and depth. Production initially increases with depth, but after a certain level, production starts to decrease with increasing depth, thereby entering the over-mature gas window.

Step 2. Normalized Production Polynomial Model: In the second model, we transform the cumulative production with 0.4 λ, the same Box-Cox method used to achieve ideal Gaussian distribution. The Q-Q plot indicates that the production data are skewed before transformation and are symmetrical afterwards (**Fig. 74**).

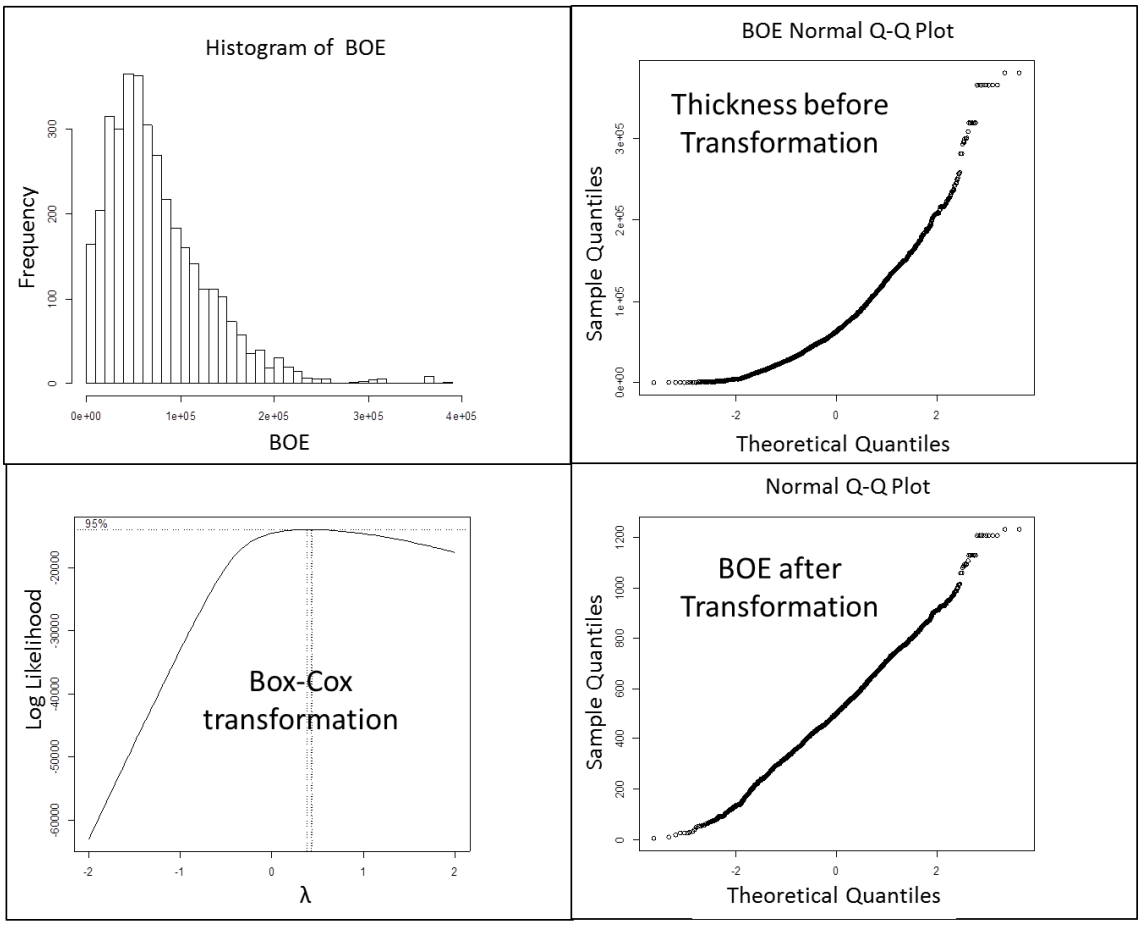

Fig. 74—Transformation of production data for Gaussian distribution without skewness.

Step 3. Scaled Geological Data Normalized Production Polynomial Model: So far, our prediction model has been accurate. But which geological parameter out of the five inputs has the primary on regional production? The traditional method was used to compare the coefficients of the linear regression equation. The magnitudes of the geological data sets, however, are different. Therefore, to directly compare the control weight on oil production, we converted the geological data into unit values by dividing the data by the maximum value of that data set. Therefore, for each geological parameter data set, the values now range from 0 to 1.

All three models provide acceptable production estimation (**Figs. 75 through 77**). There are, however, huge differences in terms of residual value. The second and third production models result in a significantly lower residual; the median is as low as 2 bbl, whereas the median residual of model 1 is as high as 600 bbl. Therefore, normalized production is necessary to achieve a more accurate model.

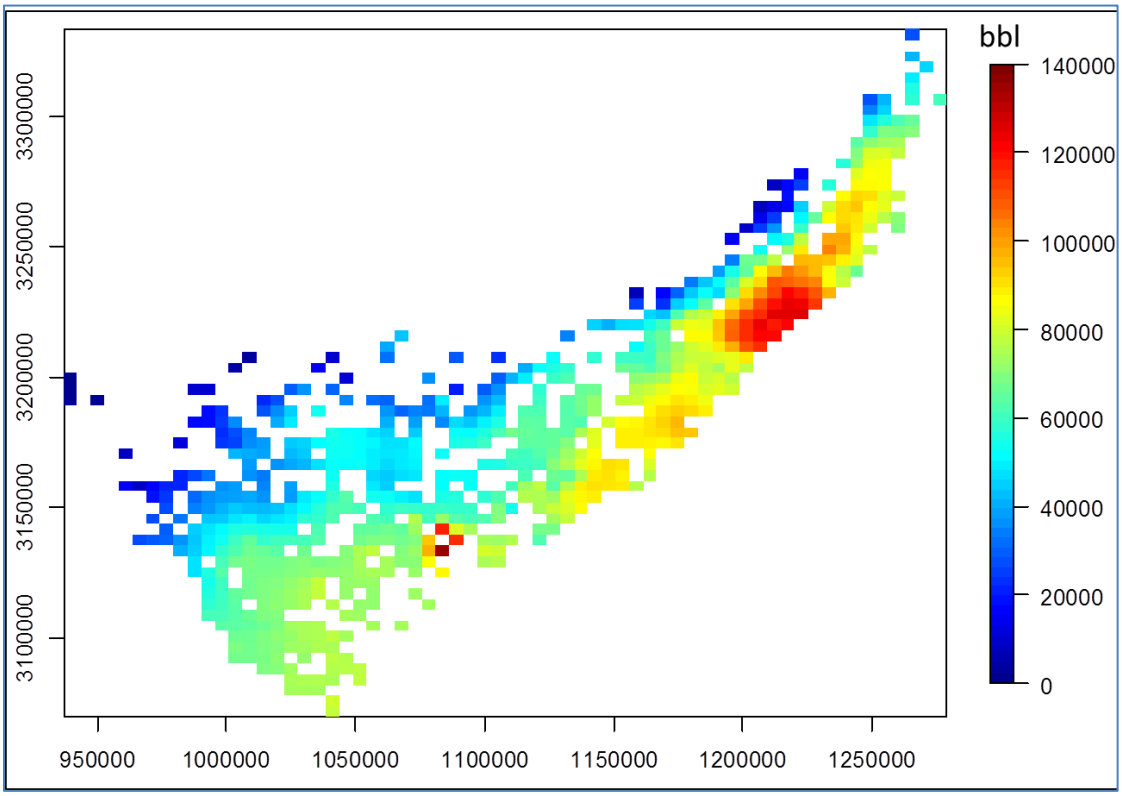

Fig. 75—First 6 months' BOE prediction from model 1. Coordinates uses NAD27 system in meters.

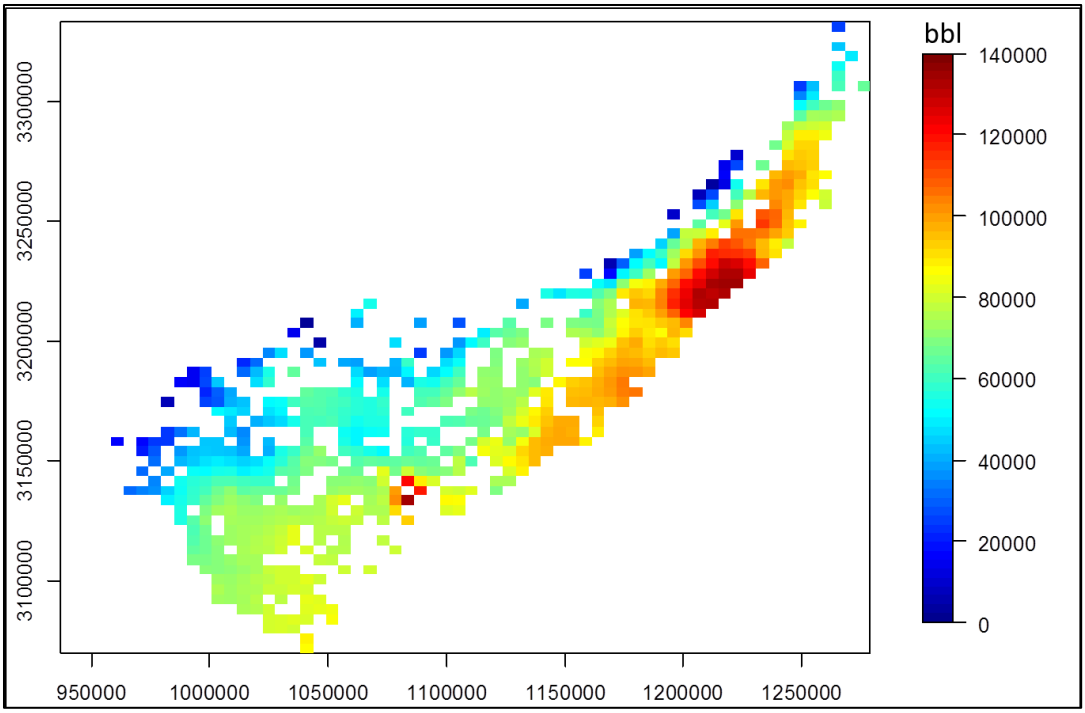

Fig. 76—First 6 months' BOE prediction from model 2. Coordinates uses NAD27 system in meters.

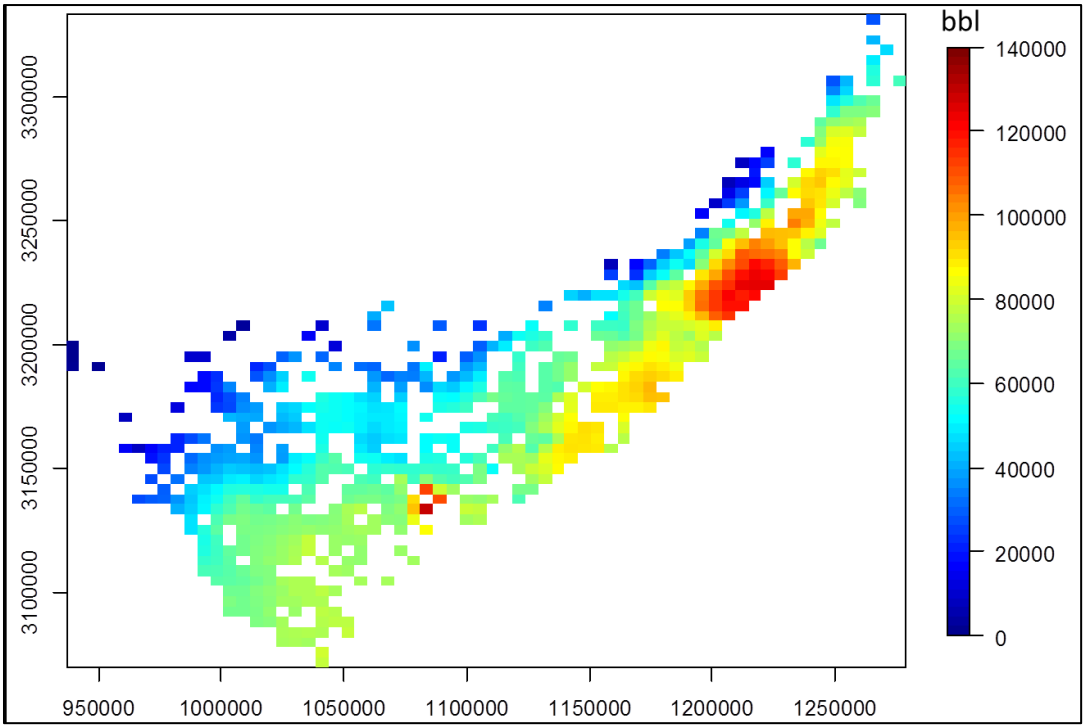

Fig. 77—First 6 months' BOE prediction from model 3. Coordinates uses NAD27 system in meters.

REGRESSION RESULT INTERPRETATION

Coefficient Analysis

The coefficients of depth, thickness, average bed thickness, TOC, and number of limestone beds from three regression models were compared (**Table 2**). Although the coefficient magnitudes of the same parameters from three different models are different, the overall positive or negative influences remain the same. The coefficients from model 3 could be used to analyze the relative importance of each geological parameter on production, since the geological parameters have been converted and range from 0 to 1 (Table 2).

TABLE 2—THE COEFFICIENTS OF GEOLOGICAL PARAMETERS FROM THREE MODELS

	Model 1	Model 2	Model 3
	Polynomial	Norm Polynomial	Unit Norm Polynomial
Depth	3.11E+01	1.63E-01	2.37E+03
$Depth^2$	-7.94E - 04	-5.03E-06	-1.06E+03
Thickness	1.12E+03	3.92E+00	1.19E+03
$Thickness^2$	-3.12E+00	-1.12E-02	-1.03E+03
TOC	5.13E+04	1.78E+02	1.72E+03
TOC	-3.83E+03	-1.40E+01	-1.30E+03
Number of Limestone Beds	-9.72E+03	-3.43E+01	-9.01E+02
Number of Limestone $Beds^2$	3.99E+02	1.43E+00	9.84E+02
Average Bed Thickness	7.11E+04	2.85E+02	2.60E+03
Average Bed $Thickness^2$	-5.05E+03	-2.00E+01	-1.66E+03

The maximum coefficients are from depth and average bed thickness of the Lower Eagle Ford, which suggests that these two parameters play the most significant role in production. By holding the other parameters constant, we plotted each geological parameter against production with the coefficient from model 3. This allowed us to further investigate the relationship between production and these parameters.

Depth vs. BOE Production

Considering other parameters remain constant, we plotted the first 6 months' production against depth by the coefficient achieved from regression model 3. The production increases with structural depth in the entire study area (**Fig. 78**).

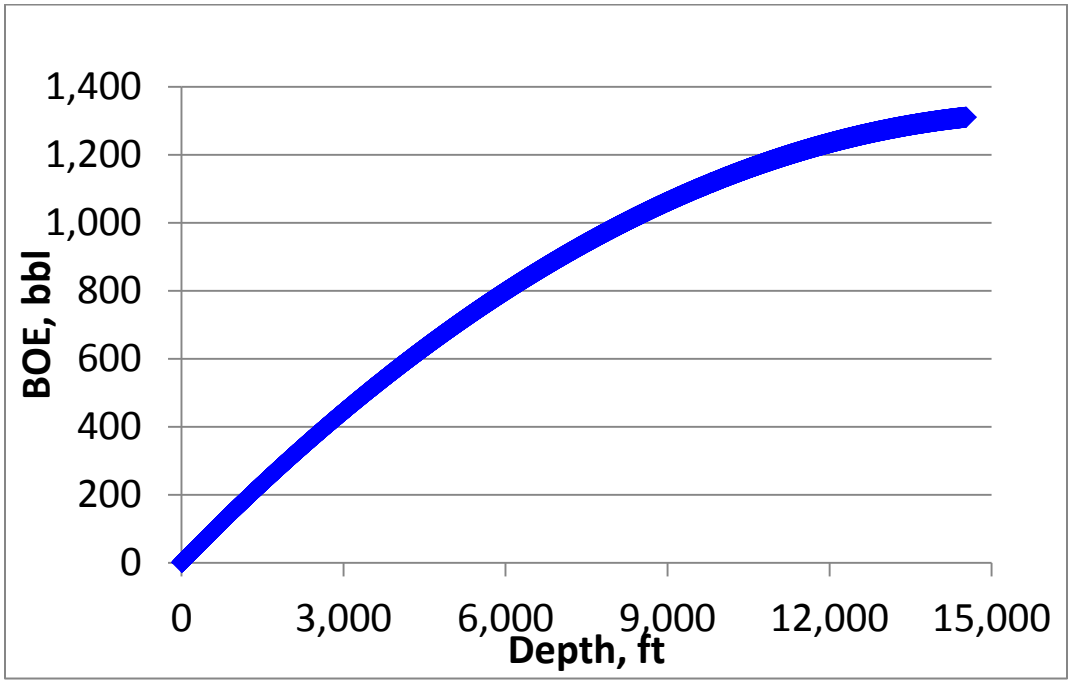

Fig. 78—Depth vs. production correlation of regression model 3.

Thickness vs. BOE

Oil production increases with thickness until the thickness reaches 180 ft. (**Fig. 79**). When the Lower Eagle Ford is thicker than 180 ft., the production declines (Fig. 19). This is reasonable and consistent with observations, because thickness exceeds 180 ft mainly in the Maverick depocenter, where production is relatively low compared to the rest of the study area (Figs.13 and 14).

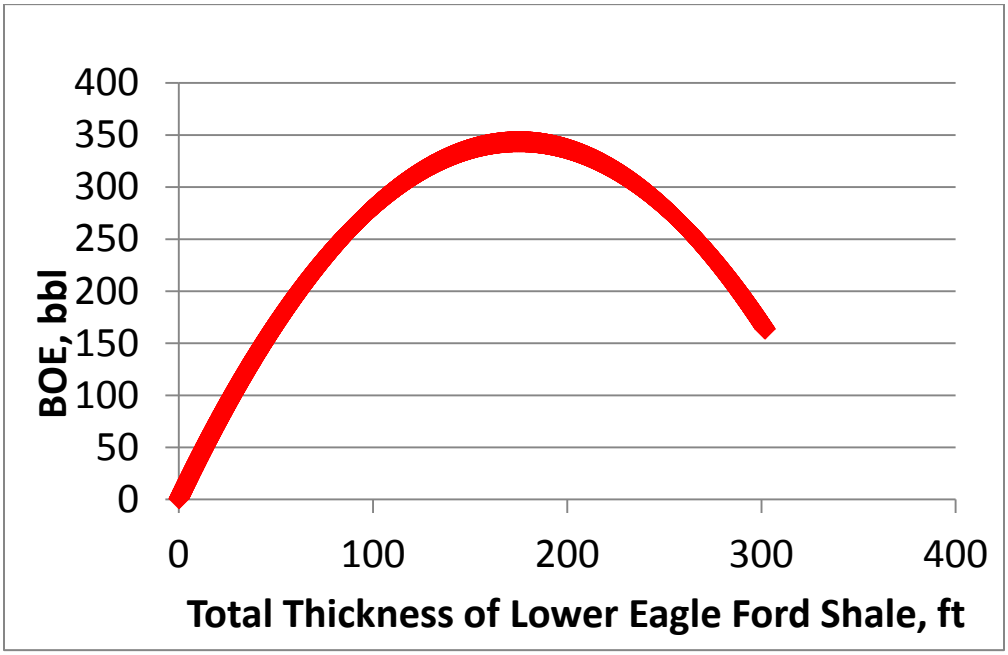

Fig. 79—Total thickness of Lower Eagle Ford Shale vs. production correlation of regression model 3.

TOC vs. BOE Production

Production from initial 6 months increases with TOC until TOC exceeds approximately 7% (**Fig. 80**). If TOC is greater than 7%, then production decreases with TOC (Fig. 80). Several factors may result in such a relationship. TOC greater than 7% may suggest low

thermal maturity and highly ductile rock, both of which have a negative role in overall production.

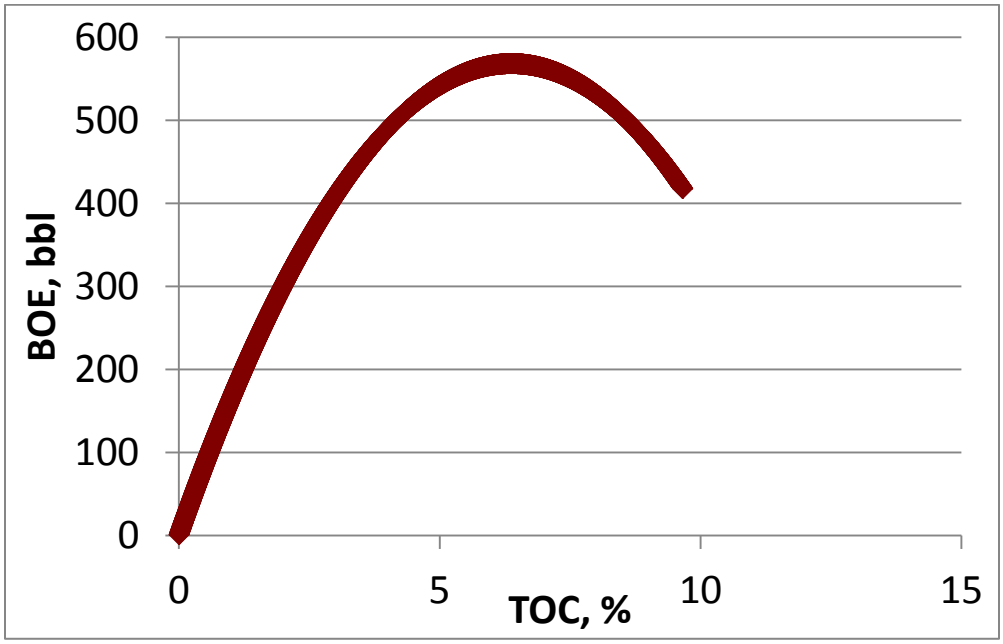

Fig. 80—Average TOC of Lower Eagle Ford Shale vs. production correlation of regression model 3.

Number of Limestone Beds vs. BOE Production

By plotting production against the number of limestone beds, a decreasing and increasing pattern was observed (**Fig. 81**). In the study area, oil production increases with the number of limestone beds. In the northern study area where the total number of limestone beds is less than 12, the correlation between production and number of limestone beds is quite complex, and overall, it negatively impacts the production regionally. In the southern study area, where the number of limestone beds exceeds 12, production is higher.

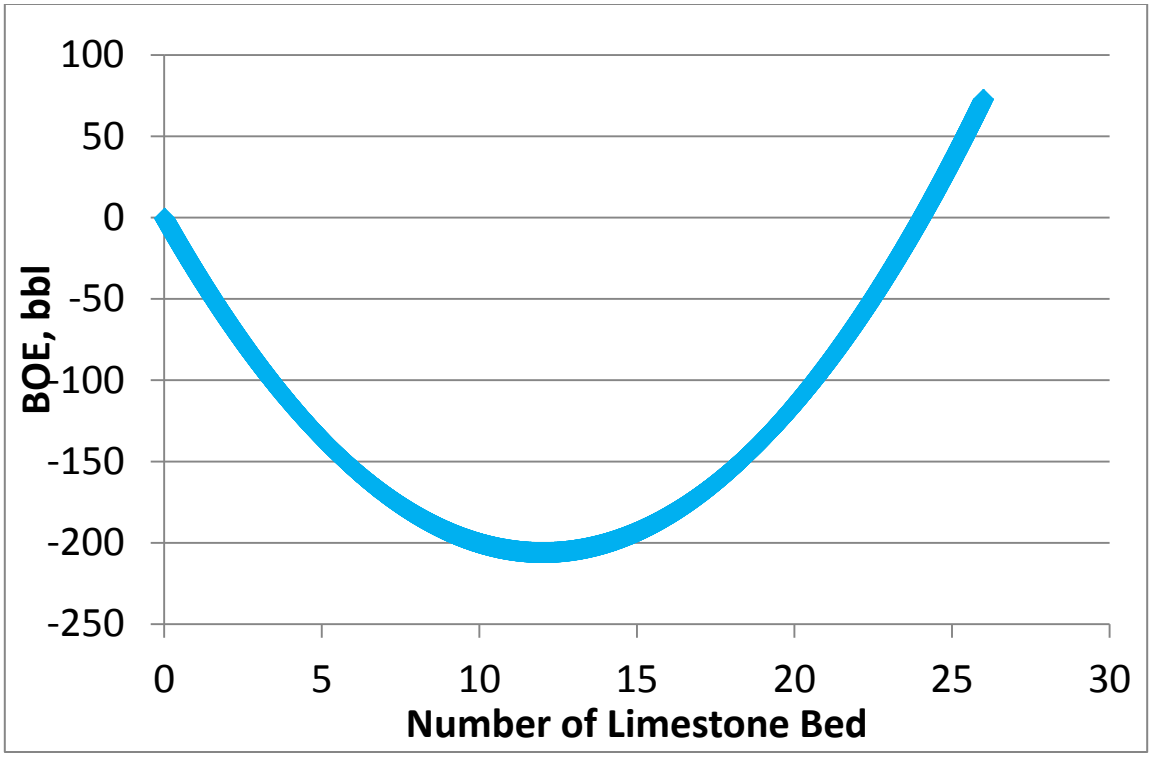

Fig. 81—Number of limestone beds in Lower Eagle Ford Shale vs. production correlation of regression model 3.

Average Bed Thickness vs. BOE Production

By plotting production against the number of limestone beds, an increasing pattern was observed. In the study area, oil production increases with the number of limestone beds. It goes against with the expectation (**Fig. 82**).

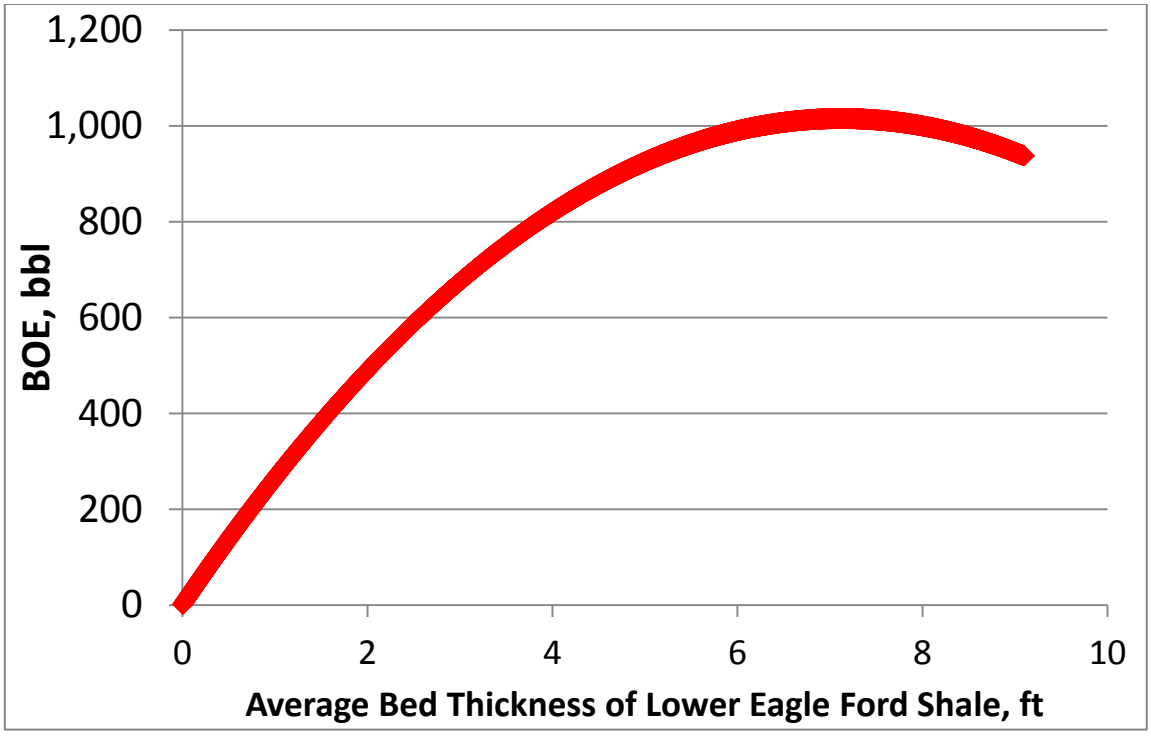

Fig. 82—Average bed thickness of Lower Eagle Ford Shale vs. production correlation of regression model 3.

P-value Analyses

In statistical significance testing, the *p*-value is the probability of obtaining a test statistic at least as extreme as the one that was actually observed, assuming that the null hypothesis is true. The *p*-value can be used to reject the null hypothesis when it is less than a certain significance level, often 0.05. In this project, *p*-values are important to understanding the significance level of data and measuring the weight of the geological data. Coordinates X and Y have high *p*-values, which indicates a high possibility of there being no relationship between production and these parameters. Depth, thickness, limestone bed number, and average bed thickness have low *p*-values, which suggests certainty of the relationship between production and these parameters. The

corresponding significance code level indicates that the most significant parameters to production are TOC and depth. The number of limestone beds also plays an important role, but it is less significant than other properties. Thickness plays a moderate role in production (**Table 3**).

TABLE 3—*P*-VALUES AND SIGNIFICANT CODES OF GEOLOGICAL PARAMETERS IN REGRESSION MODEL 3.

	p-Value	Significance Code
Depth	< 2e-16	***
$Depth^2$	4.10E-09	***
Thickness	6.63E-07	***
$Thickness^2$	2.08E-06	***
TOC	< 2e-16	***
TOC^2	5.65E-15	***
Number of Limestone Beds	3.62E-11	***
Number of Limestone $Beds^2$	5.67E-12	***
Average Bed Thickness	1.21E-04	**
Average Bed $Thickness^2$	5.57E-04	**
X Coordinate	0.168047	
Y Coordinate	0.105604	

LIMITATIONS

Kriging may be used to predict geological parameters at locations where no measured values are available, on the basis of nearby data. It is especially useful when limited well control is present. However, kriging has limitations when applied to a large area. Kriging interpolates values for unknown locations without considering the possible local heterogeneity in geological parameters. Without sufficient sample density, local geological variability will not be accurately detected, and thus, considerable geological details may be lost during the kriging. Therefore, variability identified by kriging will be less than the true variability in Eagle Ford Shale.

CHAPTER VI

RESERVOIR MODELING

PRODUCTION DATA USED IN RESERVOIR MODELING

We built reservoir models for four wells comprising two volatile oil wells, one gas condensate well, and one dry gas well **(Figs. 83 through 86)**. Volatile oil and gas condensate wells with complete histories were from the same field in the northeastern study area. Data included gas production, oil production, and bottom hole pressure; however, the well name, well geometry, stimulation treatment, and reservoir properties were unknown.

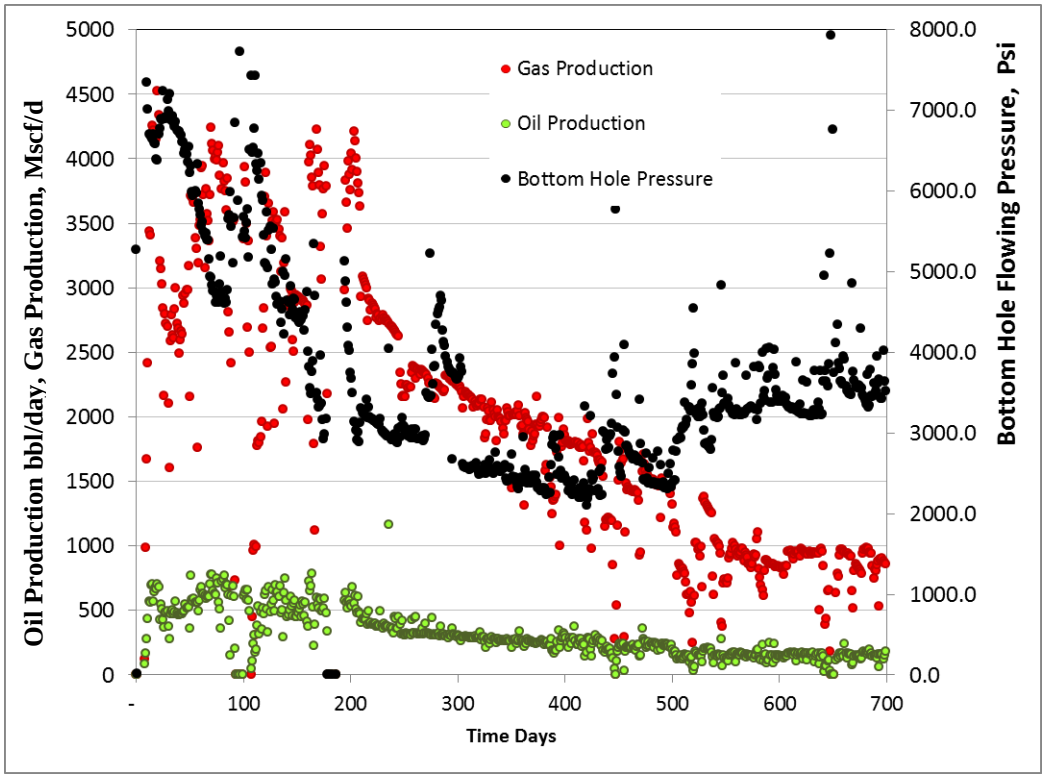

Fig. 83—Production history for gas condensate well.

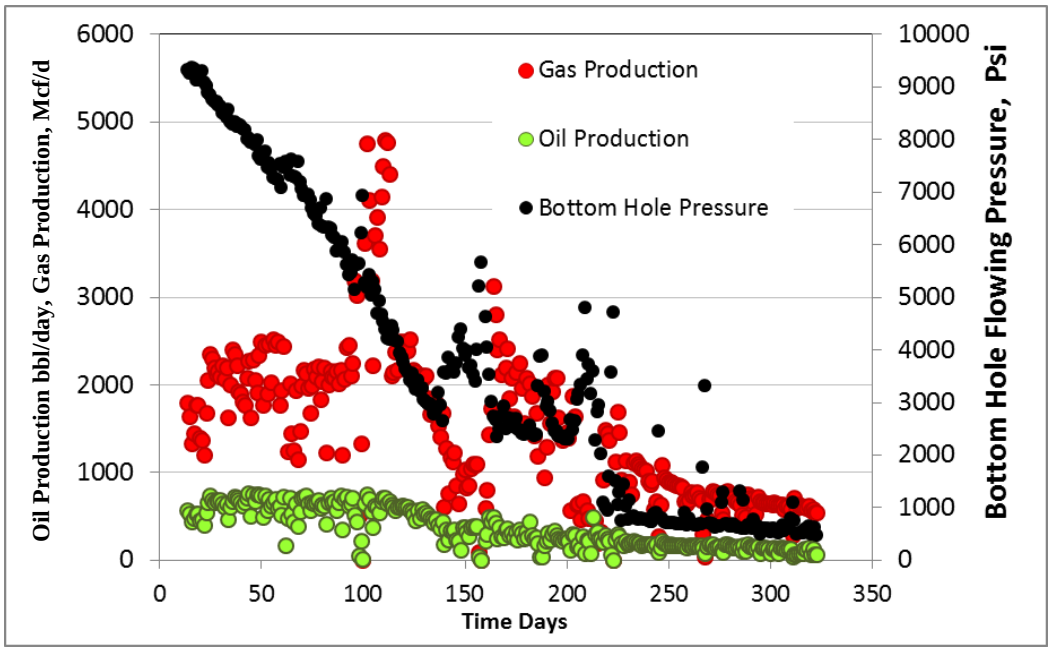

Fig. 84—Production history for volatile oil well No. 1.

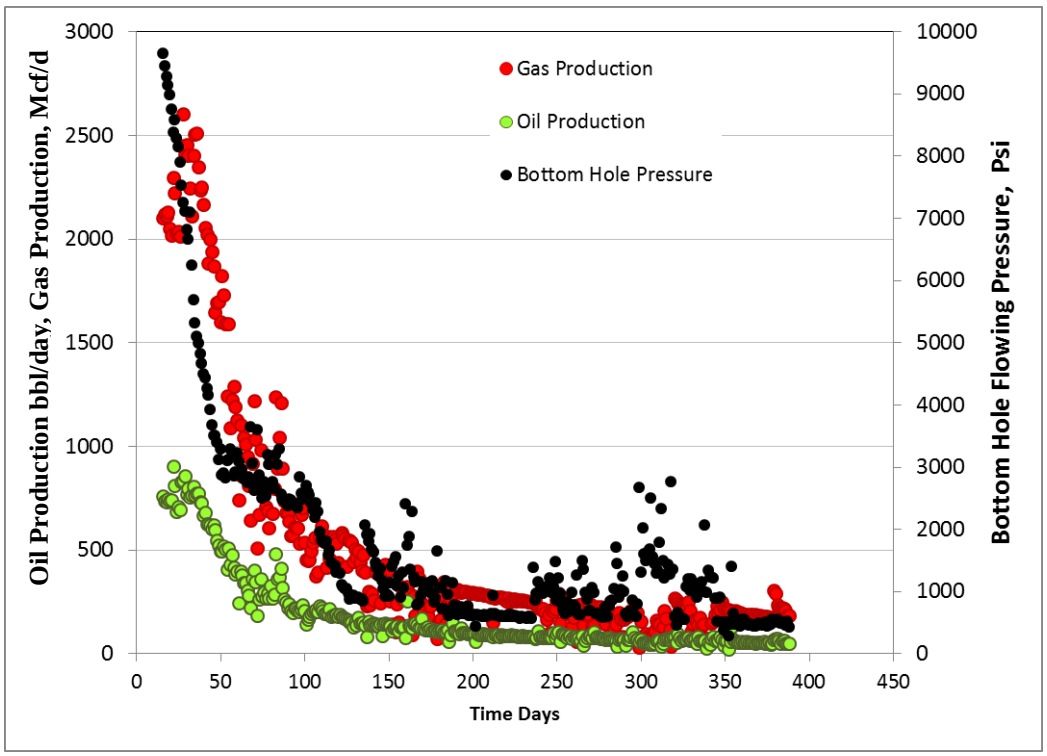

Fig. 85—Production history for volatile oil well No. 2.

Pressure and production data of a dry gas well were retrieved from a publication on Eagle Ford Shale (Fig. 86). The horizontal well geometry, stimulation treatment, production logging data and overall average reservoir properties were given for the dry gas well **(Table 4)** (Bazen et al. 2010)

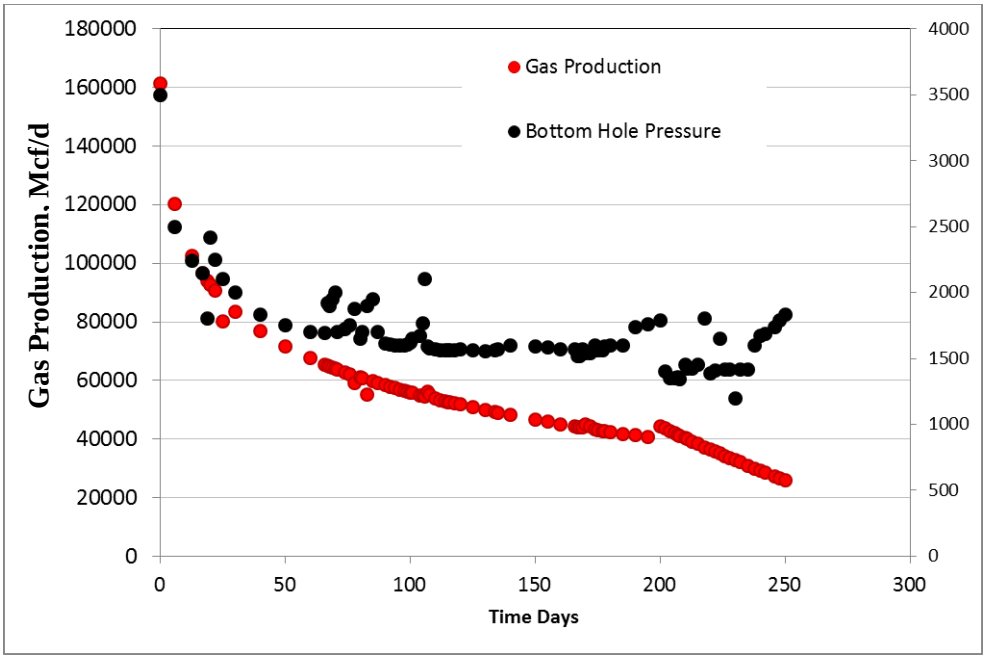

Fig. 86—Production history for dry gas well (Bazen et al. 2012).

TABLE 4—RESERVOIR AND FRACTURE PROPERTIES FOR THE DRY GAS WELLS (BAZEN ET AL. 2010)

Wellbore Radius (ft)	0.333
Lateral Length (ft)	4,000
Number of Stages	10
Number of Clusters per Stage	4
Depth, TVD (ft)	10,875
Pay Zone Height (ft)	283
HC* Porosity (%) *($\phi_{hc} = \phi_{eff}(1\text{-}S_w)$)	5.76
Reservoir Pressure (psi)	8,350
Specific Gravity	0.621
Temperature (°F)	285
BHFP (psi)	3,950 – 1,875
Drainage Area (acres)	80
Aspect Ratio, $\lambda = x_e / y_e$	1/4
Reservoir Size (x_e, y_e), (ft)	933.38, 3733.52

VOLATILE AND GAS CONDENSATE WELL MODELING

Reservoir Geometry

A single-well, base-case model was created for each production region. The dry gas model was built based on actual data from the same well, including the thickness, depth, drilling and stimulation information (Table 4). Such data were not available for the gas condensate and volatile oil wells; therefore, the geometry of the volatile and gas condensate model was carefully designed by studying the typical Eagle Ford Shale horizontal wells. First, typical drilling and completion practices in the Eagle Ford Shale were investigated using Drillinginfo (2013). The average perforated intervals for horizontal wells in the Eagle Ford Shale are approximately 4,500 ft **(Fig. 87)**

(Drillinginfo 2012). Most of Eagle Ford Shale horizontal wells were stimulated by 15 stages of hydraulic fracturing and four fracture clusters per stage (Bazen et al. 2010). The efficiency of completion and stimulation varied greatly. Previous production logging results commonly showed that two out of the four fracture clusters in each fracturing stage were successful (Bazen et al. 2010). Therefore, there are 30 fractures that contribute to total production. Each fracture cluster covers 150 ft, which is 1/30 of the entire 4,500 ft long horizontal wellbore. Each well occupies from 60 to 160 acres in the Eagle Ford Shale (drillinginfo 2013). Assuming 80 acres/well, the distance between two horizontal wells is 660 ft, which means the fracture extends 330 ft from the wellbore.

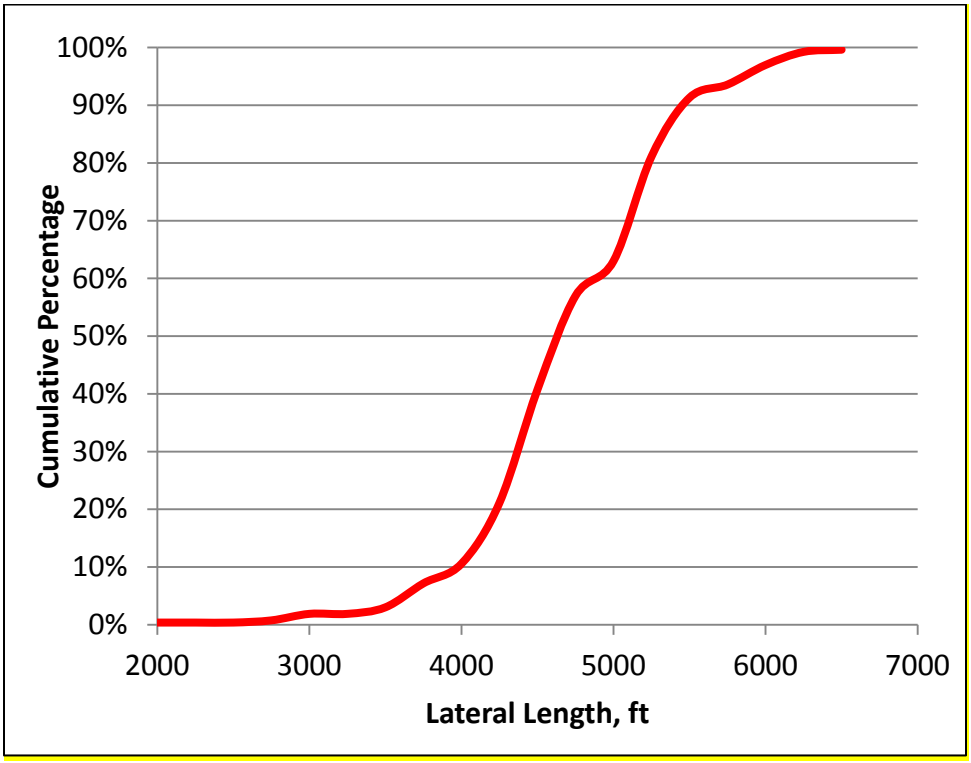

Fig. 87—Lateral length distribution of Eagle Ford Shale horizontal wells. Data from Drillinginfo (2012).

The volume of the reservoir model is 1/60 that of the entire well to reduce the amount of computation time upon reservoir simulation (**Fig. 88**, **Table 5).** The dimensions of the oil wells are 13×17×11 in the number of cells in each direction, with 2,431 grid cells in the model. To capture the pressure variation in the proximity of a fracture in the oil well, more grid cells were created as a local refinement around each fracture. The dimensions of dry gas and gas condensate wells are 9×17×11 in the number of cells in each direction, with 1,683 cells. Eleven layers were designed for the volatile oil, gas condensate, and dry gas wells.

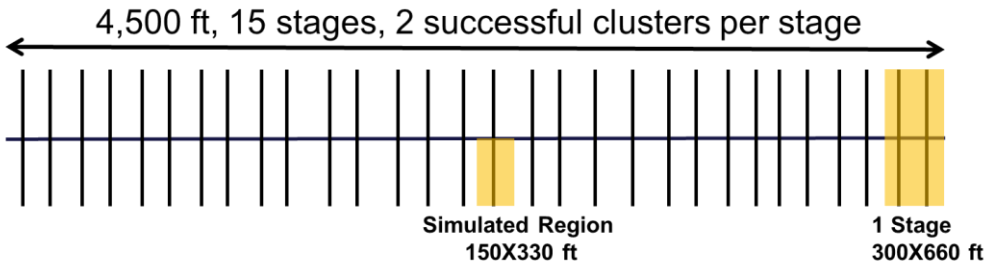

Fig. 88—Geometry for base case reservoir model for all production regions.

TABLE 5—RESERVOIR MODEL GEOMETRY DESIGN			
Typical Well in Eagle Ford		Simulation Model	
Typical lateral length, ft	4500	X, ft	150
Number of fracturing stages	15	Y, ft	330
Number of hydraulically fractures	30	Number of grid cell in X direction	11/9
Distance between fractures, ft	150	Number of gridblocks in Y direction	17
Well spacing, acres/well	80	Number of gridblocks in Z direction	11
Distance between wells, ft	660	Fraction of well	1/60

Model Setup

The model components varied by fluid regions. The dry gas model was a single-porosity, single-permeability system using the Peng–Robinson correlation equation of state. In the oil and gas condensate regions, the reservoir models were designed to be a single-porosity, single-permeability compositional system.

Reservoir Properties

Reservoir properties used in the models of the gas condensate and volatile oil wells, including depth and thickness, were determined by stratigraphic analysis from the previous chapter (Figs. 25 and 32, **Table 6**). Other parameter inputs, such as saturation and porosity, were obtained from Eagle Ford Shale publications (**Table 7**) (Quirein et al. 2013; Zhang, et al. 2013). Matrix porosity and permeability are homogeneous within each model layer and each lithology (Table 7). Instead of using uniform fracture permeability, we designed a fracturing plane with decreasing permeability from the center **(Fig. 89).** We assumed that the horizontal well lands in the middle of the Lower Eagle Ford Shale. Therefore, central layers (layers 4, 5, and 6) have the maximum fracture permeability (Fig. 89).

TABLE 6—DEPTH AND THICKNESS FOR RESERVOIR MODELS OF GAS CONDENSATE AND VOLATILE OIL REGIONS		
	Volatile Well Models	Gas Condensate Model
Depth, ft	10,000	11,000
Thickness, ft	120	160

TABLE 7—RESERVOIR PROPERTIES FOR INPUT BEFORE HISTORY MATCH			
Layers	Porosity, %	Permeability, ND	Water Saturation %
1–8	8	400	25
9	10	20	40
10	4	800	20
11	10	20	40

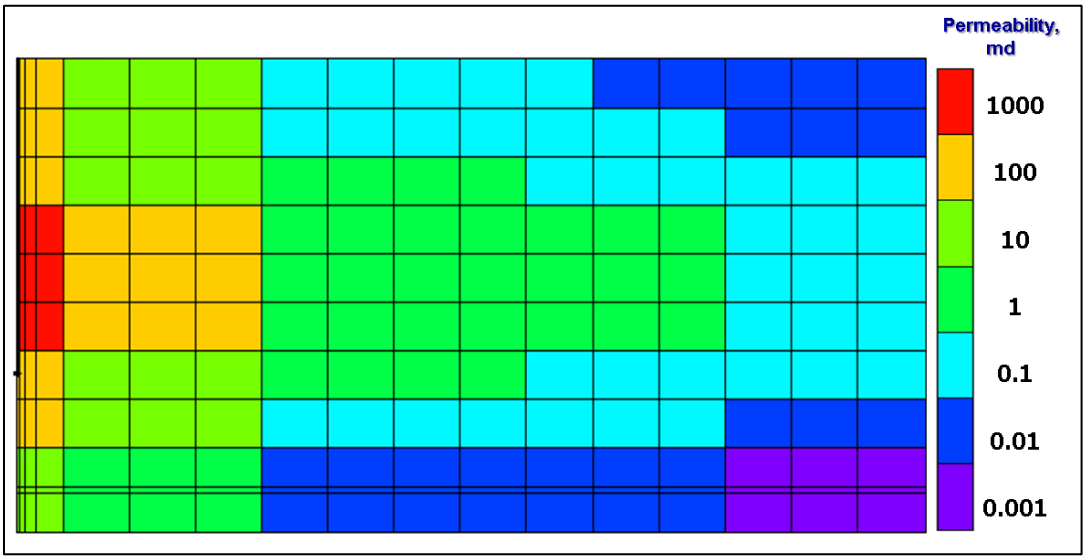

Fig. 89—Fracture permeability of the fracturing plan.

Two types of lithology were used in the reservoir models. The properties, including relative permeability **(Figs. 90 and 91),** compaction **(Figs. 92 and 93),** water saturation, porosity, and permeability, varied among the different systems. The first lithology was organic-rich marl, which has high porosity, high water saturation, high compaction, and low relative permeability. The second was a combination of limestone bed interbedded with ORM, referred to as the calcite-rich interval. Being more calcite rich, the second lithology had relatively lower porosity, low water saturation, low compaction, and high relative permeability.

Of the 11 layers, layers 1 through 8 were a mixture of the interbedded limestone and OMR. Layers 9 and 11 were thick, organic-rich marl with a thin limestone bed between them. The gridblocks of fracturing also have a different set of properties with a significantly higher permeability and compaction multiplier (Table 7).

Relative Permeability

Relative permeability data were generated using Corey's exponent correlation method for the two lithologic components in the reservoir model. The residual water saturation of ORM was as high as 40% (Fig. 90), whereas it was only 12% for the combination of both lithologies (Fig. 91).

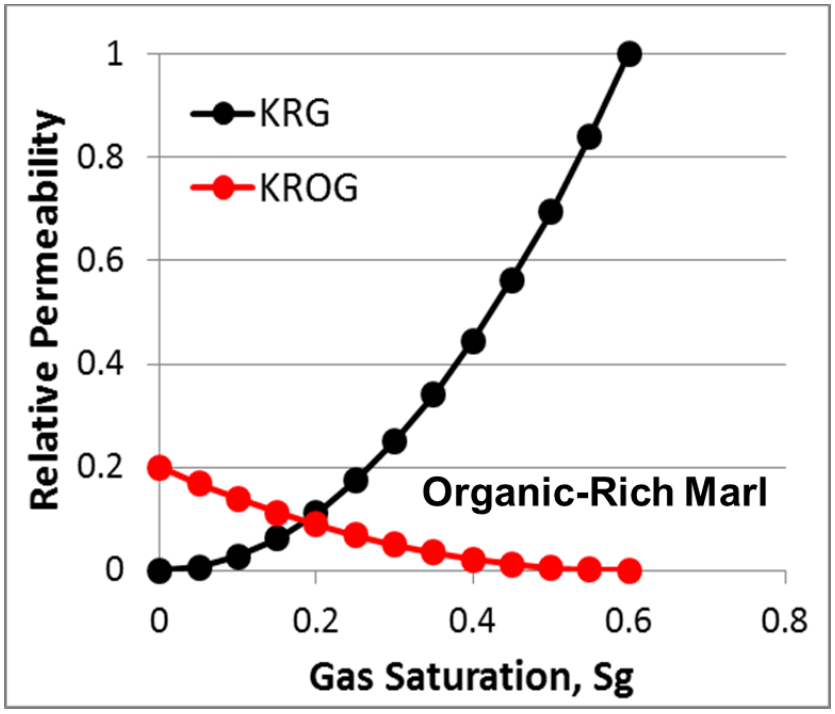

Fig. 90—Relative permeability generated by Corey's correlation for organic-rich marl.

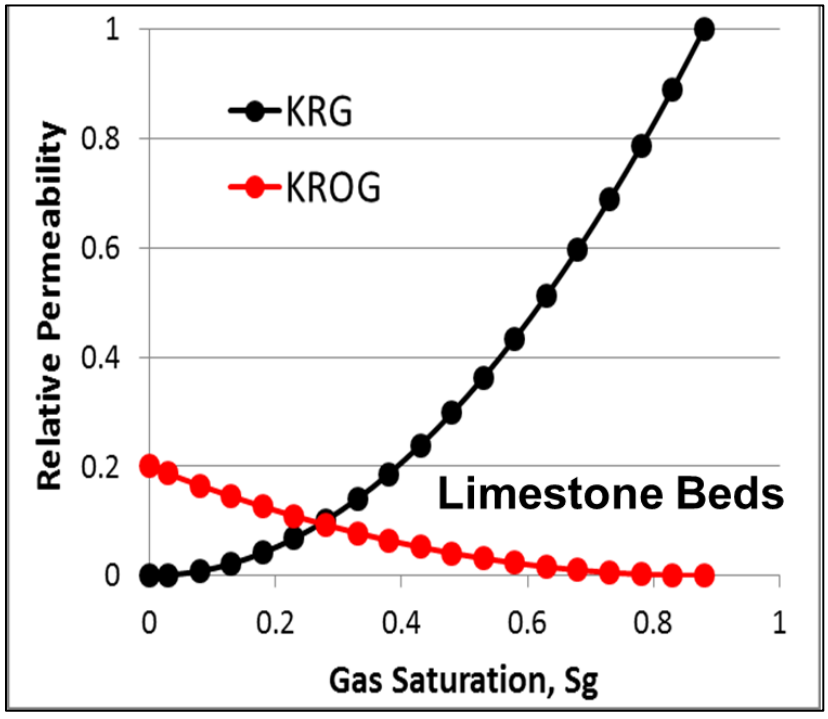

Fig. 91—Relative permeability generated by Corey's correlation for the limestone beds.

Transmissibility Multiplier

Compaction has a strong impact on fluid flow in both matrices and hydraulic fractures, which can be characterized by the relationship of transmissibility to pressure as *Trans_Multi* = C * exp(*Expo* * *p*) (Honarpour et al. 2012; Zheng et al. 2013). Three chains of transmissibility multiplier vs. pressure were used for limestone, ORM, and hydraulic fractures (Fig. 92) (Honarpour et al. 2012). Porosity transmissibility multiplier vs. pressure correlated was generated using the same equation, but with a slower decline (Fig. 93).

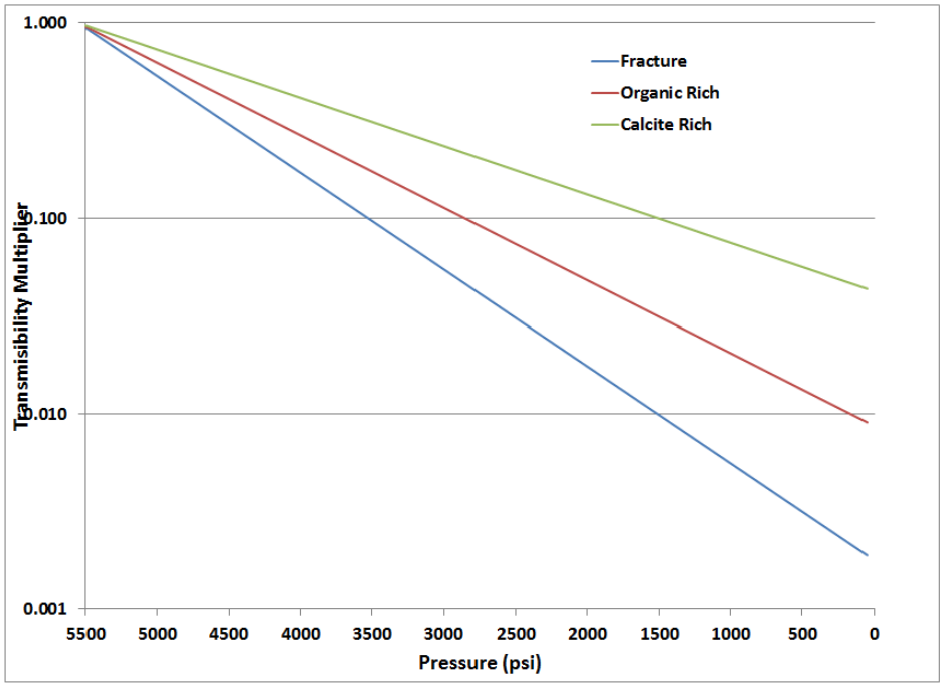

Fig. 92—Pressure-dependent permeability for hydraulic fracture, ORM, and limestone (Honarpour et al. 2012).

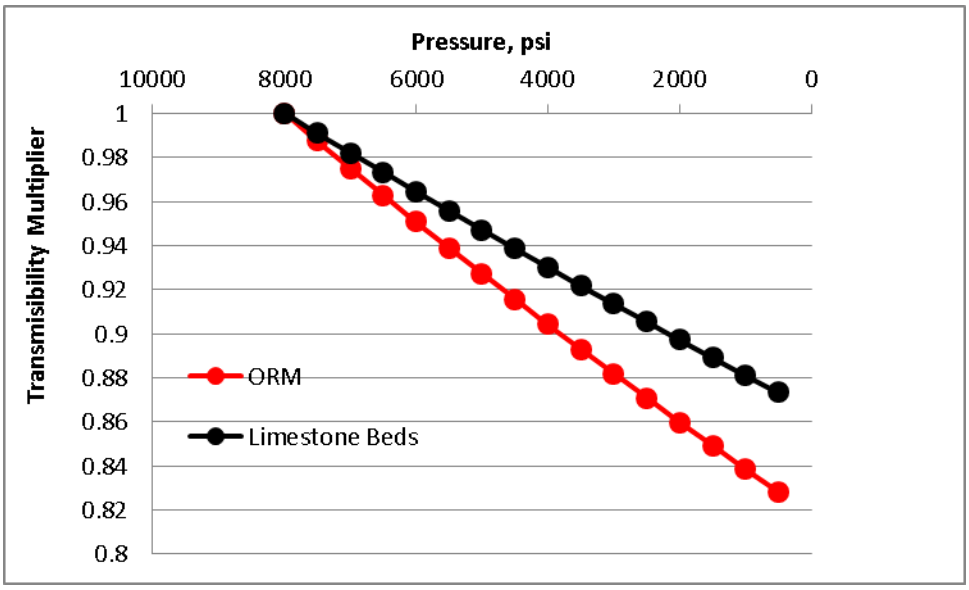

Fig. 93—Pressure-dependent porosity for ORM and calcite-rich rocks.

Pressure/Volume/Temperature (PVT) Data Acquisition

PVT reports were selected for both the oil and gas condensate regions and were built into the simulation models in Computer Modeling Group Ltd. (CMG) software. The wells tested in the PVT reports had approximately the same initial gas/oil ratio (GOR) and were from the same field as the well in the reservoir model. Reservoir temperature, oil gravity, bubble or dew point pressure (Table 8), and composition of each fluid component **(Table 9)** were imported into CMG**.** Constant composition expansion results were imported into the reservoir models, and phase diagrams were created based on the CMG phase analysis simulation for the volatile oil and gas condensate models **(Figs. 94 and 95).**

TABLE 8—SUMMARY OF FLUID PROPERTIES USED IN THE RESERVOIR MODELS FOR PVT BEHAVIOR				
	Oil API Gravity	Reservoir Temperature, °F	Bubble/Dew Point Pressure, psi	Gas/Oil Ratio, Scf/bbl
Volatile Oil	50	319	4,210	2,800
Gas Condensate	52.4	325	4,165	3,800

TABLE 9—COMPOSITION AND C7+ PROPERTIES FOR THE RESERVOIR MODELS		
	Volatile Oil, mole%	Gas Condensate, mole%
H2S	0.00	0.00
N2	0.0091	0.13
CO2	1.09	1.59
C1	56.79	59.98
C2	12.274	12.01
C3	6.404	5.64
IC4	1.440	1.47
NC4	2.575	2.49
IC5	1.092	1.32
NC5	1.041	1.25
C6	1.341	1.64
C7+	15.81	12.49
C7+ Molecular Weight	164.63	156.69
C7+ Specific Gravity	0.8	0.79

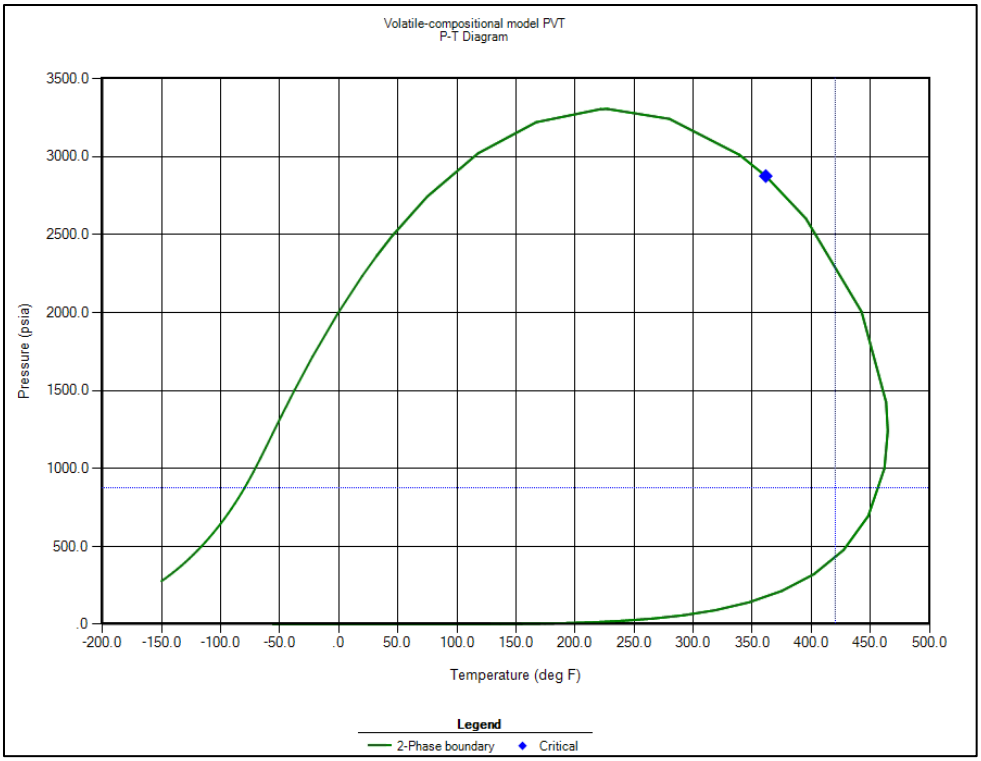

Fig. 94—Phase diagram used in the volatile oil model.

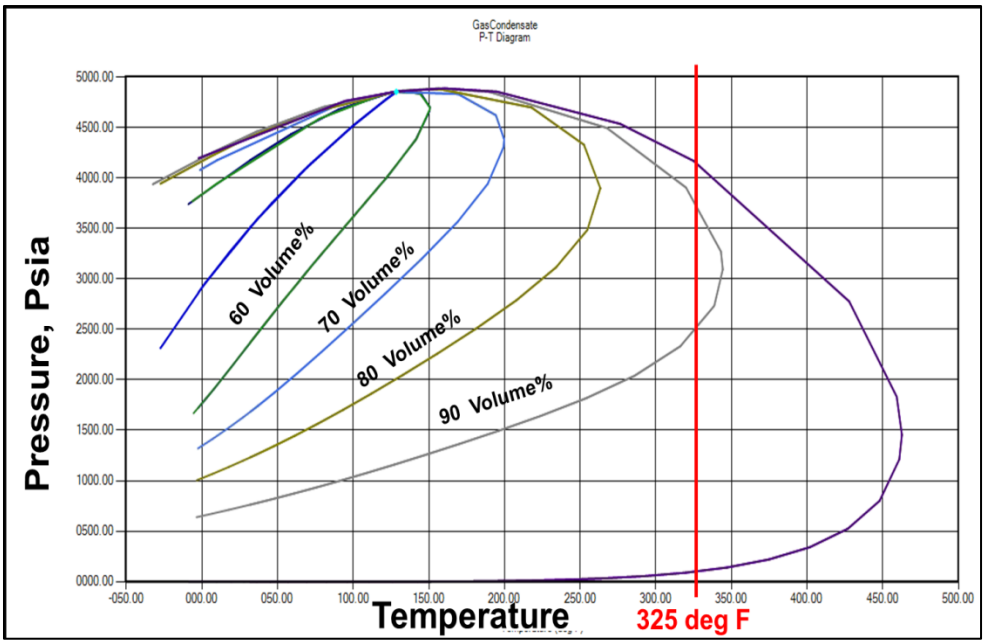

Fig. 95—Phase diagram used in the gas condensate model.

VOLATILE OIL AND GAS CONDENSATE WELLS SIMULATION RESULTS

Gas Condensate Well History Match

We used gas production as a constraint and performed a history match to characterize the simulation model. To test the uncertainty of the reservoir models, we began with various combinations of reservoir parameters. By modifying the transmissibility multiplier, we investigated how the compaction factor would impact production. A lower relative permeability dataset was created and was also used in the model to test production sensitive to relative permeability (**Fig. 96**).

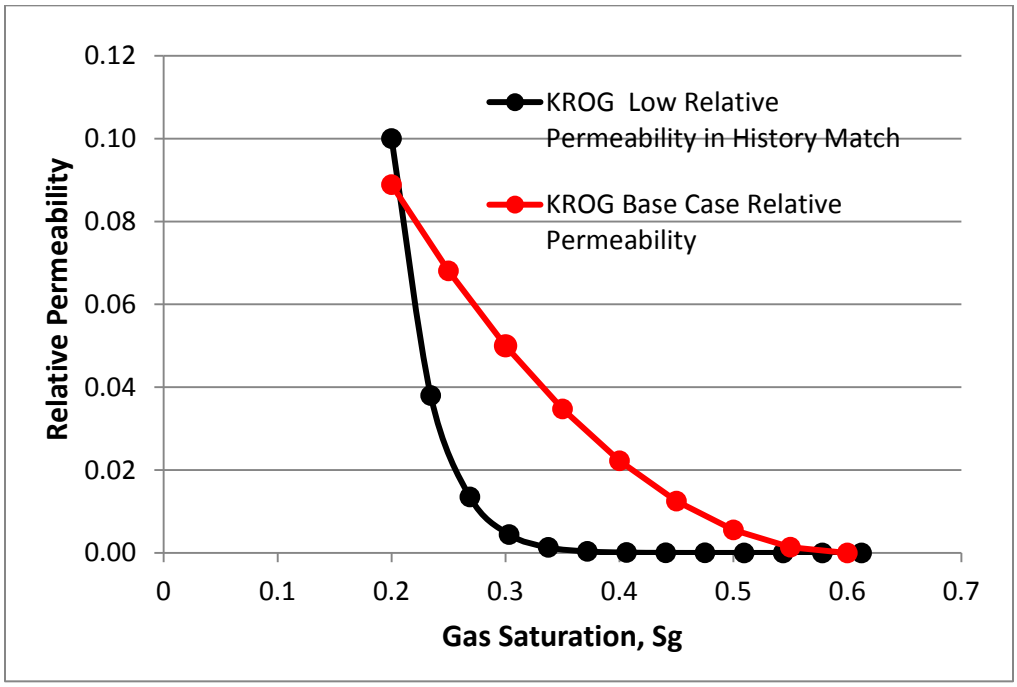

Fig. 96—Low relative permeability used in the history match process.

Several good matches were achieved for both simulated bottomhole pressure and oil production **(Figs. 97 through 103).** The reservoir properties in each model of good

history results were summarized and are presented in **Tables 10 and 11.** Overall, the parameters that influenced the match results of early phases were in-place hydrocarbon volume and fracture permeability. In the reservoir model, the hydrocarbon volume was determined by porosity, saturation, reservoir height, and area. Drainage area had been fixed by the features of the hydraulic fractures. The late phase of history was controlled more by properties of the matrix, such as matrix permeability.

Match 1 is the base case, presuming that there are both organic-rich marl and limestone beds in layers 1 through 8. There are good matches between both simulated pressure vs. pressure history and simulated GOR and GOR history **(**Fig. 97**).** Matches 2 and 3 were built to tests the possibility of good history match results with only limestone in the Eagle Ford Shale in layers 1 through 8 (Figs. 98 and 99). When significant calcite was present in Eagle Ford Shale, the relative permeability of calcite-rich data set was used, and a history match showed that lower matrix relative permeability was required. With other parameters being the same, by adjusting matrix permeability and fracture permeability, various combinations were available for good history match results.

Compared to base match 1, match 4 had lower matrix permeability and a lower transmissibility multiplier. Lower transmissibility suggested less compaction during decreasing pressure; lower matrix permeability was expected. But the fracture permeability was also higher; therefore, lower matrix permeability was needed to match the pressure decline for the same production.

Significantly lower relative permeability was used in match 5 model. We were still able to obtain history match with a matrix permeability increase of approximately 25%. The results suggest that the overall production and pressure decline were not sensitive to relative permeability.

We increased the water saturation in the reservoir models of matches 6 and 7. When water saturation was increase by 20% from the base model, the needed matrix permeability was 2.4 times greater. When water saturation was increased to as high as 40%, porosity was increased to counteract the decrease in volume. To have a good match in the early phase, fracture permeability was doubled. Because the relative permeability used in this model was twice that of the base model, matrix permeability was slightly higher than that of the base model and lower than that of match 5.

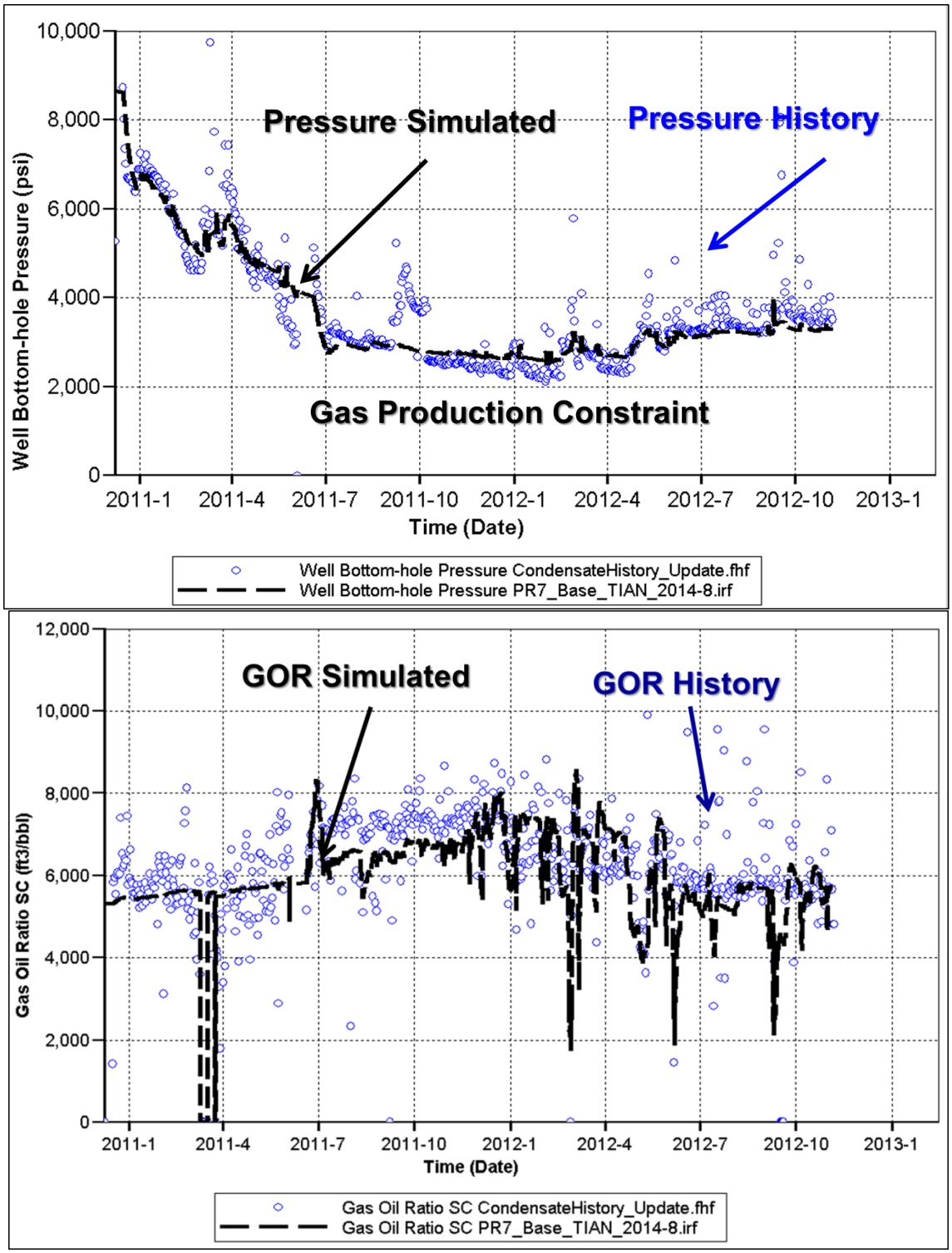

Fig. 97—Model 1 of good history match results.

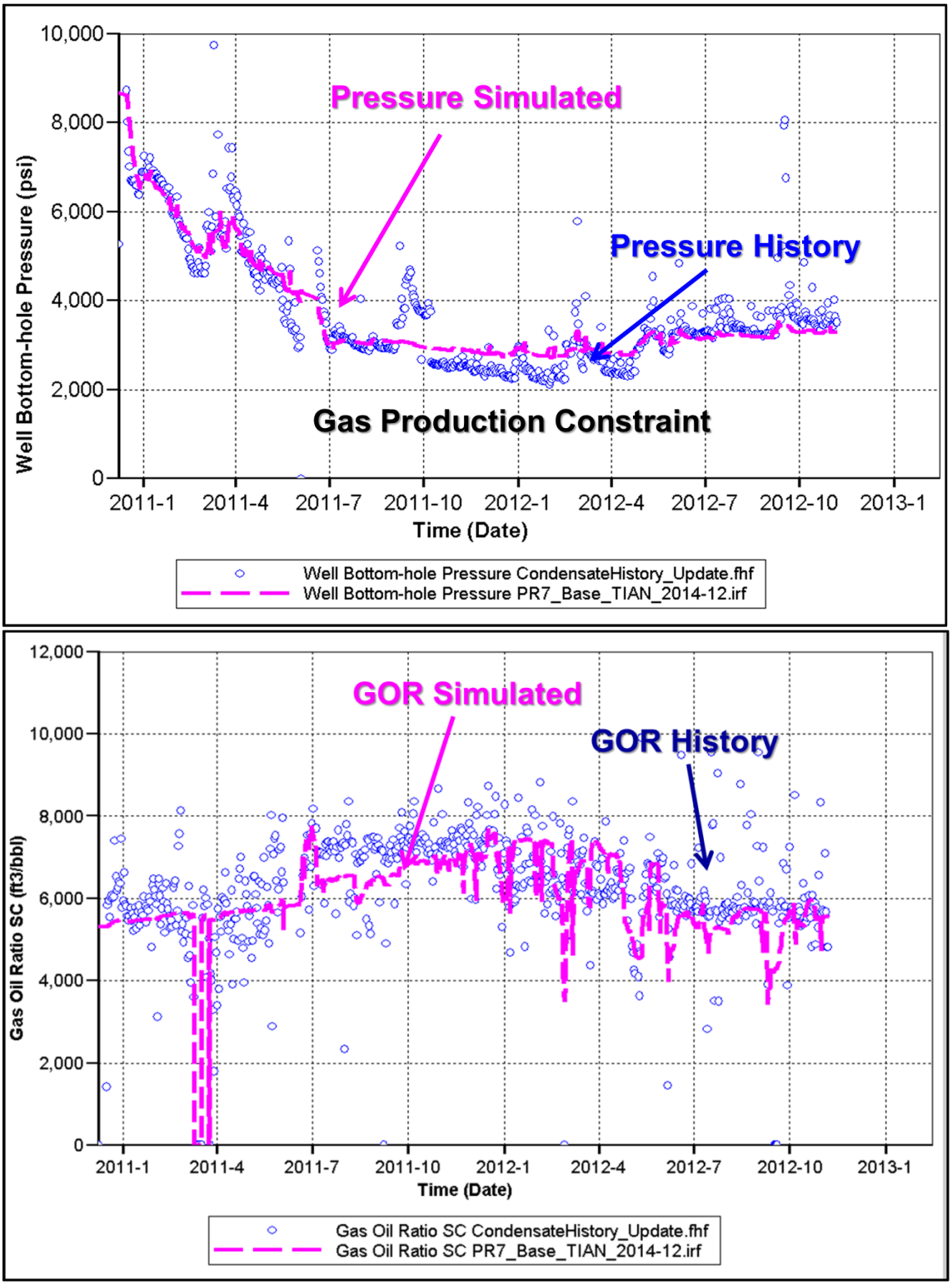

Fig. 98—Model 2 of good history match results.

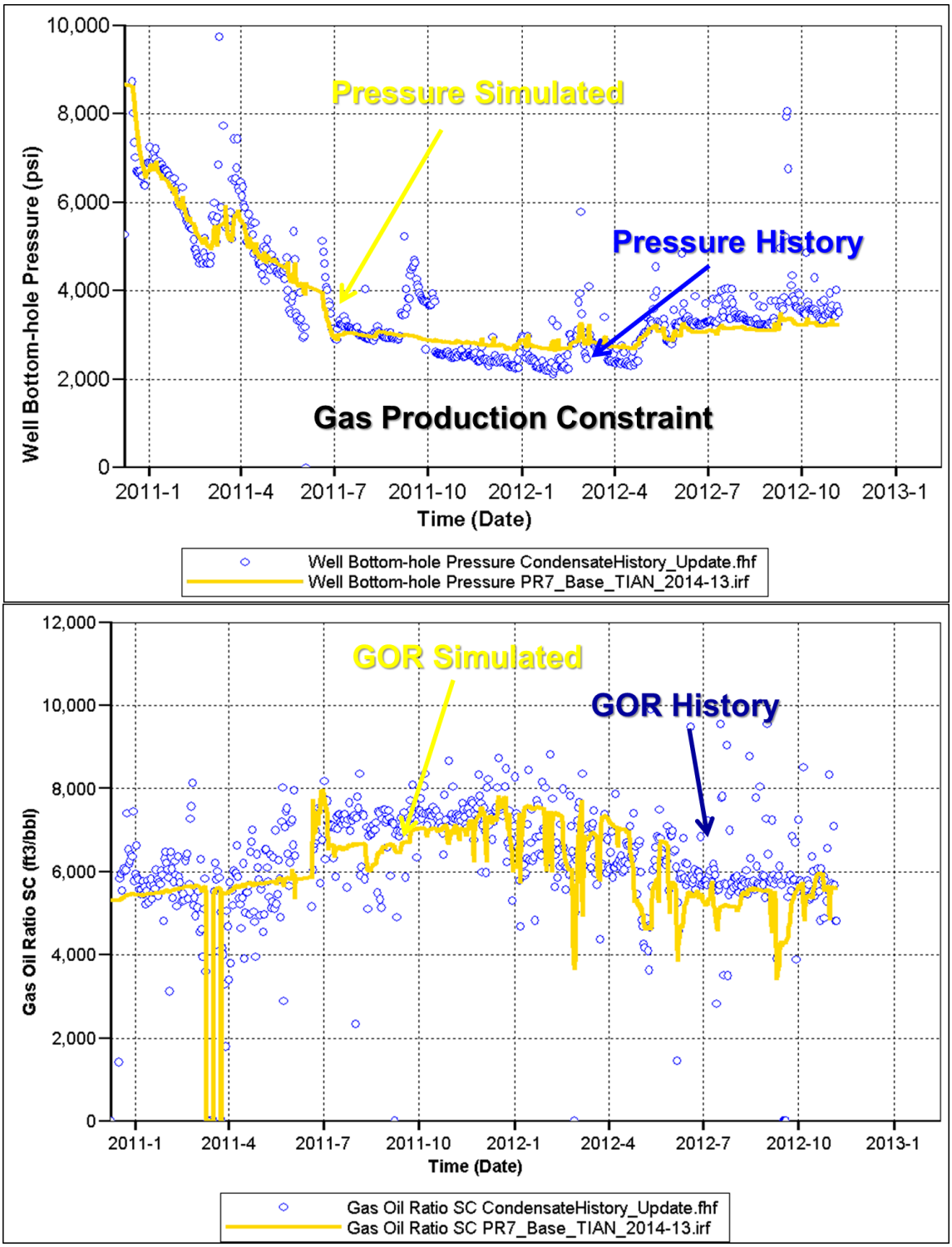

Fig. 99—Model 3 of good history match results.

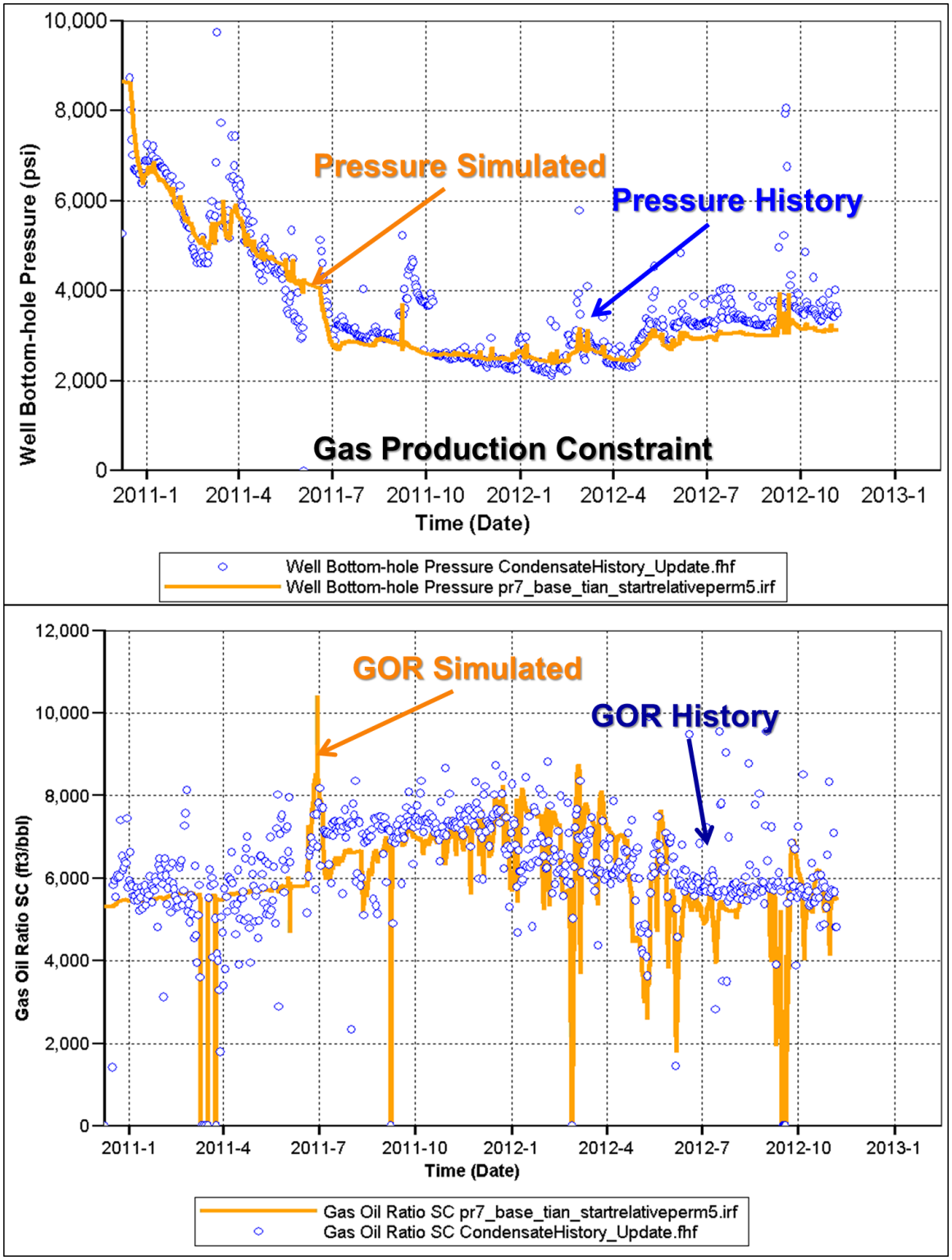

Fig. 100—Model 4 of good history match results.

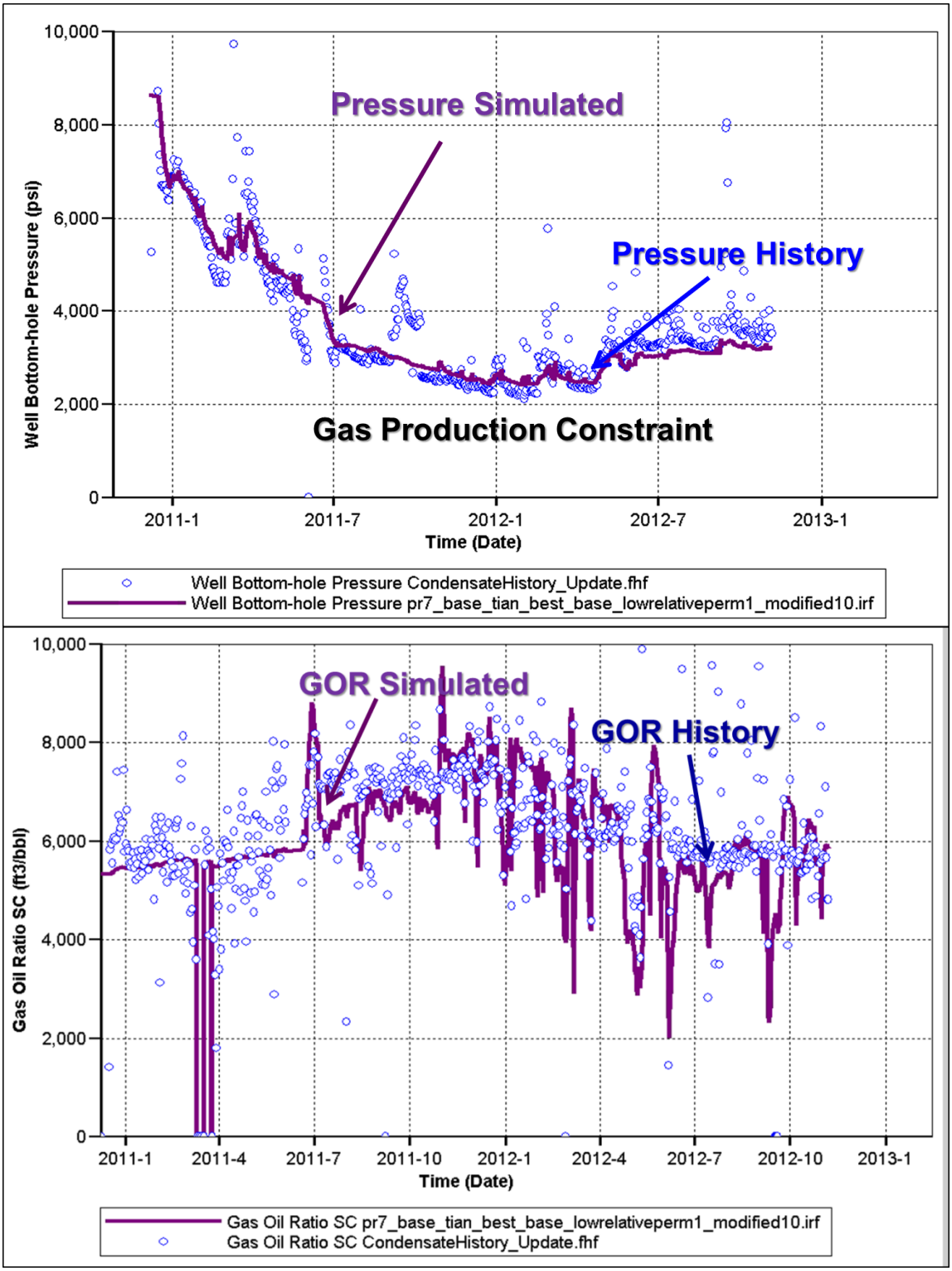

Fig. 101—Model 5 of good history match results with higher porosity.

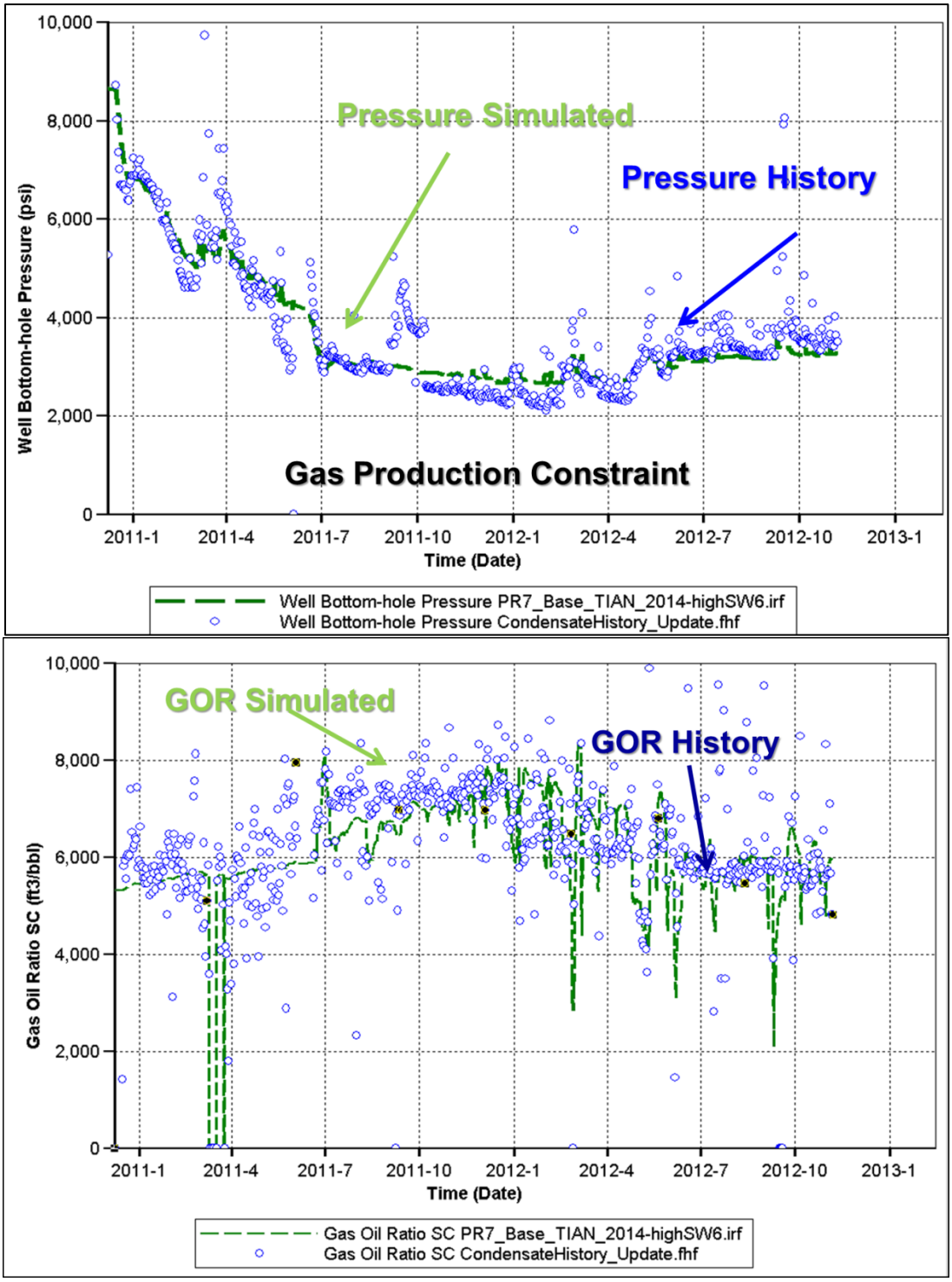

Fig. 102—Model 6 of good history match results with higher water saturation.

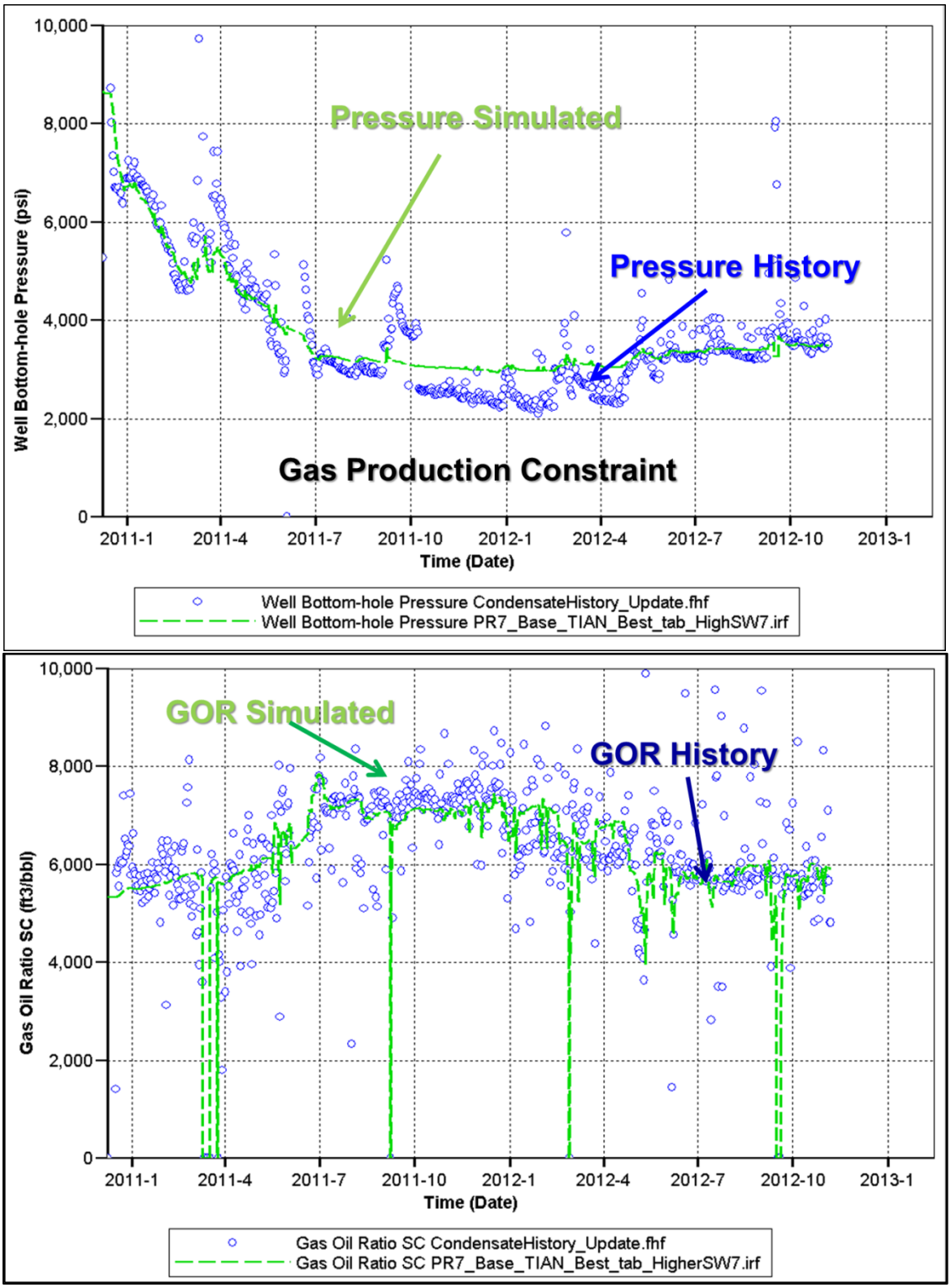

Fig. 103—Model 7 of good history match results with higher porosity and water saturation.

TABLE 10—SUMMARY OF RESERVOIR PROPERTIES OF GAS CONDENSATE MODELS WITH GOOD HISTORY MATCH RESULTS

	Phi, %	K, ND	Sw, %	Transmissibility Multiplier	Relative Permeability
Match 1	5.5	570	25	High	ORM and limestone
Match 2	5.5	430	25	High	Limestone
Match 3	5.5	480	25	High	Limestone
Match 4	5.5	500	25	Low	ORM and limestone
Match 5	5.5	800	25	Low	Limestone with low relative permeability for clay
Match 6	5.5	1200	30	Low	ORM and limestone
Match 7	6.5	850	40	High	ORM and limestone with high relative permeability

TABLE 11—FRACTURE PERMEABILITY DECREASING FROM CENTER TO OUTER BOUNDARY OF HISTORY MATCH RESULTS

Layer	1–4	5–7	8–9	10–11	12–12	13–14	15–17
Match 1	500	15	1	0.8	0.2	0.2	0.1
Match 2	500	15	1	0.8	0.4	0.2	0.1
Match 3	500	15	1	0.8	0.15	0.1	0.1
Match 4	500	15	1	0.8	0.4	0.2	0.1
Match 5	500	15	1	0.12	0.04	0.01	0.001
Match 6	500	2	1	0.8	0.4	0.2	0.1
Match 7	1,000	10	5	2	0.4	0.05	0.05

Gas Condensate Model Sensitivity Analysis

To investigate the relative importance of various parameters on production, a sensitivity analysis was conducted for some of the important parameters, such as reservoir properties**,** hydraulic fractures, and rock characteristics. Simulation runs were performed for each uncertainty under low and high values, and the impact of each parameter on the objective function was ranked. Only the impact of a few important parameters on reservoir response and well production performance will be discussed. By increasing and decreasing the water saturation, porosity, and matrix permeability by 10%, we obtained the high and low cases to compare with the base case from previous history match models.

A high relative-permeability case was obtained by doubling current permeability. The low relative-permeability case was 50% lower than the base case (**Fig. 104**). Relative permeability variability did not appear to have a strong impact on cumulative production (**Fig. 105**). This is reasonable because oil production is relatively low in the gas condensate region. An increase of porosity by 10% added approximately 1% of 18 months cumulative oil production **(Fig. 106).** A decrease of water saturation by 10% increases the 18 months cumulative oil production by less than 1% (**Fig. 107**). The sensitivity of fracture permeability suggests a strong impact from fracture permeability on cumulative production **(Fig. 108).**

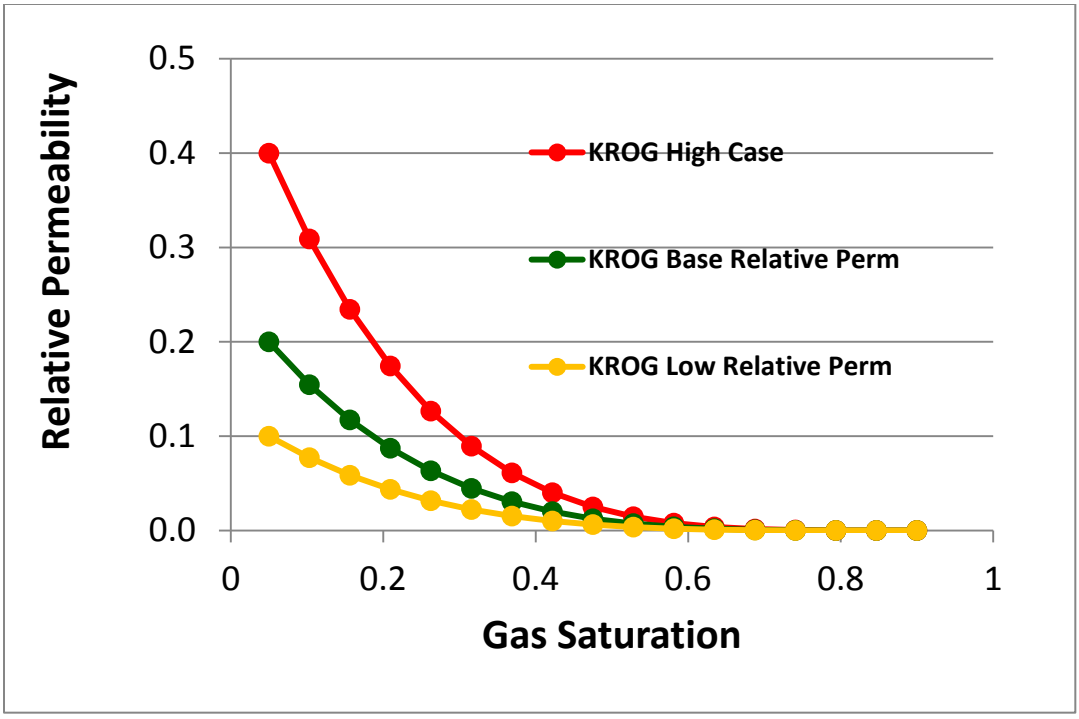

Fig. 104—Three relative permeability cases used in the sensitivity analysis.

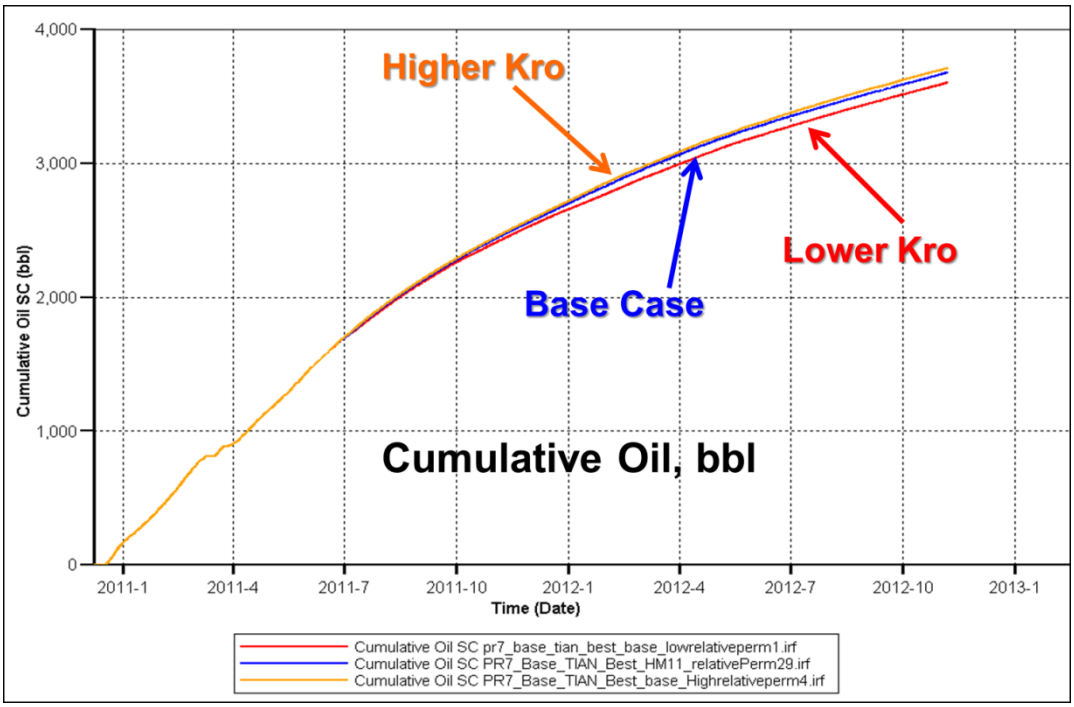

Fig. 105—Gas condensate well sensitivity analysis of relative permeability on cumulative oil production.

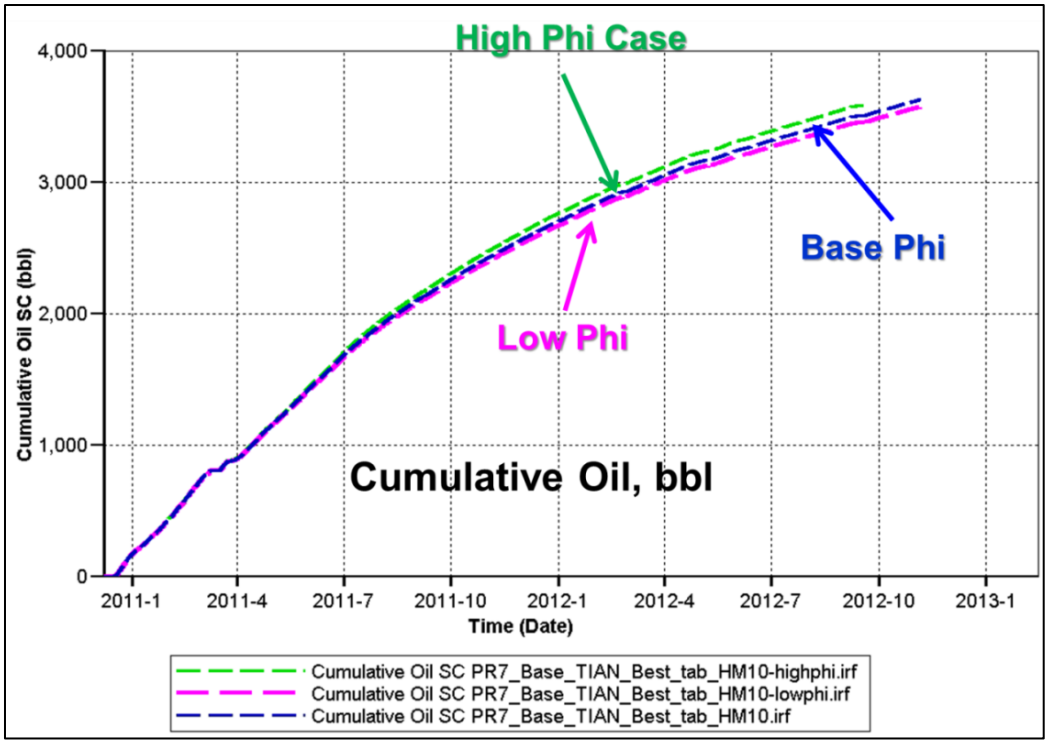

Fig. 106—Gas condensate well sensitivity analysis of porosity on cumulative oil production.

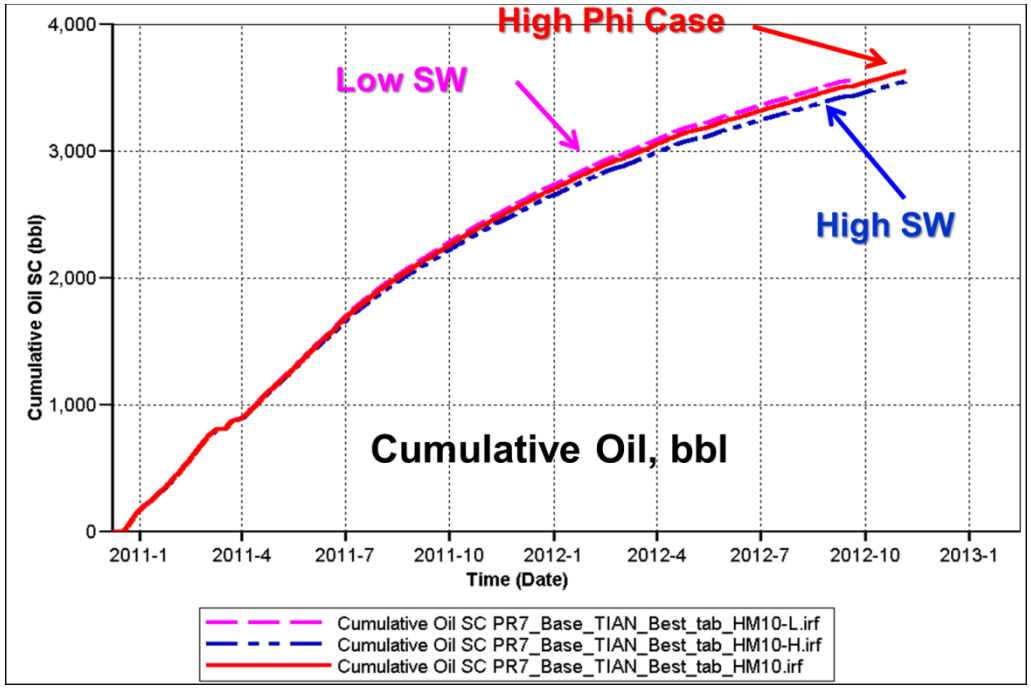

Fig. 107—Gas condensate well sensitivity analysis of water saturation on cumulative oil production.

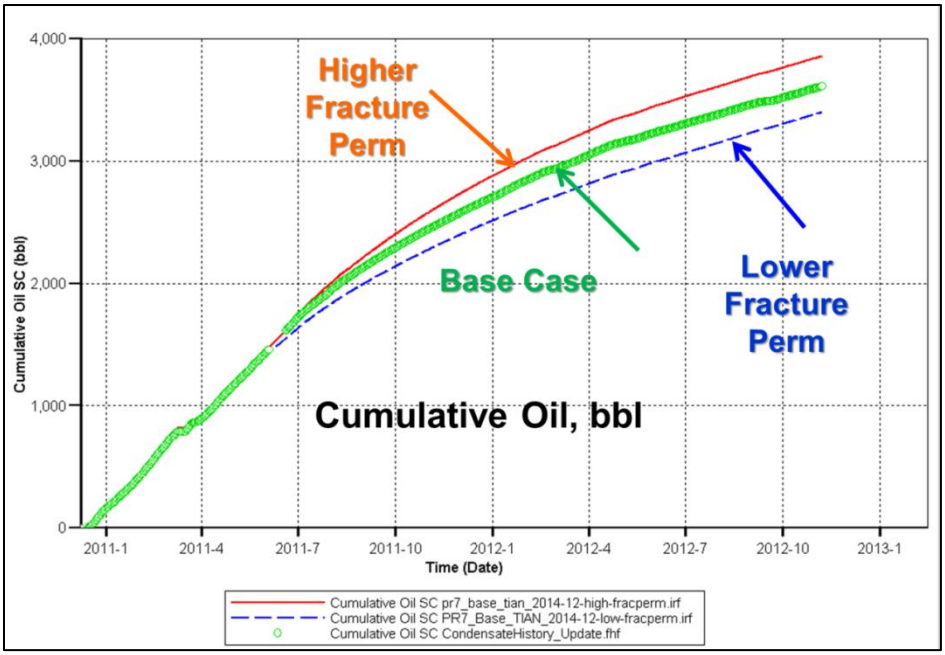

Fig. 108—Gas condensate well sensitivity analysis of fracture permeability on cumulative oil production.

Volatile Well Model Simulation Results

After successfully obtaining several good matches between simulated and historic data, we spent a significant amount of time on the volatile oil models of two different wells and characterized the reservoir by conducting a history match. We used oil production as a constraint and calculated the bottomhole flowing pressure and gas production.

Instead of having good matches to both simulated pressure and simulated gas production for both volatile wells, we could only match either the pressure plot or the gas production data mentioned above, but not both **(Figs. 109 through 111).** When matching the production data, GOR increased significantly rather than remaining somewhat constant throughout time (Figs. 109 and 110). When matching the GOR plot, pressure

remained >2,000 psi without dropping to approximately 700 psi, as shown by the history data (Fig. 111).

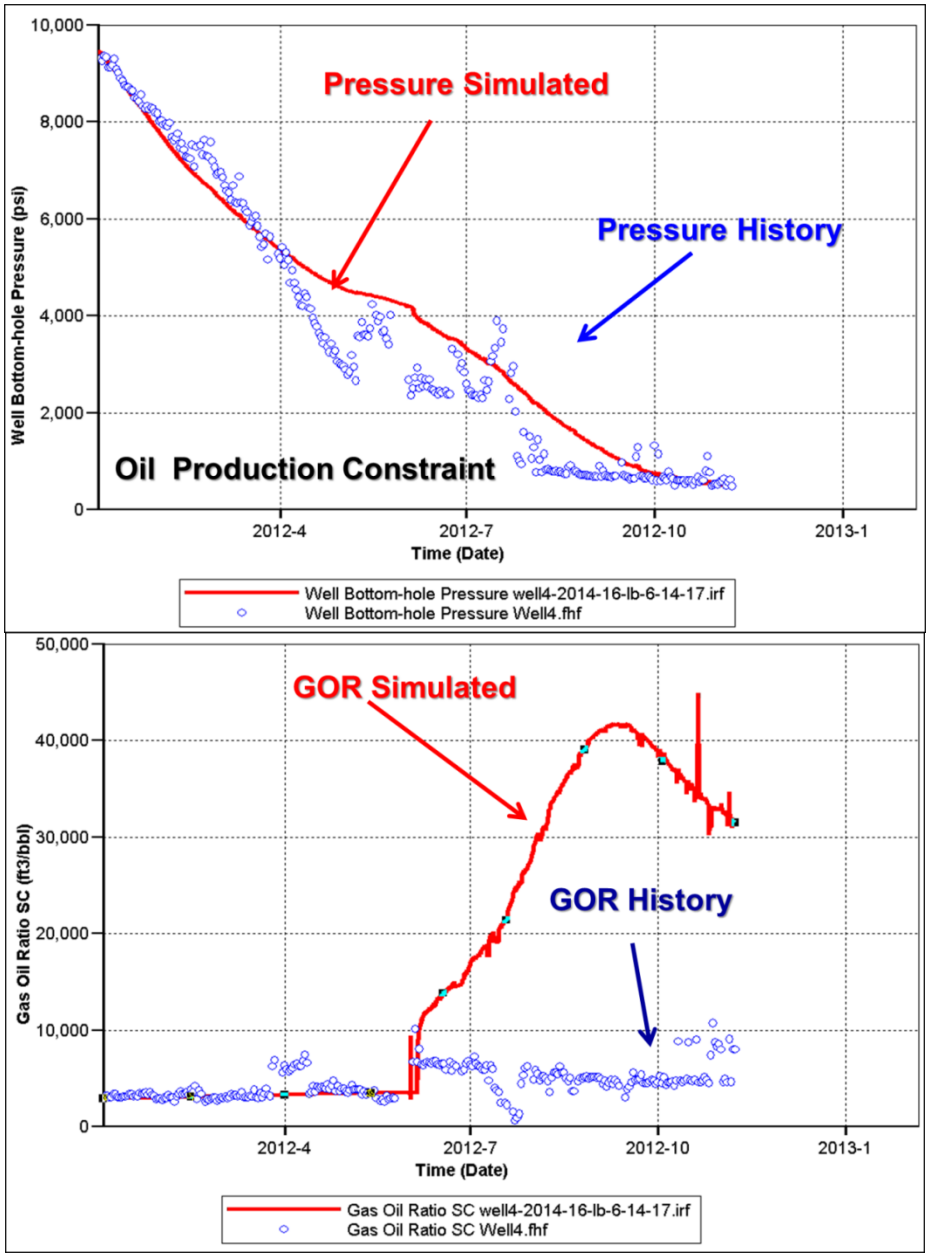

Fig. 109—Simulation results showing proper pressure decline prediction but inaccurate simulated GOR on volatile oil well model No. 1.

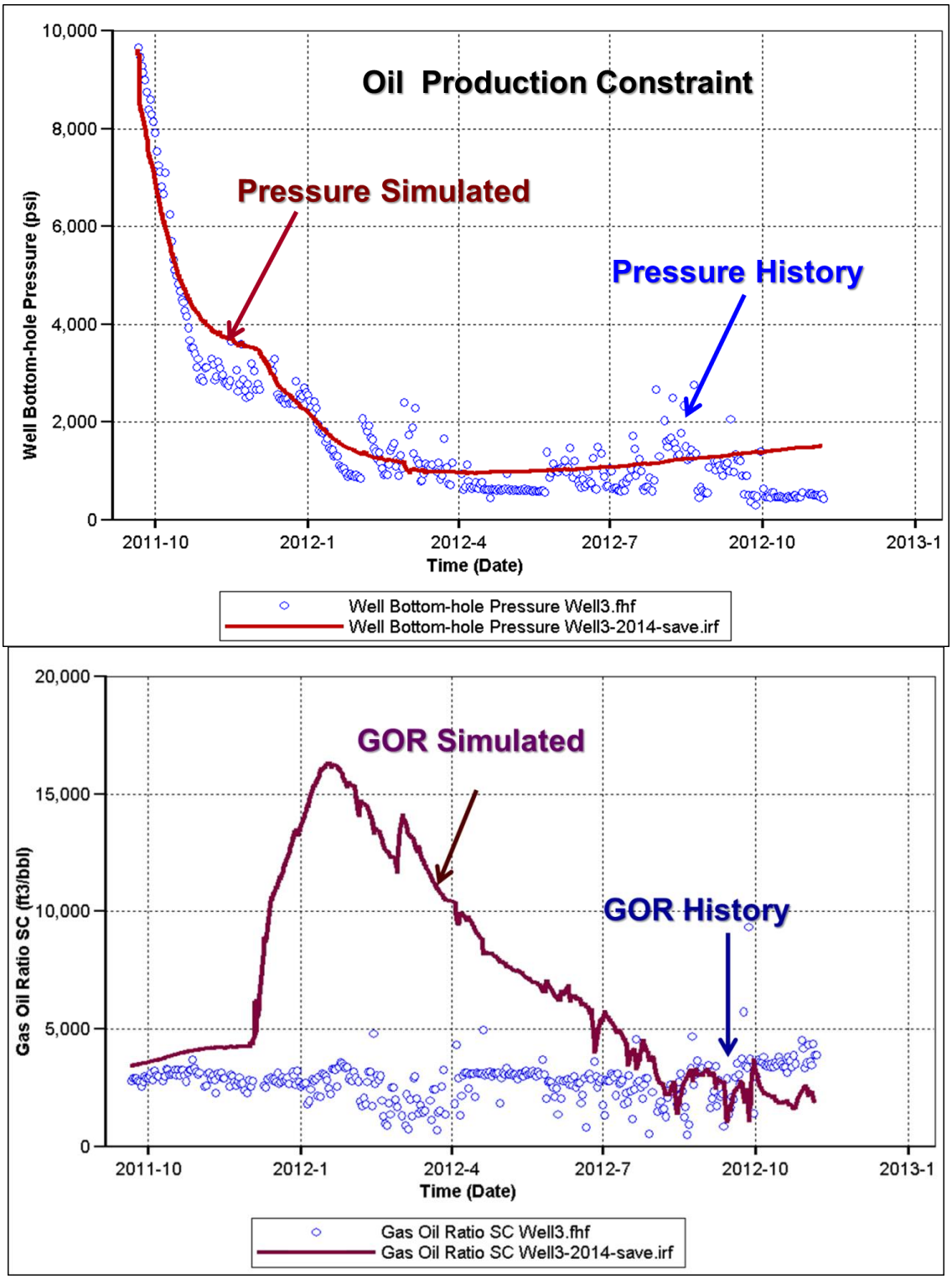

Fig. 110—Simulation results showing proper pressure decline prediction but inaccurate simulated GOR on volatile oil well model No. 2.

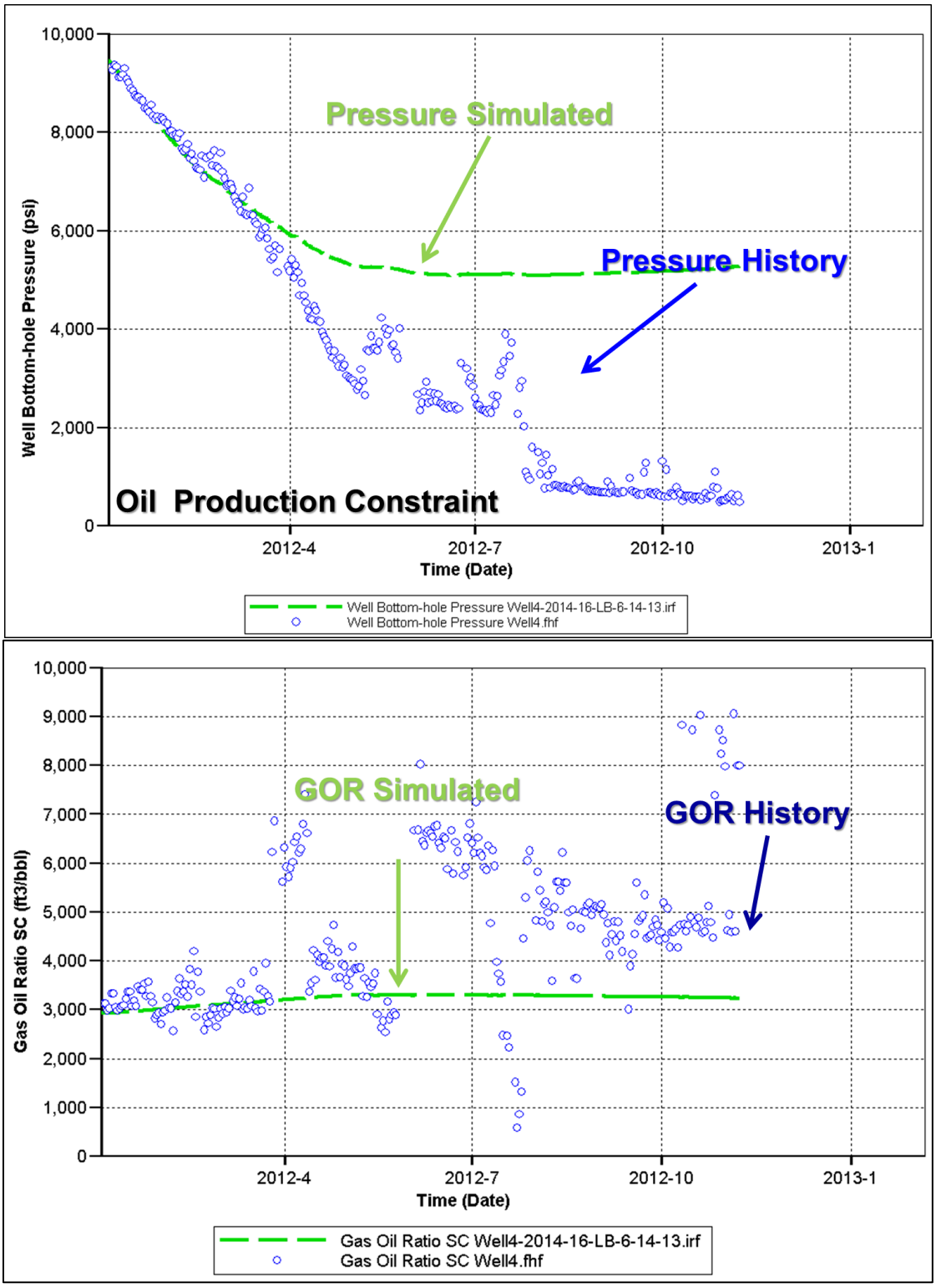

Fig. 111—Simulation results showing accurate simulated GOR but inaccurate simulated pressure on volatile oil well model No. 1.

We used several methods to try to resolve this dilemma. The measure we took was to increase reservoir permeability and decrease drainage volume. In the late phase of production history, when the bottomhole pressure was as low as 700 psi, the pressure in adjacent cells should have also been quite low; however, the fact that there was no gas coming out suggested that there was gas supply being transporting to cells near the wellbore and maintaining the pressure (Figs. 109 and 110). In this case, we needed to increase matrix permeability to achieve more gas supply. The significant pressure decline since initial production suggests limited reservoir volume (Figs. 109 and 110). This method did not work (Figs. 109 and 110).

We shed some light on the reason for not being able to obtain a good match for both pressure and GOR plots by taking a closer look at the production data. The depth of volatile oil reservoir is commonly as great as 10,000 ft (Fig. 27). If bottomhole pressure is as low as 700 psi (Fig. 84 andFig. 85), the pressure gradient inside the wellbore is 0.07 psi/ft. If the wellbore is filled with water, the pressure gradient is approximately 0.43 psi/ft for fresh water. Oil would slightly decrease the pressure gradient from 0.43 psi/ft, but 0.07 psi/ft is still too low to be practical with only oil and water.

The possible answer was gas lift, which has been used in the Eagle Ford fluid-rich region (Ferguson and Narvaes 2013). The sudden pressure decline also indicated the possibility of gas lift; therefore, the late phase of the pressure design was a result of injecting gas into the wellbore rather than a natural decline resulting from hydrocarbon

depletion. The late phase of production history should not be considered because the pressure decline did not reflect the properties of the reservoir.

OIL PRODUCTION OPTIMIZATION

Artificial lift has been used to improve ultimate recovery by controlling the bottomhole flowing pressure (Ferguson and Narvaes 2013). We tested various bottomhole flowing pressures to assess how this pressure would influence cumulative production. If bottomhole pressure was fixed at 2,000 psi without the artificial lift, 1 year after the production history, the cumulative oil production would be 500 bbl lower than the case with 700 psi as bottomhole pressure. The reservoir model represents only 1/60 of the entire horizontal wellbore; therefore, by using gas lift, the cumulative oil production for the 18 months will be 300,000 bbl higher than without gas lift **(Fig. 112).** A low bottom hole pressure plays a key role in overall oil production.

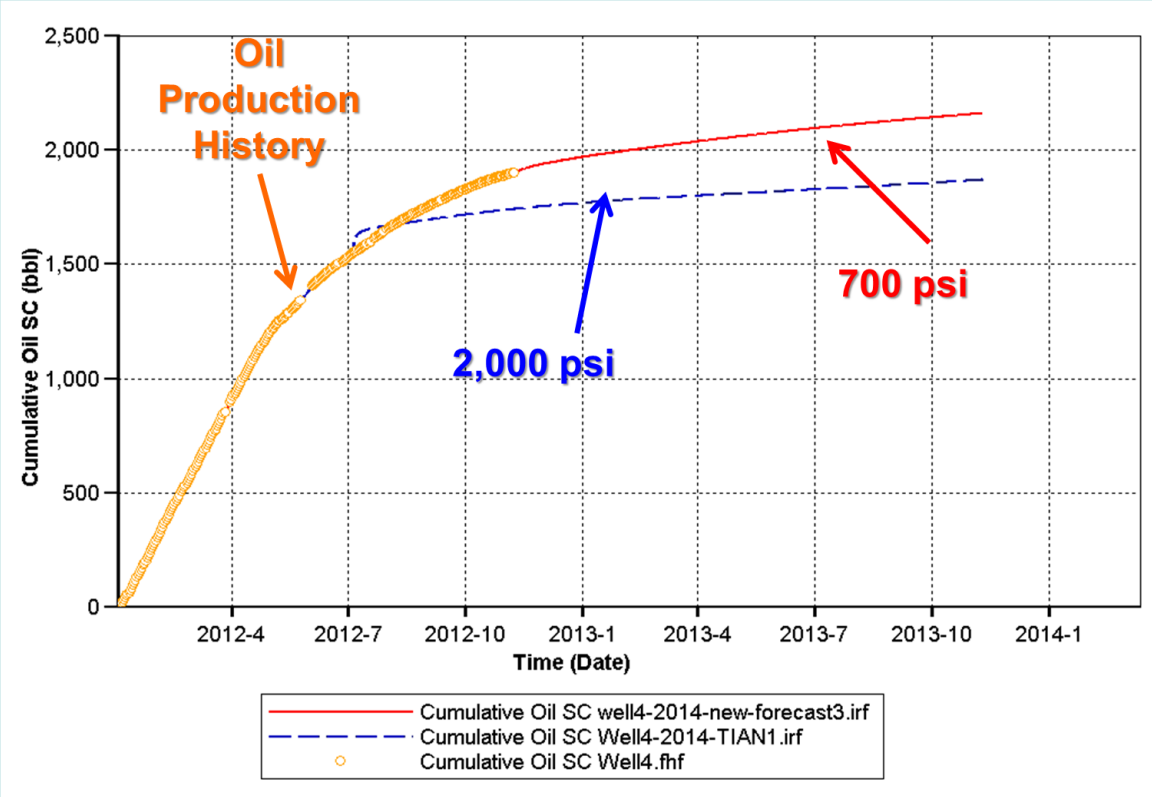

Fig. 112—Oil production forecast with two different bottomhole pressures.

DRY GAS WELL MODELLING

Data Gathering

Well geometry, fluid properties, and fracture properties, which were needed to build the dry gas well model, were from a publication **(Fig. 113)** (Bazen et al. 2010); however, reservoir properties, such as water saturation and porosity, were not. Therefore, we searched for reservoir properties in the public database, Drillinginfo (2013), using the operator name and screening by GOR and general well location.

There was one well, API 42-283-32190, that met both criteria. Comparing the image well log from Drillinginfo to the figure in the paper, a remarkable similarity was found. **(Fig. 114).** We now had two extremely close wells that would have relatively similar reservoir properties; therefore, we downloaded and digitized the image well logs, including gamma ray, resistivity, neutron, and density porosity logs. With these logs, we analyzed the porosity and fluid vertical variability, and determine the layering of the reservoir model **(Fig. 115).**

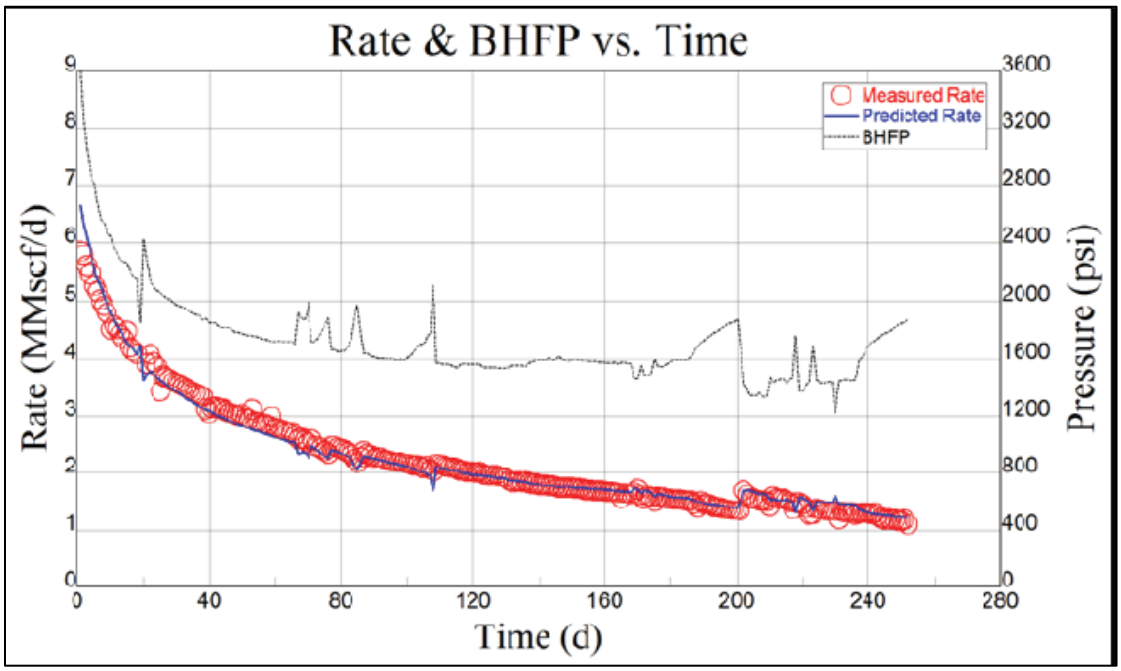

Fig. 113—Production and pressure history of 250 days for Eagle Ford dry gas well (Bazen et al. 2010).

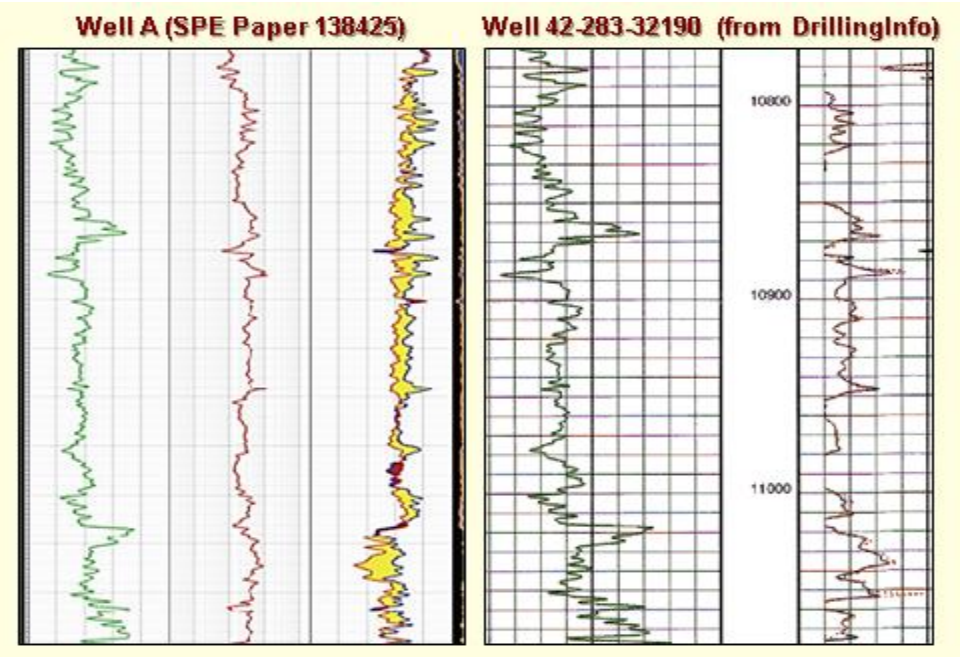

Fig. 114—Log image in publication vs. the well log images available in Drillinginfo database (Bazen et al. 2012; Drillinginfo 2013).

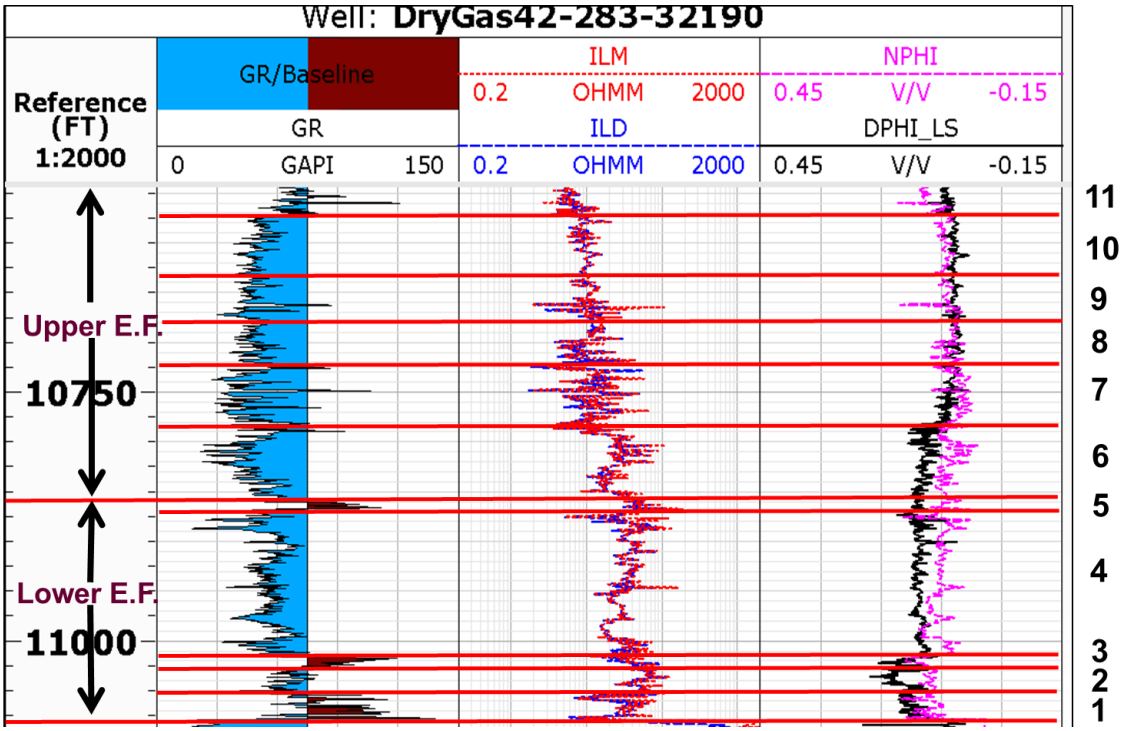

Fig. 115—Digitized well log showing layering in the reservoir model (digitized from image in Drillinginfo).

Dry Gas Model History Match Results

Using gas production as the constraint, two sets of good history matches between pressure history and pressure simulated results were achieved **(Fig. 116).** The water saturation and porosity were quite different among various layers between the two models **(Tables 12 and 13).** The matrix permeability was approximately 21 and 16.8 nd, respectively, from the two cases. There was uncertainty in the reservoir model parameters.

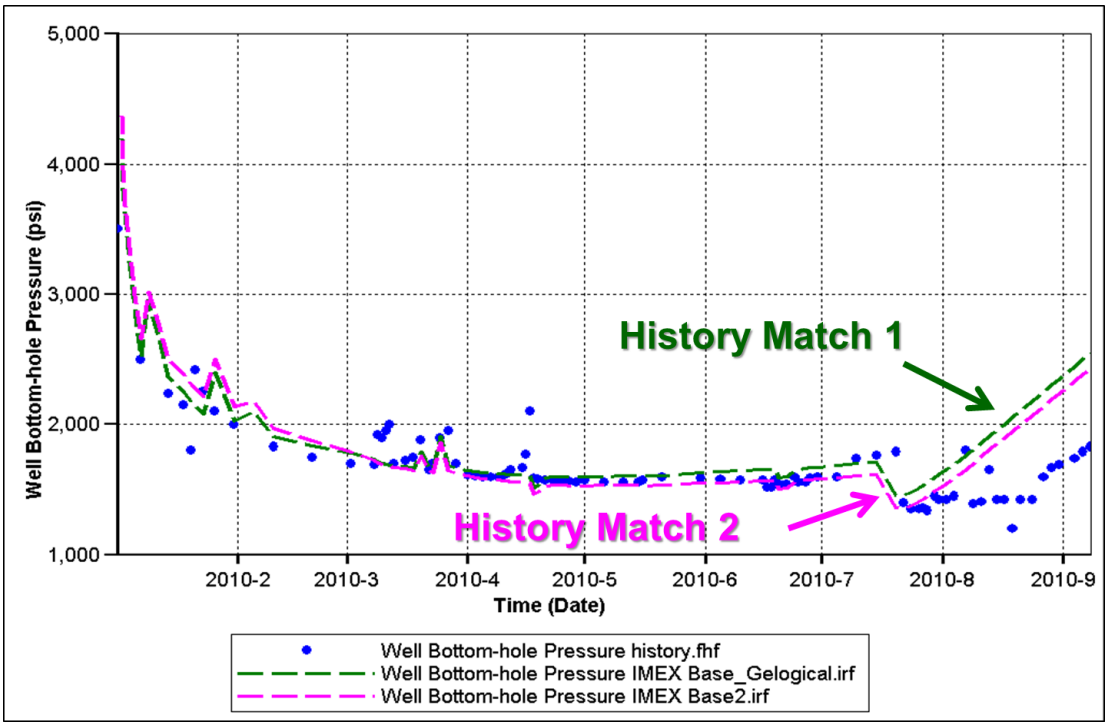

Fig. 116—Two models of a dry gas well showing good matches between pressure history and simulated pressure.

TABLE 12—WATER SATURATION USED IN THE DRY GAS RESERVOIR MODEL FROM TWO HISTORY MATCHES		
	Sw History Match 1	Sw History Match 2
Layer 11	0.9	0.7
Layer 10	0.9	0.9
Layer 9	0.8	0.8
Layer 8	0.7	0.6
Layer 7	0.7	0.6
Layer 6	0.7	0.6
Layer 5	0.3	0.3
Layer 4	0.3	0.3
Layer 3	0.4	0.5
Layer 2	0.3	0.3
Layer 1	0.4	0.5

TABLE 13—POROSITY USED IN THE DRY GAS RESERVOIR MODEL FROM TWO HISTORY MATCH RESULTS		
	Phi History Match 1	Phi History Match 2
Layer 11	0.095	0.095
Layer 10	0.12	0.12
Layer 9	0.08	0.08
Layer 8	0.06	0.06
Layer 7	0.08	0.08
Layer 6	0.15	0.08
Layer 5	0.15	0.14
Layer 4	0.12	0.08
Layer 3	0.18	0.14
Layer 2	0.13	0.1
Layer 1	0.15	0.14

CHAPTER VII

DISCUSSION

To assess geologic controls on production, we divided the South Texas Eagle Ford into 5 regions (**Table 14, Fig. 117**) based on: production and the regional trends of depth; thickness of Lower Eagle Ford Shale; average TOC, gamma ray, and bulk density; the number of ORM and limestone beds; and average bed thickness of the Lower Eagle Ford Shale (Figs. 27, 34, 47, 52 through 54). Continuity of these reservoir properties is greatest is along depositional strike, which parallels the Sligo-Stuart City Shelf Margin from DeWitt County southwestward to central La Salle County, where it turns northwestward to Kinney County in the Maverick Basin (**Fig. 118**).

TABLE 14—SUMMARY OF GENERALIZED RESERVOIR PROPERTIES OF LOWER EAGLE FORD AMONG FIVE PRODUCTION REGIONS.

	Region 1	Region 2	Region 3	Region 4	Region 5
Primary Fluid Type	Oil	Gas	Oil and Gas	None	None
Depth (ft)	8,500-13,500	10,000-12,500	6,000-10,000	2,000-5,000	0-3000
L.E.F Thickness (ft)	100-200	125-200	50-125	>150	0-100
U.E.F Thickness (ft)	0	0-300	0-400	>400	0-300
TOC (%)	4-6	3-5	5-7	6-8	>6
Number of limestone bed	>12	>14	<10	>20	0
Average bed Thickness	<6	<6	6-13	>9	4-11

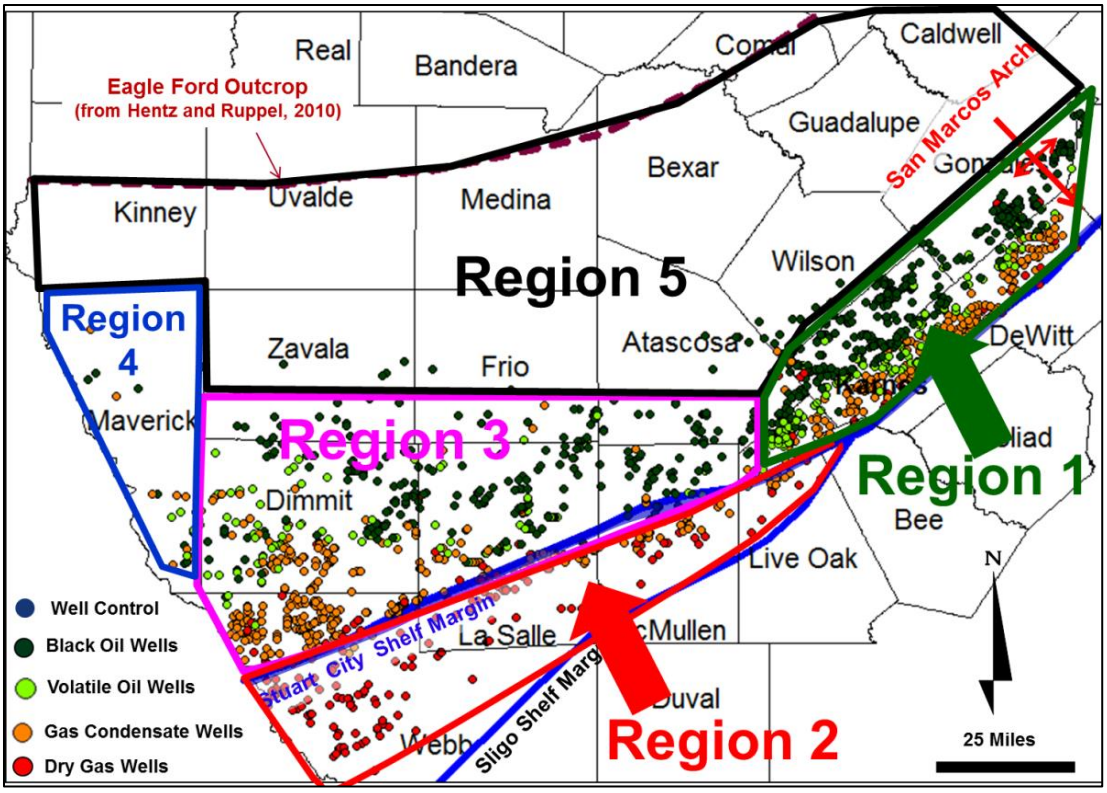

Fig. 117—Eagle Ford Shale production region subdivisions displayed on Eagle Ford GOR map (Fig. 15).

REGIONS 1 AND 2

Regions 1 and 2 are the most productive oil and gas regions, respectively (Figs. 14 and 13) and are parallel to many of the regional trends of the geological parameters (Figs. 117 and 118). Although fluid types in regions 1 and 2 vary as result of thermal maturity, the oil- and gas-productive regions share common favorable reservoir properties that contribute to high productivity.

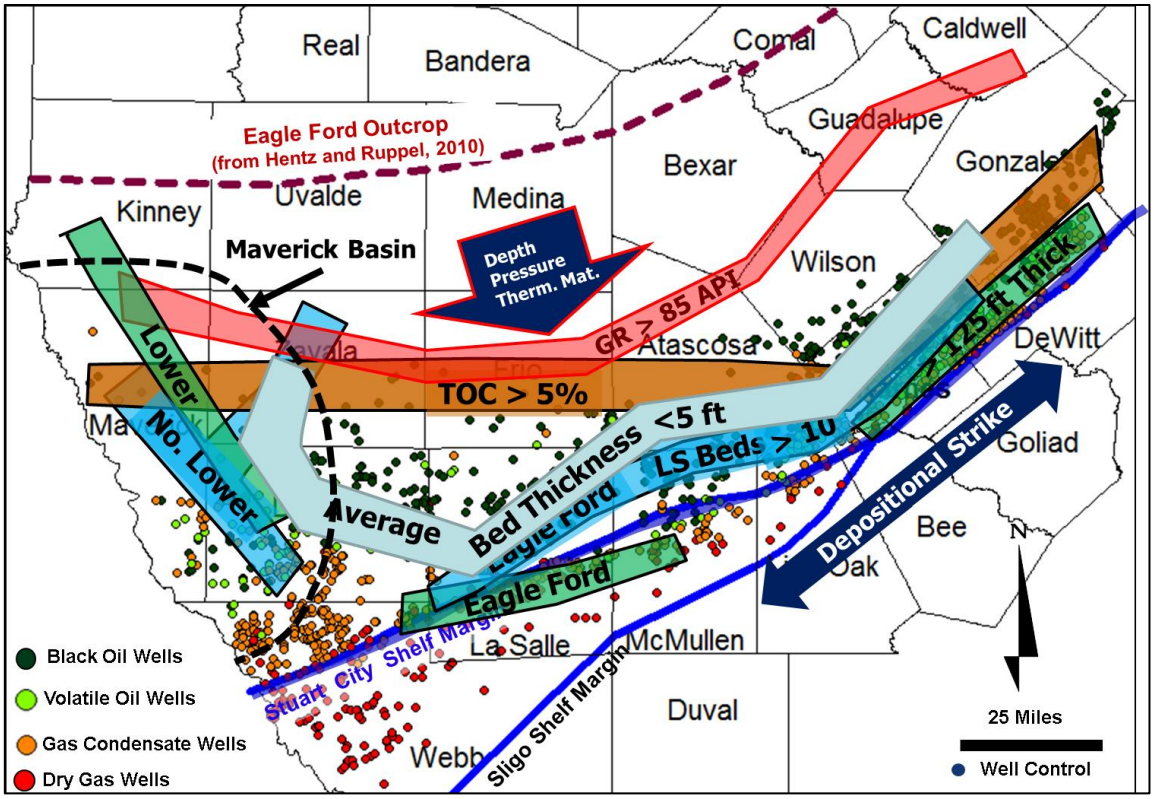

Fig. 118—Summary of "central trends" of key Eagle Ford Shale reservoir properties (Figs, 27,34, 39, 37, 47, 52 through 54) that affect productivity. Displayed on Eagle Ford GOR map (Fig. 15).

In Regions 1 and 2, depth is greater than other regions (Figs. 27, 117 and 118). There are strike-elongate trends of low gamma ray (Fig. 38), high bulk density (Fig. 39), and low TOC (Fig. 47) in these two regions (Figs. 117 and 118). A strike-elongate trend of high numbers of limestone and ORM beds, and low average bed thickness is also present (Figs. 52 through 54 and 118). The above trends suggest better completion targets than in area of high gamma ray (ductile marl and shale). The highly productive trend also coincides with a northeast-trending region of anomalously thick Lower Eagle Ford Shale (Fig. 34). Greater formation depth and thickness, lower TOC, thinner individual beds, and higher frequency of interbedding contribute to the high productivity in these two

regions (Figs. 117 and 118). Reservoir properties that differentiate the oil-productive region (Region 1) from the gas-productive region (Region 2) are the higher thermal maturity in Region 2 and the high reservoir pressure and pressure gradient in Region 1 (Fig. 20, 21, 117 and 118).

REGION 3

In Region 3, Lower Eagle Ford Shale is anomalously thinner (Fig. 34, 117 and 118) and the formation is shallow compared to Regions 1 and 2 (Fig. 27). Higher TOC suggests a better reservoir quality than Regions 1 and 2 (Fig. 47), but lower numbers of limestone (Fig. 52) and ORM beds (Fig. 53) and lower average bed thickness (Fig. 54) reduced its general completion quality compared to Regions 1 and 2 (Table 14, Fig. 118).

REGION 4

The Maverick basin, which is the depocenter of the Lower Eagle Ford Shale, has the greatest total thickness of Lower Eagle Ford Shale (Fig. 34), numbers of Lower Eagle Ford limestone (Fig. 52), and ORM interbeds (Fig. 53), and greatest average bed thickness (Fig. 54,117 and 118). The great Eagle Ford thickness in the Maverick basin suggests more potential reservoir and source rock. However, productivity of Maverick County Eagle Ford may suffer from shallow depth (Fig. 27) and resulting lower reservoir pressure. Average bed thickness in Maverick County ranges from less than 5 ft to more than 13 ft, which is relatively thick compared to the other locations with the same number of interbeds (Fig. 54).While there is a direct relation between total Lower

Eagle Ford thickness and average interbed thickness in the Maverick Basin depocenter, there is an inverse relation between total thickness and average interbed thickness in the La Salle – DeWitt County trend. Therefore, the mechanical properties of the Eagle Ford Shale in this region are different than those of others areas. Chittum Anticline, which extends through the center of Maverick Basin depocenter (Fig. 27), could cause complexity in mechanical properties and reduce the productivity of the Eagle Ford Shale.

REGION 5

In region 5, there is a strike-elongate trend of high TOC (Fig. 47 and 118) and low bulk density (Fig. 39) region which suggests as good source rock quality. This trend coincides with a strike-elongate trend of low numbers of limestone (Fig. 52) and ORM beds (Fig. 53) and high average bed thickness (Fig. 54) that extends from eastern Zavala County northeastward through Guadalupe County and coincides with low values of total Lower Eagle Ford Shale thickness (Fig. 34 and 118). Lower concentration of limestone beds makes the Eagle Ford Shale formation in this region difficult to stimulate. Lower formation thickness and thermal maturity indicates limited potential of hydrocarbon in place. But the major disadvantage of Region 5 is its shallow depth (Fig. 27), which results in low reservoir pressure.

CHAPTER VIII

CONCLUSIONS

From NW to SE, Eagle Ford fluids evolve from oil, to gas condensate and, finally, to dry gas, reflecting greater depth and thermal maturity. Oil gravity increases from less than 43 API in the northwest to more than 60 API in the southeast. Gas specific gravity increases from approximately 0.6 in the southeast to more than 0.85 in the northeast. Limited data suggest that reservoir pressure increases from less than 6,000 psi in southern Dimmit County to more than 10,000 psi in Karnes and DeWitt Counties in the northeast. Reservoir pressure gradient increases from less than 0.68 psi/ft. in the southeast to approximately 0.85 psi/ft. in the northeastern region. The most productive gas wells are located south of the Stuart City Shelf Margin, where production commonly exceeds 80 MMcf/M/W. Peak monthly oil production is greatest in Karnes and Gonzales counties, where production exceeds 16,000 bbl/M/W

From outcrop, the Eagle Ford Shale dips southeastward; depth exceeds 13,000 ft at the Sligo Shelf Margin. From more than 600 ft thick in the Maverick basin depocenter, the total Eagle Ford Shale thins to less than 50 ft on the northeast at the San Marcos Arch. We divided the Eagle Ford Shale into 3 units. The Lower Eagle Ford is present throughout the study area; it is more than 275 ft thick in the Maverick Basin depocenter and thins to less than 50 ft on the northeast. The Upper Eagle Ford Shale is present in

only the southwest, where maximum thickness exceeds 425 ft in the Maverick Basin depocenter. TOC is greatest in the Lower Eagle Ford Shale (2 to 12%).

TOC of the lower Upper Eagle Ford Shale is greatest (7%) in Zavala and Frio Counties. In the Upper Upper Eagle Ford Shale, TOC is greatest (5%) in Dimmit and Maverick Counties. A strike-elongate trend of high TOC, high average gamma ray responses, and low bulk density extends from Maverick County northeast through Guadalupe County, parallel to updip of the Sligo and Stuart City Shelf Margins. The number of both limestone and ORM beds increase from less than 2 near outcrop in the northwest to more than 20 on the southeast at Sligo Shelf Margin. Average thickness of limestone and ORM beds in the Lower Eagle Ford Shale is low (< 5 ft.) in La Salle – DeWitt trend, coincident with the most productive gas and oil regions, respectively.

Eagle Ford Shale production (BOE) increases consistently with depth, increases with Lower Eagle Ford thickness (up to 180-ft thickness), and increases with TOC (up to 7%). P values analyses suggest high certainty of the relationship between the production and five reservoir parameters tested in regression models.

Multiple good history matches of a gas condensate well suggest significant uncertainties in reservoir parameters. Oil production rate is not sensitive to oil relative permeability for the gas condensate well model. We were unable to match the production history for the volatile oil wells, possibly because gas lift was probably applied. Reservoir modeling

suggests low bottom hole flowing pressure was the key to optimize cumulative oil production.

Eagle Ford Shale was divided into 5 production regions in South Texas. Regions 1 and 2, the most productive oil and gas regions, respectively, coincide with the regional, strike-elongate trends of several geologic parameters, which suggests that these parameters significantly impact Eagle Ford Shale production.

REFERENCES

Blatt, H., Berry, W. B., and Brande, S. 1991. Principles of Stratigraphic Analysis. Oxford, United Kindom: Blackwell Science Ltd.

Bowker, K.A. 2003. Recent Development of the Barnett Shale Play, Fort Worth Basin. West Texas Geological Society Bulletin 42 (6): 4-11.

Box, G. E. and Cox, D.R. 1964. An Analysis of Tranformation. Journal of the Royal Statistical Society 26(2):211-252.

Cardneaux, A.P. 2012. Mapping of the Oil Window in the Eagle Ford Shale Play of Southwest, Texas Using Thermal Modeling and Log Overlay Analysis. MS Thesis, Louisiana State University, Baton Rouge, Louisiana (August 2012).

Childs, O., Steele, E. G., and Salvador, A.1988. Correlation of Stratigraphic Units in North America (COSUNA) Project, Gulf Coast Region. Tulsa, Oklahoma: American Association of Petroleum Geologists Bulletin Oversize Chart.

Cipolla, C., Weng, X., Onda, H., et al. 2011. New Algorithms and Integrated Workflow for Tight Gas and Shale Completions. Paper 146872 presented at SPE Annual Technical Conference and Exhibition, Denver, Colorado, 30 October-2 November.

Condon, S.M. and Dyman, T.S. 2004. Geologic Assessment of Undiscovered Conventional Oil and Gas Resources in the Upper Cretaceous Navarro and Taylor Groups, Western Gulf Province, Texas. http://pubs.usgs.gov/fs/2004/3114/FS-04-3114_508.html. Downloaded April 2010.

Dawson, W. C, 2000, Shale Microfacies:Eagle Ford Group (Cenomanian-Turonian) North-Central Texas Outcrops and Subsurface Equivalent. Gulf Coast Association of Geological Societies Transactions 50:607-621.

Dembicki, H. Jr. 2009. Three Common Source Rock Evaluation Errors Made by Geologists during Prospect or Play Appraisals. AAPG Bulletin 93(3): 341-356.

Dicman, A. and Vernik, L. 2012. A New Petrophysical Model for Organic Shales. Paper 2012-217 Presented at SPWLA 53 rd Annual Logging Symposium, 16-20 June.

Drillinginfo. 2013. Eagle Ford Shale Oil Gravity and Gas Specific Gravity. http://drillinginfo.com/ (access May 2013).

East, L.E., Grieser, W., McDaniel, B.W., et al. 2004. Successful Application of Hydrajet Fracturing on Horizontal Wells Completed in a Thick Shale Reservoir. Paper 91435 Presented at Eastern Regional Meeting in Charleston, West Virginia, U.S.A.,15-17 September.

EIA. 2011. Review of Emerging Resources: U.S. Shale Gas and Shale Oil Plays. http://www.eia.gov/analysis/studies/usshalegas/full report errata (accessed July 2011)

EIA. 2012. Review of Emerging Resources: U.S. Shale Gas and Shale Oil Plays Report. http://www.eia.gov/naturalgas/review/production.cfm (accessed March 2013).

EIA. 2014. AEO2014 Early Release Overview. http://www.eia.gov/forecasts/aeo/er/pdf/0383er (2014).pdf (Accessed 7 January 2014).

Ewing, T.E. and Lopez, R.F. 1991. Principal Structural Features. Gulf of Mexico Basin, in Salvador, The Gulf of Mexico Basin: Boulder, Colo., Geological Society of America, Geological of North America, Scale 1:2,400,000.

Fan, L., Martin, R., Thompson, J., et al. 2011. An Integrated Approach for Understanding Oil and Gas Reserves Potential in Eagle Ford Shale Formation. Paper 148751 Presented at Canadian Unconventional Resources Conference, Calgary, Canada, 15-17 November.

Gilbert, D., Holschneider, M., and Mouel, J.L. 1998. Wavelet Analysis of the Chandler Wobble: Geophysical Research 103(B11): 27,069–27,089.

Gillard, M., Medvedev, O., Pena, A., et al. 2010. A New Approach to Generating Fracture Conductivity. Paper 135034 Presented at the SPE Annual Technology Conference and Exhibition, Florence, Italy, 19-22 September.

Gong, X., Tian, Y., McVay, D.A., et al. 2013. Assessment of Eagle Ford Shale Oil and Gas Resources. Paper 167241 Presented at Canadian Unconventional Resources Conference, Calgary, Canada, 5 - 7 November.

Hentz, T. H. and Ruppel, S. C. 2010. Regional lithostratigraphy of the Eagle Ford Shale: Maverick Basin to East Texas Basin. Gulf Coast Association of Geological Societies Transactions 60: 325-338.

Heidari, Z. and Torres-Verdin, Carlos. 2011. Quantitative Method for Estimating Total Organic Carbon and Porosity, and for Diagnosing Mineral Constituents from Well Logs in Shale-gas Formations. Paper SPWLA-2011-Q Presented at

SPWLA 52rd Annual Logging Symposium, Colorado Springs, Colorado, 14-18 May.

Jarvie, D.M. 2004. Evaluation of Hydrocarbon Generation and Storage in the Barnett Shale, Ft. Worth Basin, Texas: The Barnett Shale Fractured Shale Gas Model (abst.): 21st International Meeting on Organic Geochemistry, Krakow, Poland, 8–12 September.

Jarvie, D.M., Hill, R.J., Ruble, T.E., et al. 2007. Unconventional Shale-Gas Systems: The Mississippian Barnett Shale of North-Central Texas as One Model for Thermogenic Shale-Gas Assessment. AAPG Bulletin 91 (4): 475-499.

Ketter, A.A., Daniels, J.L., Heinze, J.R., et al. 2006. A Field Study Optimizing Completion Strategies for Fracture Initiation in Barnett Shale Horizontal Wells. Paper 77441 Presented at SPE Annual Technical Conference and Exhibition in San Antonio, Texas, 24-17 September.

Labrecque, P.A., Jensen, J.L., and Hubbard, S.M. 2011. Ciclicity in Lower Cretaceious Point Bar Deposits with Implications for Reservoir Charaterization, Athabasca Oil Sands, Alberta, Canada. Sedimentary Geology 242 (2011): 18-33.

Lau, K.M. and Weng, H. 1995. Climate Signal Detection Using Wavelet Transform: How to Make a Time Series Sing. Bullitin of the American Meteorological Society 76 (12): 2391–2402.

Lewan, M.D. 2002. New Insights on Timing of Oil and Gas Generation in the Central Gulf Coast Interior Zone Based on Hydrous-Pyrolysis Kinetic Parameters. Transactions of the Gulf Coast Association of Geological Societies 52 (2002): 607-619.

Liro, L.M., Dawson, W.C., Katz, B., et al. 1994. Sequence Stratigraphic Elements and Geochemical Variability within a “Condensed Section”: Eagle Ford Group, East-Central Texas. Transactions of the Gulf Coast Association of Geological Societies 44 (1994): 393-402.

Mott, R.E., Cable, A.S., and Spearing, M.S. 2000. Measurements of Relative Permeabilities for Calculating Gas-Condensate Well Deliverability. SPE Reservoir Evaluation and Engineering 3(6):473-479.

McCain, W.D. Jr. 1990. The Properties of Petroleum Fluids, Second Edition. Tulsa, Oklahoma: PennWell Publishing Company.

Montgomery, S.L., Jarvie, D.M., Bowker, K.A., et al. 2005. Mississippian Barnett Shale, Fort Worth Basin, North-Central Texas: Gas-Shale Play with Multi-Trillion Cubic Foot Potential. AAPG Bulletin 89 (2): 155-175.

Mullen, J. 2010. Petrophysical Chaterization of the Eagle Ford Shale in South Texas. Paper 138145 Presented at Canadian Unconventional Resources & Petroleum Conference, Calgary, Alberta, Canada, 19-21 October.

Mullen, J., Lowry, J.C., and Nwabuoku, K.C. 2010. Lesson Learned Developing the Eagle Ford Shale. Paper 138446 Presented Tight Gas Completions Conference in San Antonio, Texas, 18-20 March.

Passey, Q.R., Creaney, S., Kulla, J.B., et al. 1990. A Practical Model for Organic Richness from Porosity and Resistivity Logs. AAPG Bulletin 74 (12): 1777-1794.

Passey, Q.R., Bohacs, K.M., Esch, W.L., et al. 2010. From Oil-Prone Source Rock to Gas-producing Shale Reservoir-Geologic and Petrophysical Characterization of Unconventional Shale Gas Reservoirs. Paper 131350 Presented at International Oil and Gas Conference and Exhibition in Beijing, China, 8-10 June.

Petrohawk. 2009. Leaders in Industry Luncheon. http://www.petrohawk.com/presentations.php. (accessed May 2009).

Pollastro, R.M., Jarvie, D.M., Hill, R.J., et al. 2007. Geologic Framework of the Mississippian Barnett Shale, Barnett-Paleozoic Total Petroleum System, Bend Arch-Fort Worth Basin, Texas. AAPG Bulletin 91 (4): 405-436.

Quirein, J., Praznik, G. Galford, J., et al. 2013. A Workflow to Evaluate Mineralogy, Porosity, TOC, and Hydrocarbon Volume in the Eagle Ford Shale. Paper 167012 Presented at SPE Unconventional Resources Conference and Exhibition-Asia Pacific Help in Brisbane, Australia, 11-13 November.

Rehrin, T., Loayza, M., Kirkham B., et al. 2011. Channel Fracturing in Horizotnal Wellbores: the New Edge of Stimulaion Techniques in the Eagle Ford Formation. Paper 145403 Presented at SPE Annual Technical Conference and Exhibition in Denver, Colorado, 30 October - 02 November.

Rickman, R., Mullen, M, Petre, E., et al. 2008. A Practical Use of Shale Petrophysics for Stimulation Design Optimization: All Shale Plays Are Not Clones of the Barnett Shale. Paper 115258 Presented SPE Annual Technical Conference and Exhibition, Denver, Colorado, 21-24 September.

Rivera, N.A., Ray, S., Jensen, J.L., et al. 2004. Detection of Cyclic Patterns Using Wavelets: An Example Study in the Ormskirk Sandstone. Irish Sea. Mathematical Geology 36 (5):529-543.

Rushing, J.A. and Sullivan, R.B. 2003. Evaluation of a Hybrid Water-Frac Stimulation Technology in the Bossier Tight Gas Sand Play. Paper 84394 Presented at SPE Annual Technical Conference and Exhibition in Denver, Colorado, 5-8 October.

Scott, D. and Lane, D.M. 2008. Box-Cox Transformations. Online Statistics Education: A Multimedia Course of Study. http://onlinestatbook.com/.

Skbkekas. 2009. Normal Quantile Plot of a Set of 100 Independent Standard Exponential Values. http://en.wikipedia.org/wiki/File:Normal_exponential_qq.svg.

Spears, R.W. and Jackson, S.L. 2009. Development of a Predictive Tool for Estimating Well Performance in Horizontal Shale Gas Wells in the Barnett Shale, North Texas, USA. Petrophysics 50 (1): 19-31.

Tanyel, E.D. 2006. Formation Evaluation Using Wavelet Analysis on Logs of the Chinji and Nagri Formations, Northern Pakistan. M.S. thesis, Texas A&M University, College Station, Texas (August 2006)

Texas Railroad Commission. 2013a. Texas Eagle Ford Shale Gas Well Gas Production 2008 through 2012. https://www.rrc.state.tx.us/eagleford/EagleFordGWGProduction.pdf (accessed April 2013)

Texas Railroad Commission. 2013b. Texas Eagle Ford Shale Oil Production 2008 through 2012 https://www.rrc.state.tx.us/eagleford/EagleFordOilProduction.pdf (accessed April 2013)

Texas Railroad Commission. 2013c. Texas Eagle Ford Shale Gas Condensate Production 2008 through 2012 https://www.rrc.state.tx.us/eagleford/EagleFordCondensateProduction.pdf (accessed April 2013)

Texas Railroad Commission. 2013d. http://www.rrc.state.tx.us/data/online/index.php. (accessed Febuary 2013).

Texas Railroad Commission. 2014. Texas Eagle Ford Shale Drilling Permit Issued Each Year https://www.rrc.state.tx.us/eagleford/EagleFordDrillingPermitsIssued.pdf (accessed February 2014).

Tian, Y. and Ayers, W. B. 2009. Regional Stratigraphic and Sedimentory Analyses, Barnett Shale, Fort Worth Basin, Texas. Proc., Coalbed & Shale Gas Symposium, Alabama, 0919.

Tian, Y. 2010. An Investigation of Regional Variations of Barnett Shale Reservoir Properties, and Resulting Variability of Hydrocarbon Composition and Well Performance. Master Thesis, Texas A&M U., College Station, Texas (May 2010).

Tian, Y., Ayers, W. B., and McCain, W. D. Jr. 2012. Regional Analysis of Stratigraphy, Reservoir Characteristics, and Fluid Phases in the Eagle Ford Shale. Paper Presented at Gulf Coast Association of Geological Societies and the Gulf Coast Section of SEPM, Austin, Texas, 21-24 October.

Tian, Y., Ayers, W.B., and McCain, W.D. Jr. 2013. The Eagle Ford Shale Play, South Texas: Regional Variations in Fluid Types, Hydrocarbon Production and Reservoir Properties. Paper 16808 presented at the International Petroleum Technology Conference, Beijing, China, 26–28 March.

Tian, Y., Ayers, W.B., and McCain, W.D. Jr. 2014. Regional Impacts of Lithologic Cyclicity and Reservoir and Fluid Properties on Eagle Ford Shale Well Performance. Paper 169007 presented for SPE Unconventional Resources Conference in the Woodlands, TX, 1-4 April.

TXCO. 2009. The Emerging Resource Company, TXCO Resources. http://www.txco.com/presentation.html. Downloaded 20 May 2009.

Wan, J., Barnum, R.S., DiGloria, D.C., et al. 2013. Factors Controlling Recovery in Liquid Rich Unconentional Systems. Paper IPTC 17103 Presented at the International Petroleum Technology Convergence, Beijing, China, 26-28 March.

Wells, L.E. 1990. Holocene History of the El Niño Phenomenon in Flood Sediments of Northern Coastal Peru. Geology 18:1134–1137.

Wilk, M.B. and Gnanadesikan, R. 1968. Probability Plotting Methods for the Analysis of Data. Biometrika 55(1):1-17.

Yu, S., Lee, J., Miocevic, D., et al. 2013. Estimating Proved Reserves in Tight/Shale Wells Using the Modified SEPD method. Paper 166198 Presented at SPE Annual Technical Conference and Exhibition in New Orleans, Louisiana, USA, 30 September–2 October.